

POLITECNICO DI TORINO

College of Chemical and Material Engineering

**Master Degree
in Chemical and Sustainable Process Engineering**

Master Thesis

Impedance spectroscopy for the assessment of demineralized tooth lesions



Supervisors

Prof. Sabrina Grassini
Prof. Leonardo Iannucci
Prof. Nicola Scotti

Candidate

Marta Pireddu

March 2023

Riassunto

Introduzione

Le malattie del cavo orale sono le malattie croniche più comuni, colpiscono quasi 3,5 miliardi di persone a livello globale, secondo il Global Burden of Disease Study 2017 [2], e possono provocare la carie dentale.

La carie è una malattia ad eziologia multifattoriale, irreversibile, infettiva, cronica, che distrugge i tessuti dentali duri (smalto e dentina). Le carie hanno un impatto importante sulla qualità della vita dell'uomo, infatti se non vengono curate, possono causare ansia, dolore, stress, problemi sociali causati dalla possibile perdita dei denti, limitazioni funzionali, infezioni e persino la morte [1, 10].

I denti sono strutture mineralizzate molto resistenti, di diverse forme e dimensioni, e sono alloggiati nelle mascelle, all'interno di cavità. Ci sono 16 denti per arco, classificati come incisivi (quattro), canini (due), premolari (quattro) e molari (sei) (**Figure 1.2**). La struttura del dente è divisa in tre parti (**Figure 1.3**): la corona, il colletto e la radice. Ogni dente è formato da smalto, corona, gengive, cavità pulpare, colletto, dentina, parete ossea (o osso) mascellare (o alveolare), canale radicolare, cemento, e legamento parodontale [15] (**Figure 1.4**).

Lo smalto dentale, che ricopre la parte esterna della corona, è l'elemento più duro del corpo umano. Si tratta di un tessuto calcificato, traslucido, che tende a dissolversi se a contatto con acidi, e costituito per il 96% da minerali (matrice inorganica) e per il restante 4% da sostanze organiche (proteine e lipidi) e acqua. Inoltre, non contiene cellule viventi ed è molto più bianco e più duro della dentina.

Lo smalto dentale contiene circa il 96% di apatite di calcio, chiamata idrossiapatite (HAP) ($\text{Ca}_{10}(\text{PO}_4)_6(\text{OH})_2$) o fluorapatite ($\text{Ca}_{10}(\text{PO}_4)_6\text{F}_2$) [18]. A causa di questo elevato contenuto di minerali, i denti sono i materiali biologici più duri e più mineralizzati nel corpo umano [19]. La microstruttura dello smalto è composta da prismi esagonali allineati perpendicolari che si sviluppano dalla giunzione dentina-smalto (DEJ) verso la superficie del dente [18]. Ogni prisma è impacchettato e forma aste di circa 4 μm di diametro, creando una struttura meccanicamente dura ed altamente resistente. La matrice inorganica occupa le lacune tra i cristalli di apatite.

La dentina è formata da minerali per circa il 70% in peso (principalmente fosfato di calcio), mentre la matrice organica è presente per il 20%, e il 10% rimanente è occupato dall'acqua. I cristalli di idrossiapatite nella dentina hanno la forma di piastre appiattite con una lunghezza pari a circa 60-70 nm, 20-30 nm di larghezza e 3-4 nm di spessore. Il collagene di tipo I è il componente principale della matrice organica della dentina, infatti è presente per circa l'85%, mentre i tipi di collagene III e V sono presenti in quantità inferiori. La matrice organica è costituita non soltanto da collagene ma anche da una fosfoproteina (per circa il 50%), mentre la matrice inorganica rimanente è prevalentemente composta da idrossiapatite (HA) [29].

La demineralizzazione è il processo di rimozione dei minerali sotto forma di ioni dai cristalli di HA dei tessuti duri, come smalto, dentina e cemento, mentre la remineralizzazione è il processo di ripristino di questi ioni; entrambi i processi si verificano sulla superficie del dente [4]. L'erosione e le lesioni cariose sono le due principali conseguenze della demineralizzazione.

La demineralizzazione è causata dall'azione dei batteri normalmente presenti all'interno del cavo orale, che si accumulano nel biofilm batterico della placca dentale. I prodotti acidi, derivanti dalla fermentazione batterica degli zuccheri e degli amidi presenti in cibi e bevande [47], aggrediscono inizialmente lo smalto e successivamente la dentina.

La demineralizzazione causa un aumento della porosità nella struttura del dente, che può essere riempita dal liquido ricco di ioni proveniente dall'ambiente orale, portando ad una maggiore conduttività elettrica. Se invece i cristalli di HA parzialmente demineralizzati a causa degli acidi sono esposti ad ambienti orali che favoriscono la re-mineralizzazione, possono raggiungere le loro dimensioni originali, infatti la demineralizzazione è un processo reversibile [49]. La forma più stabile di idrossiapatite si ha in un ambiente con un pH di 7,4, mentre la dissoluzione dei cristalli avviene quando il pH della placca scende sotto 5,5 [50, 51].

L'erosione dentale, cioè la perdita di tessuto dentale dovuta a danni meccanici o a dissoluzione causata da acidi di origine non batterica, può essere causata dall'esposizione ad un ambiente acido o può essere di tipo chimico. Un acido in soluzione forma ioni idronio, che si legano con un fosfato o un carbonato nella idrossiapatite, rilasciando gli anioni in soluzione; in base al pH dell'acido, si possono verificare tre forme di attacco acido [68]. L'erosione dentale può essere dovuta al pH, infatti è più rapida a pH più basso [77], ma può dipendere anche da un altro parametro, cioè la concentrazione molare di acido, misurata con l'acidità titolabile [79], il cui aumento è correlabile ad un aumento della perdita di smalto [80]. Anche la temperatura influenza la cinetica di dissoluzione, infatti più la temperatura all'interno della bocca è alta rispetto alla temperatura ambiente, più la velocità della cinetica di reazione aumenta [45].

La demineralizzazione e la successiva erosione sono processi dinamici che dipendono da molte variabili. Gli acidi provenienti dal cibo o dalle bevande e l'attacco microbico dei batteri presenti nella bocca sono le principali cause di un attacco acido [47]. I fattori che influenzano la demineralizzazione sono suddivisi in due gruppi principali: estrinseci (abitudini alimentari e farmaci) e intrinseci (malattie trattabili con farmaci). Questi fattori possono essere modificati dai fattori modificatori, che possono essere i cambiamenti nelle caratteristiche biochimiche di un fattore intrinseco o estrinseco, i fattori comportamentali (pulizia regolare dei denti, tipi di bevande consumate) o fattori socioeconomici [72].

La re-mineralizzazione è un processo naturale di ripristino di ioni minerali nella struttura dell'idrossiapatite per le lesioni non cavitate. Gli agenti re-mineralizzanti sono composti utilizzati per aumentare la saturazione minerale (fluoruri, fosfopeptide di caseina-fosfato di calcio amorfo (CPP-ACP), vetro bioattivo, fosfato tricalcico (TCP), nanoparticelle di HAP e fosfato beta tricalcico (TCP)), modificatori del biofilm come arginina, triclosan, xilitolo, probiotici e composti a base di erbe [22]. I sistemi preventivi per la demineralizzazione dei denti sono la terapia al fluoro, la saliva, e i batteri probiotici.

Per identificare la presenza di carie dentali sono stati sviluppati molti criteri di misurazione, ma uno dei più conosciuti è il sistema internazionale di rilevamento e valutazione della carie (ICDAS). Si tratta di una procedura standardizzata di rilevamento visivo, utilizzato per ridurre la variabilità dipendente dall'operatore, per l'identificazione e la valutazione dell'attività della carie, utilizzato nell'istruzione odontoiatrica, nella pratica clinica, e nella ricerca [11].

I nuovi metodi diagnostici presentano tipicamente un'elevata sensibilità ed una buona riproducibilità, ma una bassa specificità [112], quindi la scelta migliore rimane l'esame visivo, in quanto è affidabile, semplice ed accurato [113, 114].

Solitamente l'esame visivo è combinato con la radiografia bitewing (BWR) [115]. La scelta di utilizzare molti metodi diagnostici privi di raggi X, come la misura della fluorescenza indotta da laser (LF), la transilluminazione nel vicino infrarosso (NILT) e la spettroscopia di impedenza elettrochimica (EIS), è causata dalla necessità di ridurre il rischio per la salute dall'esposizione alle radiazioni ionizzanti [113, 117, 18, 119]. Due degli approcci più promettenti sono basati sulla spettroscopia di impedenza (IS) e sulle misurazioni della conduttanza elettrica (ECM) [119]. Ci sono altri metodi avanzati per la rilevazione della carie [122], ad esempio i metodi radiografici digitali, la transilluminazione con fibra ottica quantitativa, la transilluminazione con fibra ottica digitale (DIFOTI) e la fluorescenza quantitativa indotta con luce/laser, e DIAGNOdent pen.

Obiettivo del lavoro

Lo scopo di questa tesi è l'analisi del processo di demineralizzazione dentale tramite l'utilizzo di misure di spettroscopia di impedenza elettrochimica, al fine di valutare l'attuabilità di questa tecnica e quindi la fattibilità di una diagnosi non invasiva delle carie. L'analisi del fenomeno di demineralizzazione nei campioni presi in considerazione, un set di cinquanta denti sani, ha lo scopo di identificare diverse proprietà dei denti, come quelle elettrochimiche, morfologiche e chimiche. I campioni sono stati esaminati sia prima che dopo il trattamento di demineralizzazione, attuato tramite una soluzione demineralizzante preparata in laboratorio.

Materiali e metodi

I denti sani utilizzati per questa indagine (terzi molari umani non eruttati e canini) sono stati estratti da non più di un anno, per motivi parodontali, da diversi pazienti dopo il consenso informato presso il Dipartimento di Scienze Chirurgiche-Dental School dell'Università di Torino. Il comitato etico dell'Università di Torino ha approvato il protocollo di studio DS 00071 2018.

Per questo studio è stato utilizzato un set di cinquanta denti senza otturazioni o sigillanti in superficie e con la radice completamente intatta. Dopo l'estrazione, i denti, esaminati e classificati da un dentista esperto, sono stati puliti e sono stati rimossi i tessuti molli ed i frammenti ossei rimanenti sulla superficie. Per evitare la disidratazione, i denti estratti sono stati conservati in provette ermeticamente sigillate contenenti una soluzione 0,5% in volume di ipoclorito di sodio (NaClO).

Le prime misure sono state condotte su denti sani, che poi sono stati demineralizzati utilizzando una soluzione demineralizzante, la quale è stata preparata con acqua distillata, acido acetico, cloruro di calcio, diidrogenofosfato di potassio, idrossido di sodio o acido cloridrico per regolare il pH. Inizialmente la superficie dei campioni è stata ricoperta da uno smalto organico, eccetto che in una piccola area rettangolare a contatto con la soluzione (**Figure 2.1**). Successivamente, i denti all'interno di provette contenenti la soluzione demineralizzante sono stati collocati in una camera climatica a 38 °C per 96 ore per indurre la demineralizzazione.

Tutte le analisi sono state effettuate immediatamente dopo aver rimosso i campioni dalla soluzione di ipoclorito e dopo averli asciugati.

Le misure di impedenza sono state effettuate utilizzando un potenziostato Ivium-n-Stat e i dati sono stati elaborati utilizzando il software Iviumsoft. Il setup sperimentale (**Figure 2.4**) delle misure di impedenza elettrochimica è formato da una cella di misura con una configurazione a due elettrodi:

- l'elettrodo di lavoro (filo di platino a contatto con la cavità dentale, posizionato sulla superficie del dente),
- il controlettrodo (filo di platino parzialmente immerso nella soluzione fisiologica salina).

Il supporto del campione è un supporto PLA stampato in 3D e posizionato nella cella di misura per garantire una corretta misura senza danneggiare il dente. Dai due terzi ai tre quarti della radice del dente vengono immersi nella soluzione salina fisiologica allo 0,9% p/v di cloruro di sodio (NaCl), la quale offre una buona visibilità del campione durante la misurazione ed evita l'essiccazione dei campioni umidi.

Dopo la valutazione visiva delle superfici dentali, sono state effettuate misure di impedenza utilizzando un segnale sinusoidale di intensità pari a 10 mV tra l'elettrodo di lavoro ed il controlettrodo, nell'intervallo di frequenze da 10^{-1} Hz a 10^4 Hz, acquisendo 5 punti per decade di frequenza.

La spettroscopia di impedenza elettrochimica (EIS) è una tecnica sensibile, rapida, non invasiva e non distruttiva per misurare la resistenza al flusso di corrente alternata attraverso un determinato materiale. È comunemente utilizzata per la caratterizzazione delle proprietà elettriche di solidi o liquidi [153], per misurare la resistenza elettrica dei tessuti biologici e per rilevare il maggiore contenuto di liquido nel dente, correlato all'aumento della porosità dovuto alla perdita di minerale che si ha a causa dal processo carioso.

Gli spettri di impedenza possono essere correlati ai cambiamenti nella morfologia superficiale dei denti, misurati tramite la microscopia elettronica a scansione (SEM).

Per un'analisi più dettagliata di questi risultati d'impedenza, gli spettri sono stati modellati tramite un circuito elettrico equivalente (**Figure 2.6**): questo è costituito da una resistenza R_0 (resistenza di contatto o di interfaccia tra il filo di platino ed il dente) collegata ad un elemento a fase costante CPE_1 (capacità di doppio strato) in parallelo con un secondo resistore R_1 (resistenza di trasferimento di carica).

Come scritto precedentemente, la microscopia elettronica a scansione (SEM) è una tecnica di caratterizzazione che permette di rilevare i cambiamenti morfologici nei denti, tramite un fascio di elettroni che interagisce con la superficie del campione. Questa tecnica sfrutta gli elettroni che sono riflessi dalla regione vicino alla superficie di un campione per creare un'immagine; l'intera colonna di elettroni deve essere sottovuoto.

Le analisi di microscopia elettronica a scansione sono state effettuate tramite uno strumento Phenom Desktop SEM (**Figure 2.7**). Le immagini sono state ottenute utilizzando differenti valori di ingrandimento, una tensione di accelerazione pari a 15 kV ed una pressione pari a 60 Pa.

Un'altra tecnica, la spettroscopia Raman, è stata utilizzata a supporto delle misure di spettroscopia di impedenza elettrochimica. Questa tecnica è semplice, non invasiva e non distruttiva, richiede una preparazione minima o nulla del campione [172] e fornisce risultati riproducibili [171]. Viene utilizzata per monitorare i modi vibrazionali associati all'idrossiapatite, $Ca_{10}(PO_4)_6(OH)_2$, che è uno dei principali componenti dello smalto dentale e la cui demineralizzazione è legata al processo di decadimento.

Le misure di spettroscopia Raman sono state eseguite utilizzando uno spettrometro modulare portatile prodotto da BWTEK (**Figure 2.8**), dotato di un laser monocromatico (λ : 785 nm) e di uno spettrometro BTC675N (intervallo di misura: da 65 cm^{-1} a 3350 cm^{-1} , risoluzione pari a 6 cm^{-1}) accoppiato ad un sensore CCD. L'analisi è stata effettuata collegando lo strumento ad un microscopio compatto (BAC151) che permette di osservare l'area di analisi e di focalizzare il fascio sulla superficie.

Risultati e discussione

Il processo di demineralizzazione viene analizzato attraverso due tecniche di supporto alla spettroscopia di impedenza elettrochimica: la microscopia elettronica a scansione e la spettroscopia Raman. In questo modo è possibile differenziare un dente sano da un dente demineralizzato.

La superficie di un dente sano appare liscia e senza difetti correlabili ad un possibile fenomeno di demineralizzazione (**Figure 3.1**), mentre un dente demineralizzato presenta una superficie caratterizzata da prismi composti da cristalli esagonali di idrossiapatite, che creano un aspetto a nido d'ape (**Figure 3.2**) [198].

I due spettri Raman acquisiti (**Figure 3.5**), uno sulla superficie di un dente sano e uno su quella di un dente demineralizzato, permettono di valutare il grado di demineralizzazione dello smalto monitorando le variazioni di intensità del picco a 960 cm^{-1} relativo all'idrossiapatite. L'intensità del picco, correlata alla vibrazione del gruppo PO_4^{3-} nell'idrossiapatite, diminuisce con l'aumento del grado di demineralizzazione.

Mediante la spettroscopia Raman accoppiata alla spettroscopia di impedenza elettrochimica è possibile correlare la risposta di corrente con un'informazione di tipo chimico, ottenendo così una caratterizzazione completa dello stato di salute del dente.

Il setup sperimentale precedentemente presentato (**Figure 2.4**), utilizzato per eseguire le misure di impedenza, è facilmente replicabile nelle applicazioni in-vivo perché coinvolge due elettrodi, uno a contatto con il dente e l'altro all'interno della cavità orale (nella saliva), quindi non comporta una rottura del dente. Inoltre, esso permette di utilizzare strumenti portatili ed a basso costo, e non prevede l'utilizzo dei raggi X, quindi è adatto a giovani pazienti ed a donne in gravidanza [122].

Le misure di spettroscopia di impedenza sono eseguite sull'intero set di campioni sia prima che dopo il trattamento di demineralizzazione. L'obiettivo è dimostrare che la demineralizzazione provoca una modifica delle proprietà elettriche del tessuto dentale (**Figure 3.6**). Gli spettri ottenuti mostrano un comportamento resistivo alle alte frequenze, correlato alla resistenza di contatto platino/dente, che diventa capacitivo alle basse frequenze, in relazione alla capacità di doppio strato. La forma degli spettri associati ai denti sani e quella degli spettri associati ai denti demineralizzati sono simili, ma nel primo caso la parte resistiva occupa un intervallo di frequenze maggiore.

I campioni appartenenti ai due diversi gruppi, sani e demineralizzati, hanno un comportamento elettrochimico diverso, infatti, nel caso dei denti demineralizzati, alle alte frequenze, il modulo di impedenza ha valori inferiori rispetto al caso dei denti sani. Inoltre, per questi ultimi la fase di impedenza mantiene un valore pari a 0° per un intervallo di frequenze maggiore e tende ad avvicinarsi a -60° soltanto sotto 1 Hz, mentre per i denti demineralizzati raggiunge il massimo a circa -70° .

È stata condotta anche un'analisi quantitativa dei risultati delle misure di impedenza, infatti gli spettri sono stati modellati utilizzando il circuito elettrico equivalente proposto precedentemente (**Figure 2.6**). Il parametro che varia maggiormente tra i due diversi gruppi di misure è la resistenza di contatto R_0 , ottenuta dal valore di impedenza alle alte frequenze: essa presenta un valore inferiore in corrispondenza dell'area demineralizzata. Inoltre, si osserva un aumento della capacità di doppio strato Q_1 nel dente demineralizzato, che è però trascurabile. Questi risultati sono supportati anche dalla letteratura precedente [1].

Nonostante sia possibile misurare la superficie dei campioni analizzati durante queste analisi in vitro, sarebbe impossibile fare ciò in una procedura in-vivo. Di conseguenza si è scelto di non normalizzare i valori di impedenza rispetto all'area del campione.

Ogni misura di impedenza è caratterizzata dai parametri elettrici (R_0 , R_1 e Q_1) e dalle variazioni percentuali di questi ultimi. È stato riscontrato che in tutti i campioni esaminati, prima e dopo la demineralizzazione, questi parametri mantengono i seguenti ordini di grandezza: R_0 è circa pari a $10^5 \Omega$ per i denti sani e $10^4 \Omega$ per quelli demineralizzati, R_1 è circa pari a $10^7 \Omega$ per tutti i campioni, e Q_1 è circa pari a $10^{-7} \text{ s}^N/\Omega$ per tutti i denti.

Nonostante analizzare lo spettro completo rappresenti una buona scelta per differenziare un dente sano da uno demineralizzato, c'è un altro modo per valutare la demineralizzazione: l'uso della fase di impedenza. Viene esaminato il valore di frequenza a cui la fase raggiunge -45° per tutti i campioni (**Figure 3.16**), che è correlata alla diversa capacità misurata. Si riscontra che questa frequenza ha un valore superiore a 10 Hz nel caso dei denti demineralizzati, mentre è inferiore a 10 Hz per le misure relative ai denti sani.

Questo valore di soglia risulta essere un buon metodo per classificare i denti sani e demineralizzati, anche se si riscontrano dei problemi con alcune misure d'impedenza.

I valori anomali (outliers) sono esaminati tramite i diagrammi di Bode, tramite le immagini ottenute attraverso il SEM e tramite i grafici che riportano la frequenza a cui la fase raggiunge un valore pari a -45° . Eliminando i campioni con comportamento anomalo, si ottiene un grafico con la frequenza nelle ordinate in cui è evidente una netta separazione tra i campioni pre e post demineralizzazione (**Figure 3.32**). Di conseguenza, si è deciso di distinguere i due gruppi di campioni analizzando la fase (e non il modulo di impedenza), la quale non dipende dall'area del campione, ma soltanto dalle sue proprietà dielettriche.

Al fine di fornire una visione più dettagliata di ciascun campione, le misure di impedenza riportate nella presente tesi sono eseguite in cinque punti per dente, ed è stata riscontrata una certa variabilità per ogni misura.

Conclusioni

La cura delle malattie dentali è stata rivoluzionata grazie ai progressi scientifici del secolo scorso, ma la carie dentale rimane la più rilevante malattia cronica nel mondo.

La presente tesi sperimentale propone l'utilizzo della spettroscopia di impedenza elettrochimica come metodo diagnostico per valutare la presenza di demineralizzazione nei denti. Sono condotte anche misure di spettroscopia Raman e di microscopia elettronica a scansione per valutare tramite altre tecniche i risultati di impedenza. I risultati ottenuti mostrano la possibilità di distinguere i denti sani dai denti demineralizzati attraverso la variazione delle caratteristiche elettriche del campione.

Nel caso dei denti demineralizzati, i valori del modulo di impedenza alle alte frequenze sono inferiori a quelli dei denti sani, mentre la fase raggiunge valori pari a circa -70° sotto 1 Hz. Nel caso dei denti sani, la fase mantiene valori vicini a 0° per un intervallo di frequenza più ampio e tende a valori vicini a circa -60° sotto 1 Hz.

Gli spettri modellati tramite un circuito elettrico equivalente mostrano un comportamento capacitivo, associato alla capacità di doppio strato, alle basse frequenze ed un comportamento resistivo, associato all'interfaccia del dente, alle alte frequenze.

Tutti i parametri sono influenzati dalla variabilità delle dimensioni dei campioni, ma il parametro che presenta la maggiore variabilità tra denti sani e denti cariati è la resistenza R_0 .

L'andamento della fase non dipende dalle dimensioni del campione: il valore della fase pari a -45° è raggiunto ad una frequenza superiore a 10 Hz nel caso dei denti demineralizzati e ad una frequenza inferiore a 10 Hz nel caso dei denti sani. Questo è un parametro soglia che permette di distinguere i denti prima e dopo la demineralizzazione.

Le immagini ottenute tramite il SEM mostrano una superficie liscia ed omogenea nel caso dei denti sani, mentre nel caso dei denti demineralizzata la superficie è caratterizzata da strutture esagonali, con un aspetto alveolare. L'intensità del picco di 960 cm^{-1} , monitorata tramite spettroscopia Raman, diminuisce con l'aumentare del grado di demineralizzazione.

La ricerca futura si può focalizzare sulla valutazione della medesima metodologia (EIS) ma in diverse soluzioni, come la saliva artificiale, o tramite l'utilizzo di sonde differenti. Altri studi possono migliorare la statistica al fine di convalidare questo approccio su un maggior numero di campioni ed al fine di valutarne l'accuratezza. Inoltre, una volta convalidato, il metodo proposto può essere utilizzato per valutare lo stato di demineralizzazione della dentina umana, anche tramite lo sviluppo di una nuova sonda. La spettroscopia di impedenza può essere proposta per studiare le micro-perdite fra i materiali dentali e di riempimento. Infine, possono essere studiati algoritmi di elaborazione più complessi, ad esempio analisi multivariata o strumenti di machine learning [202-204].

Contents

<i>Riassunto</i>	III
List of Figures	iii
List of Tables.....	vi
1. Introduction	1
1.1 The structure of human teeth	3
1.2 The chemical composition of human tooth.....	6
1.3 Tooth demineralization	10
1.3.1 Acid erosion mechanisms	13
1.3.2 Chemical erosion mechanisms.....	15
1.3.3 Modifying factors	16
1.4 Remineralization	18
1.5 Caries detection methods	20
1.5.1 Electrochemical Impedance Spectroscopy (EIS).....	24
1.5.2 Raman Spectroscopy.....	25
1.5.3 Scanning Electron Microscopy (SEM)	26
1.6 Aim of the work	28
2. Materials Characterization and Methodologies	29
2.1 Human Teeth Samples Preparation.....	29
2.2 Impedance Measurements and Data Acquisition.....	31
2.2.1 Main impedance concepts	31
2.2.2 Impedance Measurements	33
2.3 Equivalent Electrical Circuit.....	35
2.3.1 Main aspects.....	35
2.3.2 Proposed Equivalent Electrical Circuit	37
2.4 Scanning Electron Microscopy	38
2.5 Raman Spectroscopy.....	39
3. Results and discussion.....	41
3.1 Analysis of the demineralization process through SEM and Raman measurements	41
3.2 Experimental set-up	45
3.3 Impedance measurements	46
3.4 Equivalent electrical circuits.....	48
3.5 Variations in EEC Pre and Post Demineralization	52
3.6 Discrimination using the phase value	59

3.7 Variability of measurements	61
3.8 Effect of outliers	68
3.9 Demineralization process examined in different surface points	73
4. Conclusions and future developments	75
List of Abbreviations.....	76
List of Symbols	77
References	79
Acknowledgments.....	92

List of Figures

Figure 1.1: Tooth decay starts with the acid from plaque attacking the enamel and repeated attacks lead to tooth decay [6].....	1
Figure 1.2: Lower jaw (mandible) and upper jaw (maxilla) [13]	3
Figure 1.3: Teeth structure [14]	3
Figure 1.4: A cross sectional view of a tooth [15]	4
Figure 1.5: HAP structure [148]	6
Figure 1.6: Triple helix structure of collagen [149]	8
Figure 1.7: Collagen fibre [150]	8
Figure 1.8: The equilibrium between dynamic demineralization and remineralization at the plaque-enamel interface [22]	10
Figure 1.9: Citric acid structure [151]	13
Figure 1.10: Formula of hydroxyapatite and fluorapatite [152]	18
Figure 1.11: Basic components of a SEM [197]	26
Figure 2.1: Tooth with an organic burnish.....	30
Figure 2.2: Bode Plot for 1 mm/year Corrosion Rate [206].....	32
Figure 1.3: Nyquist Plot for 1 mm/year Corrosion Rate [206].....	32
Figure 2.4: Experimental set-up for impedance measurements.....	33
Figure 2.5: Simplified Randles cell schematic diagram [206].....	36
Figure 2.6: Equivalent electrical circuit.....	37
Figure 2.7: Phenom Desktop SEM [196]	38
Figure 2.8: BWTEK portable modular spectrometer.....	39
Figure 3.1: SEM image of a healthy tooth.....	40
Figure 3.2: SEM image of a demineralized tooth.....	41
Figure 3.3: SEM image at lower magnification.....	42
Figure 3.4: SEM image of a demineralized tooth.....	42
Figure 3.5: Raman spectra acquired on a healthy and demineralized tooth.....	43
Figure 2.4: Experimental set-up for impedance measurements.....	44
Figure 3.6: Impedance spectra of healthy (green lines) and demineralized (red lines) teeth as Bode diagram.....	45
Figure 2.6: Equivalent electrical circuit.....	47
Figure 3.7: Bode diagrams of a healthy tooth modelled through IviumSoft software, blue dots are experimental data, while the continuous line represents the model.....	48
Figure 3.8: Nyquist diagram of a healthy tooth modelled through IviumSoft software, blue dots are experimental data, while the continuous line represents the model.....	49

Figure 3.9: Bode diagrams of a demineralized tooth modelled through IviumSoft software, blue dots are experimental data, while the continuous line represents the model	49
Figure 3.10: Nyquist diagram of a demineralized tooth modelled through IviumSoft software, blue dots are experimental data, while the continuous line represents the model	50
Figure 3.11: Impedance spectra of healthy (green lines) and demineralized (red lines) teeth as Bode diagram.....	51
Figure 3.12: Impedance spectra of healthy (green lines) and demineralized (red lines) teeth as Bode diagram.....	53
Figure 3.13: Impedance spectra of healthy (green lines) and demineralized (red lines) teeth as Bode diagram.....	54
Figure 3.14: Impedance spectra of healthy (green lines) and demineralized (red lines) teeth as Bode diagram.....	55
Figure 3.15: Impedance spectra of healthy (green lines) and demineralized (red lines) teeth as Bode diagram.....	56
Figure 3.16: Frequency value at which the phase value of -45° is reached in each of the impedance measurements acquired on healthy teeth (green markers) and demineralized teeth (red markers) [1].....	58
Figure 3.17: Impedance spectra, as Bode diagram, of the healthy (green lines) and demineralized (red lines) tooth which shows an opposite behaviour.....	60
Figure 3.18: SEM image of a demineralized tooth.....	61
Figure 3.19: SEM image of a demineralized tooth.....	61
Figure 3.20: Impedance spectra, as Bode diagram, of the healthy (green lines) and demineralized (red lines) tooth which shows different trends.....	62
Figure 3.21: SEM image of a demineralized tooth.....	63
Figure 3.22: SEM image of a demineralized tooth.....	63
Figure 3.23: Impedance spectra, as Bode diagram, of the healthy (green lines) and demineralized (red lines) tooth which shows different trends.....	64
Figure 3.24: SEM image of a demineralized tooth.....	64
Figure 3.25: SEM image of a demineralized tooth.....	65
Figure 3.26: Impedance spectra, as Bode diagram, of the healthy (green lines) and demineralized (red lines) tooth which shows different trends.....	65
Figure 3.27: SEM image of a demineralized tooth.....	66
Figure 3.28: Frequency values at which the phase value of -45° is reached in each of the impedance measurements acquired on healthy tooth (green markers) and demineralized tooth (red markers) related to Figure 3.17.....	67
Figure 3.29: Frequency value at which the phase value of -45° is reached in each of the impedance measurements acquired on healthy tooth (green markers) and demineralized tooth (red markers) related to Figure 3.20.....	68

Figure 3.30: Frequency value at which the phase value of -45° is reached in each of the impedance measurements acquired on healthy tooth (green markers) and demineralized tooth (red markers) related to Figure 3.23.....69

Figure 3.31: Frequency value at which the phase value of -45° is reached in each of the impedance measurements acquired on healthy tooth (green markers) and demineralized tooth (red markers) related to Figure 3.25.....70

Figure 3.32: Frequency value at which the phase value of -45° is reached in each of the impedance measurements acquired on healthy teeth (green markers) and demineralized teeth (red markers).....71

Figure 3.33: Impedance spectra, as Bode diagram, of the healthy (green lines) and demineralized (red lines) tooth.....72

Figure 3.34: SEM image of a demineralized tooth.....73

Figure 3.35: SEM image of a demineralized tooth.....73

List of Tables

Table 1.1: Interaction of different factors in relation to tooth surface loss [4].....	17
Table 2.1: Principal equivalent elements present in equivalent circuits with IviumSoft symbols [206].....	35
Table 3.1: Equivalent electrical circuit parameters computed for a healthy and a demineralized tooth (results coming from the spectra reported in Figure 3.6)	47
Table 3.2: Equivalent electrical circuit parameters computed for a healthy and a demineralized tooth (results coming from the spectra reported in Figure 3.11)	52
Table 3.3: Percentage changes relative to the equivalent electrical circuit parameters reported in Table 3.2.....	52
Table 3.4: Equivalent electrical circuit parameters computed for a healthy and a demineralized tooth (results coming from the spectra reported in Figure 3.12).....	53
Table 3.5: Percentage changes relative to the equivalent electrical circuit parameters reported in Table 3.4.....	53
Table 3.6: Equivalent electrical circuit parameters computed for a healthy and a demineralized tooth (results coming from the spectra reported in Figure 3.13)	54
Table 3.7: Percentage changes relative to the equivalent electrical circuit parameters reported in Table 3.6.....	54
Table 3.8: Equivalent electrical circuit parameters computed for a healthy and a demineralized tooth (results coming from the spectra reported in Figure 3.14)	55
Table 3.9: Percentage changes relative to the equivalent electrical circuit parameters reported in Table 3.8.....	55
Table 3.10: Equivalent electrical circuit parameters computed for a healthy and a demineralized tooth (results coming from the spectra reported in Figure 3.15)	56
Table 3.11: Percentage changes relative to the equivalent electrical circuit parameters reported in Table 3.10.....	56

1. Introduction

Oral disease is considered as one of the most common chronic disease that affects people throughout their lives, resulting in dental caries. Dental caries have an important impact on the quality of their lives, indeed if they are not treated, they can cause anxiety, pain, stress, social handicap, functional limitations, and disfiguration due to tooth loss, infection and even death [1, 10].

Oral disease affects almost 3.5 billion people globally, according to the 2017 Global Burden of Disease Study [2]. Among them, untreated caries in permanent teeth afflict 2.4 billion people and this is one of the most common health problems in the world. People of all ages may have cavities once they have teeth, from childhood until old age, in fact untreated cavities in primary teeth affect more than 530 million people globally [3].

Tooth decay can be defined as a multi-factor, irreversible, infectious, chronic, and highly prevalent disease worldwide that destroys dental hard tissues over time, caused by the demineralization and remineralization of enamel in the presence of fermentable carbohydrates, saliva, and cariogenic oral flora. When exposed to carbohydrates, oral microorganisms can produce organic acids (acidic products from bacterial fermentation) that lower the pH of dental plaque [4].

The bacteria inside the bacterial biofilm (dental plaque) form an acid due to the contact with sugars, starchy foods, and beverages [5]. This acid can attack different parts of the tooth, including the enamel covering the crown, the cementum (a thin layer which covers the root), and the dentine (the tissue underneath both the enamel and the cementum), causing the loss of minerals and eventually leading to a small hole in the tooth, known as a cavity [5].

Caries progresses through demineralization and remineralization phases on the tooth surface before invading deeper layers. **Figure 1.1** shows the different stages of tooth decay, from demineralization in the enamel to decay in the pulp.



Figure 2.1: Tooth decay starts with the acid from plaque attacking the enamel and repeated attacks lead to tooth decay [6]

The progression of dental caries is slow in most people, and, at the beginning of dental caries, there are generally no symptoms. As the decay progresses, usually when the carious lesion reaches the dentine, it may cause a toothache or tooth sensitivity [7].

The disease is initially reversible, but can be stopped anytime, even when part of the dentine or enamel is damaged (cavitation). It is therefore crucial to hinder the development of caries by intervening as soon as possible to avoid other dental damage and invasive procedures [8]. Tooth decay can be found during a regular dental check-up, by accurate visual inspection of clean teeth made by trained examiner [9, 10].

Dental decay is a complex disease, but several measuring criteria have been developed to determine its presence. One of the most popular is the International Caries Detection and Assessment System (ICDAS), a standardized visual detection system, with a clinical scoring system used in dental education, clinical practice, research, and epidemiology for detection and assessment of caries activity [11].

There is still little public awareness of dental erosion, and its differential diagnosis among dentists turned out to be difficult [12].

1.1 The structure of human teeth

Teeth are very strong mineralized structures which come in different shapes and sizes, and they are housed in the jaws, within the cavities called sockets. There are 16 teeth per arch, classified as incisors, canines, premolars, and molars. They are subdivided as follows: four incisors, two canines, four premolars, and six molars.

Figure 1.2 shows the permanent dentition, that consists of 32 teeth: there are four incisors, two canines (or cuspids), four premolars (or bicuspid), four molars and two wisdom teeth (also called third molars) in each jaw. Each type of tooth has its own specific function: canines are for grasping and snatching food, the incisors are to tear it apart and the premolars and molars are to chew it with a mechanical grinding movement.

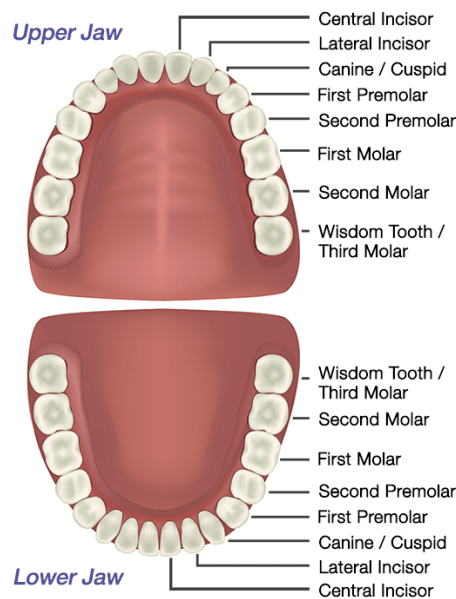


Figure 1.2: Lower jaw (mandible) and upper jaw (maxilla) [13]

The teeth structure can be divided into three parts, the crown, the neck (collar) and the root, as is shown in **Figure 1.3**. The teeth are even composed of four dental tissues: three hard tissues (enamel, dentin, and cementum) and the pulp, that is a soft (uncalcified) tissue. The pulp is also called the centre of the tooth, and it contains nerves, blood vessels and connective tissue [15].

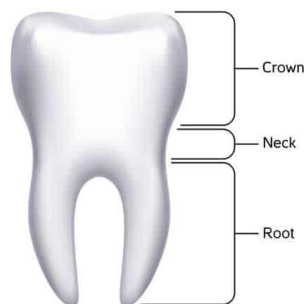


Figure 1.3: Teeth structure [14]

The crown is the visible part of the tooth that emerges from the cavity and the gums, and its form depends on the type of tooth. Canines are sharp, incisors are flat, and molars and premolars come with grooves and cusps [16].

The neck is the zone between the crown and the root, around which the gingival line develops. Bacterial plaque tends to accumulate in this area, so the gingival collar must be thoroughly cleaned to prevent dental caries [16].

The root is the non-visible part of the tooth that is inserted in the socket, connected with the bone by the periodontal ligament. It is longer than the crown and there are teeth that have only one root (canines, incisors, and the lower premolars), and others that can have double or triple roots (molars and premolars) [16].

The different parts of the teeth are enamel, crown, gums (or gingiva), pulp chamber, neck, dentin, jawbone (or alveolar bone), root canal, cementum, and periodontal ligament [15]. This structure is shown in **Figure 1.4**.



Figure 1.4: A cross sectional view of a tooth [15]

The external portion of the crown is covered by a layer of dental enamel, the single hardest element in the human body. This is a hard calcified tissue with minerals accounting for 96% of its composition and the remaining 4% consisting of organic substances. The enamel is translucent, and when it comes into contact with acidic foods, it tends to dissolve, which is why it must be protected with adequate, effective oral hygiene. It contains no living cells, so the tooth enamel cannot repair damage from decay or from wear (only the intervention of a dentist can correct these conditions). The enamel is much whiter and harder than dentin.

The anatomical crown is the visible part of the tooth, normally covered by enamel.

The gums are soft tissues that cover and protect the roots of your teeth and cover teeth that have not yet erupted.

The pulp chamber is the space occupied by the dental pulp, the portion that gives the tooth its vitality. The pulp is the soft tissue at the centre of the teeth containing nerves, blood vessels, connective tissue, and the cells (the odontoblasts that produce the dentin). The pulp is found inside the crown (pulp chamber), from where it extends along the roots (radicular pulp).

The neck is the area where the crown joins the root.

The dentin is the bulk of the tooth, underneath enamel and cementum, extends within both the crown and root, and it is the substance that gives the teeth their colour. This yellowish tissue contains microscopic tubules (small hollow tubes or canals) and when it loses its protective covering (enamel), the tubules allow heat and cold or acidic or sticky foods to stimulate the nerves and cells inside the tooth, causing sensitivity. The dentin consists of about 70% inorganic matter and 30% of organic material and water and it is generated by the odontoblasts, which are cells found in the pulp.

The jawbone is the part of the jaw that surrounds the roots of the teeth.

The root canal is the portion of the pulp cavity inside the root of a tooth; it is the chamber within the root of the tooth that contains the pulp.

The cementum hard connective tissue covering the tooth root, giving attachment to the periodontal ligament. Cementum is deposited only in the root area on the recently mineralized dentin matrix.

The periodontal ligament (PDL) is a system of collagenous connective tissue fibres that connect the root of a tooth to its socket (alveolar bone) [15]. It is a connective tissue structure that surrounds the tooth root and connects each tooth to the alveolar bone through a specialized set of collagen fibres.

Odontogenesis (tooth development) is the complex process to form dental mineralized tissues from embryonic cells (ameloblasts, cementoblasts, and odontoblasts).

Ameloblasts produce enamel, that has an epithelial origin and covers every tooth's crown. Cementum, that is made by cementoblasts, and dentin, that is secreted by odontoblasts, are of mesenchymal origin [17].

1.2 The chemical composition of human tooth

Teeth, like other natural biomaterials, are mainly inorganic/organic composites with high strength and toughness. In human teeth, enamel contains approximately 96% calcium apatite, which is called hydroxyapatite (HAP) ($\text{Ca}_{10}(\text{PO}_4)_6(\text{OH})_2$) or fluorapatite ($\text{Ca}_{10}(\text{PO}_4)_6\text{F}_2$) [18]. Due to this high mineral content, teeth are the hardest and one of the strongest biological materials within the human body [19]. The HAP structure is shown in the **Figure 1.5**.

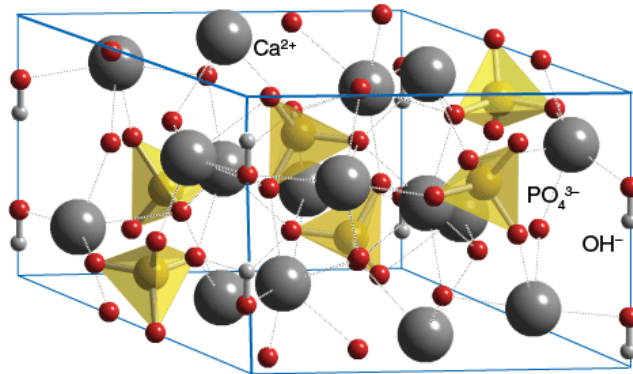


Figure 1.5: HAP structure [148]

Calcium hydroxyapatite [$\text{Ca}_{10}(\text{PO}_4)_6(\text{OH})_2$] is the most abundant mineral in human teeth. Other calcium phosphates and magnesium phosphates have been linked or not with apatite: brushite ($\text{CaHPO}_4 \cdot 2\text{H}_2\text{O}$), octacalcium phosphate ($\text{Ca}_8\text{H}_2[\text{PO}_4]_6 \cdot 5\text{H}_2\text{O}$), tricalcium-phosphate or whitlockite (b-TCP, b- $\text{Ca}_3[\text{PO}_4]_2$), calcium pyrophosphate dehydrate ($\text{Ca}_2\text{P}_2\text{O}_7$), and amorphous calcium phosphates, struvite ($\text{MgNH}_4\text{PO}_4 \cdot 6\text{H}_2\text{O}$), newberyite ($\text{MgHPO}_4 \cdot 3\text{H}_2\text{O}$), and amorphous calcium magnesium pyrophosphates [21]. Enamel and dentine are predominately composed of hydroxyapatite crystals [20].

In both the adult and deciduous teeth, enamel is the outer structure that envelops the crown. In general, the deciduous teeth are whiter, softer, smaller, and weaker than permanent ones; their enamel is thinner and has a higher organic content.

Tooth enamel is the most mineralized tissue of human body: its composition is 96 wt.% inorganic matrix and 4 wt.% organic material (proteins and lipids) and water [26], which occupy the gaps among the apatite crystals in the enamel. The microstructure of the enamel is almost fully mineralized with highly aligned prisms running approximately perpendicular from the dentin-enamel-junction (DEJ) towards the tooth surface [18]. Each rod consists of packed carbonated hydroxyapatite crystals coated with a nanometre-thin layer of enamelin and oriented along the rod axis. Each hexagonal prism is bundled to form approximately 4 mm diameter rods, making a mechanically hard and highly resistant structure.

The outer layer of deciduous teeth is usually devoid of the normal prismatic structure, but it is still unknown whether HAP crystals and enamel rods are similar in size and distribution for both tooth types [19].

Enamel consists of hydroxyapatite, water, protein, and trace elements, such as fluoride. The organic matrix consists of non-collagenous protein, amelogenin, and inorganic components consist of enamel's biological apatite. Enamel apatite has a hexagonal unit cell composed of prismatic crystals and contains more inorganic material than dentin, bone, and cementum [23].

The surface layer of enamel is composed of hydroxyapatite (HA) crystals that form the prism of enamel. HA is a crystalline form of calcium, hydroxyl (OH), and phosphate ions (PO_4^{3-}) that compose the mineral structure of bones and teeth [22]. The surface layer's hardness is primarily the result of a high concentration of phosphate ions, fluorine, calcium, and chlorine. Enamel adjacent to dentine is softer due to its high magnesium, sodium, and potassium ion content [4, 24].

The dentine is about 70% mineralized by weight, with 20% of organic matrix, and 10% of water by weight, and it forms the largest portion of a tooth. This 70 wt.% of inorganic material is mainly composed by a calcium phosphate related to the hexagonal hydroxyapatite, it is a HAP mineralized collagen matrix surrounding tubular extensions of the dentinoblast cells.

The hydroxyapatite crystals in dentine are in the form of flattened plates with approximate dimensions of 60-70 nm length, 20-30 nm width, and 3-4 nm thickness. X-ray energy dispersive spectroscopy (EDS) analysis also indicated the presence of other elements (Na, Cl and Mg) in small quantities [25, 26].

The calcium and phosphorus (as phosphate) content of the teeth range 34–39% and 16–18% by weight, respectively. Cations and anions are incorporated into cationic (Ca^{2+}) and anionic centres (OH^- , PO_4^{3-}) of the hydroxyapatite matrix. Sodium (Na^+), potassium (K^+), and magnesium (Mg^{2+}) can substitute in the calcium position, fluoride (F^-) and chloride (Cl^-) in the hydroxyl position and carbonate (CO_3^{2-}) in the hydroxyl and phosphate positions [27].

This less mineralized tissue gives the tooth the toughness necessary to resist a catastrophic fracture in case of masticatory stress. The dentin-enamel-junction can arrest crack propagation [28]. Until now, the influence of age on structure-property relationships in both tooth types has not been completely understood [19].

Type I collagen is the main component of the organic part of the dentine, representing more than 85%, while the remaining amounts are the types of collagen III and V. The non-collagen portion of the organic matrix consists of approximately 50% dentin phosphoprotein, while the remaining inorganic matrix is predominantly composed of HA [29].

Generally, more than 90% of collagen in the human body is collagen I, and it is most abundant in bones, tendons, ligaments, while collagen II, an $\alpha 1(\text{II})$ chain homotrimer, is the primary component of collagen in joint and hyaline cartilage. On the other hand, collagen III, a homotrimer of collagen made up of $\alpha 1(\text{III})$ chains, forms long and inflexible collagen fibrils and it is the main component of collagen in reticular fibres, which provide a supporting mesh in soft tissues and organs.

It is generally believed that HAs are encompassed and covered by the organic matter found in the tooth structure.

Previous theories suggest that a small percentage of collagen is preserved after the enamel matures [30, 31]. Other theories propose that, when the enamel matrix is mineralized and matured, collagen is eliminated along with all other organic components [32, 33].

A more recent study found that in mineralized and mature enamels, the collagen content, primarily types I and V, is minimal compared to dentin [34, 35].

The physical properties of teeth are widely ascribed to the presence of enamel, but collagen is also assumed to act as a protective protein sheath of the underlying HA crystalline lattice.

The type I collagen is a heterotrimer of two $\alpha 1(I)$ chains and one $\alpha 2(I)$ chain folded in a triple helix structure, like a rod (diameter of 1.5 nm and length of more than 300 nm), as shown in **Figure 1.6**. The three-helix domain is flanked by nonhelical N- and C-propeptides, creating a procollagen, that is secreted from cells (fibroblasts, odontoblasts, and osteoblasts into the extracellular spaces where it is converted into tropocollagen by the removal of N- and C-propeptides) [4].

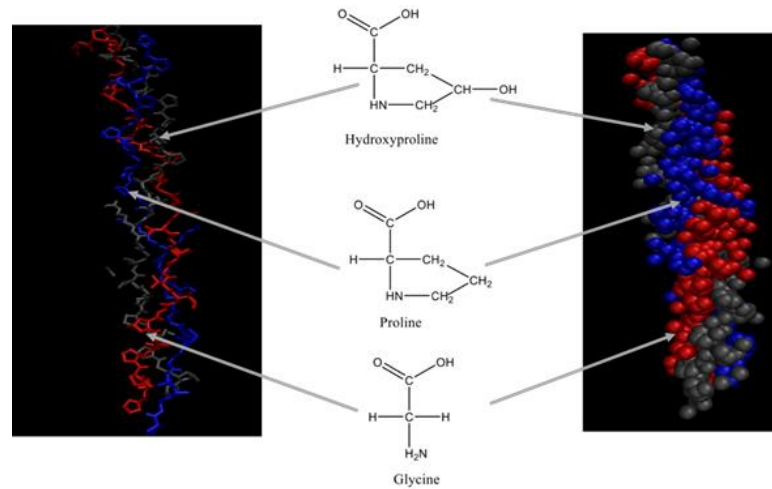


Figure 1.6: Triple helix structure of collagen [149]

Tropocollagen can then spontaneously self-assemble into fibrils, as shown in **Figure 1.7**. The fibril is constructed from the staggered packaging of the individual collagen molecules so that there are periodic gaps along the fibril surface and channels extending through the fibril [36]. Each collagen unit is approximately 300 nm in length and overlaps neighbouring units by about 67 nm [36]. Fibrils contain gap regions of 40 nm between end-to-end collagen units.

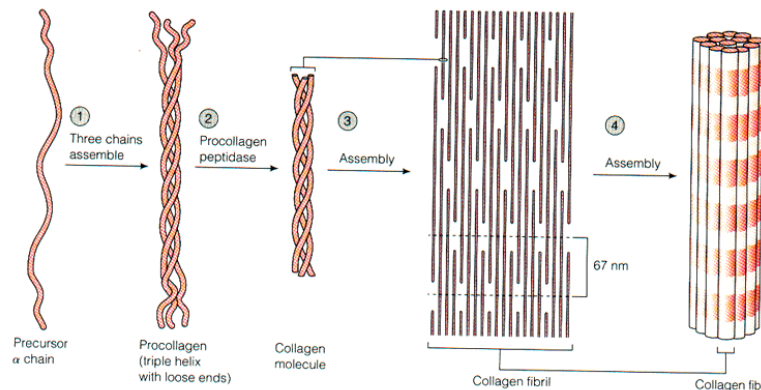


Figure 1.7: Collagen fibre [150]

Weak dispersive and hydrogen interactions and strong intermolecular cross-link stabilize packing of collagen, and this is necessary for the structural stability and insolubility of collagen in water [37]. The increase of collagen fibrils' diameter and the migration toward the place where they are mineralized occur due to elongation and lateral aggregation of them [38].

In dentin, type I collagen contains about 56% of mineral in its fibril holes and pores. The non-collagenous proteins act as inhibitors, promoters, and/or stabilizers of mineral deposits, for example glycoproteins or dentin matrix protein-1 [39].

Odontoblasts secrete an acid mucopolysaccharide, for example, chondroitin sulfate, which is a prerequisite for start of mineralization. Three types of mineralization usually occur during dentinogenesis: matrix vesicle-derived mineralization (in mantle dentin), ECM molecule-derived mineralization (in majority of dentin), and blood–serum-derived mineralization (in peritubular dentin) [40].

Twenty percent of a tooth's matrix consists of organic material, which makes up the majority of the tooth's dentine. Most of the organic portion of dentine comprises Type I collagen, while the remainder consists of collagen types III and V [22, 41].

Calcium phosphate is fundamental for the formation of teeth. The HA (stoichiometric formula $\text{Ca}_5(\text{PO}_4)_3(\text{OH})$) in teeth varies from empirically derived HA, and, due to fluorine substitutions, it is often calcium deficient. The formula (formula 1.1) of HA, calcium deficient and carbonated, shows the sites for atomic substitution.



With X, calcium substitution with metal cation, Y, phosphate substitution with carbonate, and Z, hydroxide substitution with fluoride [42].

1.3 Tooth demineralization

Demineralization is the process of removing mineral ions from HA crystals of hard tissues, like enamel, dentin, and cementum. On the other hand, the remineralization is the process of restoration of these mineral ions again to the HA crystals. Both processes occur on the tooth surface [4]. Erosion and carious lesions are the two main consequences of demineralization.

Teeth consist of the phosphate-based mineral HA in the enamel, collagen in the dentine, and living tissues [43, 44], and they are different from bones due to their location and anatomical arrangement [45]. They are exposed to the microbiota of the mouth, food, and drink, and the enamel layer that covers their crown give them a high resistance to localized demineralization [46, 47].

Chemical demineralization of teeth is caused by acidic attack: due to the acid diffusion in and the mineral content out of tooth, chemical dissolution of both the organic and inorganic matrix components takes place, facilitated by the water content of enamel and dentine [48].

Organic acids produced by plaque microorganisms destroy the mineral content from the surface of HA crystals. The big loss of mineral ions from HA does not destroy the integrity of HA latticework, whose lacking can produce cavities, but causes a high sensitivity to heat, cold, pressure, and pain. When the partially demineralized HA crystals are exposed to oral environments that favour remineralization, they can reach their original size, indeed demineralization is a reversible process [49].

The most stable form of hydroxyapatite exists in an environment with a pH of 7.4. There is a constant chemical equilibrium between the hydroxyapatite in the enamel ($\text{Ca}_{10}(\text{PO}_4)_6(\text{OH})_2$) and the dissolved hydroxyapatite in the plaque biofilm. Mineral crystal dissolution takes place when the pH level of the plaque falls below 5.5 [50, 51].

When the minerals are dissolved, the inter-crystalline space expands, and the enamel surface becomes softer and more porous, leading to the formation of cavities [51]. Demineralization of the enamel occurs due to the acidic metabolism of cariogenic microorganisms in the dental plaque biofilm.

There is an equilibrium between demineralization and remineralization, as shown in **Figure 1.8**.

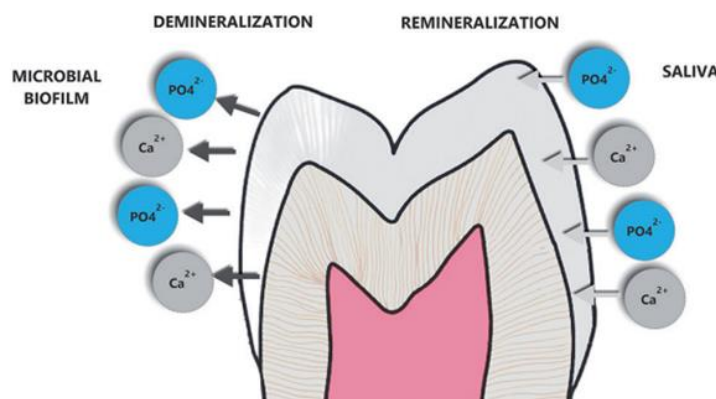


Figure 1.8: The equilibrium between dynamic demineralization and remineralization at the plaque-enamel interface [22]

The highest degree of demineralization in enamel caries occurs at a subsurface level covered by a surface layer unaffected by the attack, indeed most of the mineral loss during the initial stages of demineralization occurs at a distance away from the enamel surface. This subsurface lesion is a “white spot lesions”, which is an opaque white area different from healthy enamel.

White spots are the first visible symptom caused by the demineralization of enamel, that affects the subsurface layer, maintaining smooth the enamel surface smooth due to the chemical composition of the substrate.

Demineralization leads to an increase of the interprismatic space, and water is replaced by air. When the refractive index is different between the two phases, the light scattering effect occurs.

There are no interfaces in healthy enamel because the refractive index of healthy enamel is the same as that of hydroxyapatite (1.62). In hypo-mineralized enamel there is a difference of the refractive index, indeed light passes through mineral and fluid phases, and the result is a white optical phenomenon on the enamel surface called “white spot”. During a routine dental clinical examination these initial caries are seen as white spots and they can turn brown due to the absorption of pigments into enamel pores [22].

The dissolution of mineral salts is caused by alternating phases of demineralization and remineralization, followed by reprecipitated minerals on the enamel surface, forming an intact surface layer (20–50 μm deep). Under this layer, the carious lesion extends in a half-moon (or “cone”) shape toward the demineralization zone [52].

Hypo-mineralization leads to an enlargement of the enamel pores and to mineral dissolution [53]. The most affected area is the central layer (or body) of the lesion, with 5% mineral loss in the peripheral part and 25% in the central part. When the mineral deficit reaches 10% compared to healthy enamel, there is a clinically visible lesion. The dark zone at the front of the lesion is a decomposition phase after the translucent zone and previous the body of the lesion.

In vitro studies reported large pores in the translucent zone, while in the dark zones an additional micropore system represents areas of demineralization [54, 55].

Dental caries are small lesions (cavities) on the tooth surface that progress and cause the loss of tooth structure. First changes in ultrastructural level caused by demineralization can only be observed with an electron microscope, and only when the disease progresses, the dentist can observe a reduction of the enamel’s translucency. In dental plaque, bacteria accumulate, ferment dietary carbohydrates and acids are not neutralized by the buffering capacity of saliva, leading to demineralization of the teeth and to cavities [56].

Previous in vitro experiments using buffers of organic acid as a de-mineralizing medium outlined the presence of the unaltered surface enamel resistant to acid dissolution by adsorption of organic matter on enamel crystallites [4, 57]. Subsequent studies have recognized the reprecipitation process regarding the saturation of calcium and phosphates at the level of the underlying enamel layer [58, 59].

In vivo microscopic studies revealed that a mineral loss takes place in the interprismatic regions and later proceeds into the enamel prisms [60, 61].

According to studies carried out with a polarizing microscope, the porous subsurface enamel is positively birefringent, whereas the surface zone retains its negative birefringence [62, 63]. This shows that the subsurface enamel is characterized by a demineralized zone with a pore volume greater than 25%, while the pore volume of the surface enamel is lower than 5% [64].

1.3.1 Acid erosion mechanisms

Dental erosion is defined as the loss of hard tissue due to mechanical damage or dissolution by acids of nonbacterial origin. When teeth are exposed to acid environment, HA is solubilized, making them more flexible and more susceptible to mechanical wear. The two chemical methods are either direct acid attack or chelation [65, 66, 67].

An acid in solution forms hydronium ions, that bind with phosphate or carbonate in HA, releasing the anions into solution as a chemical etching. Carbonate is more reactive than phosphate and it requires a lower concentration of hydronium for the reaction, so HA is weaker with an excess of carbonate [65].

There are three forms of acidic attack in relation to the pH of the acid [68]:

- Acids with pH lower than 1 and exposed to teeth for very short periods may cause surface attack. An example is the hyperemesis episode with alcoholism, through which teeth are exposed to acids with a pH of 1 [42], that is lower than the demineralization pH, indeed it may cause important superficial attack.
- A short exposure at pH of 2 to 4 causes nanoscale surface softening [69, 70].
- A weak acid with pH of 4.5-6.9 (not the most common case) causes the dissolution of the subsurface, that can lead to the formation of carious lesions with bacteria.

Weak acid dissolution can be due to a variety of causes. Fruits commonly have carboxylic or citric acids [70, 71]. The hydronium ion formed by carboxylic acids is bound to phosphate, forming phosphate cations [42], that can form a calcium acid chelation complex, debonding mineral ions in the surrounding lattice, causing demineralization [66]. These may stay close to the HA layer, with minimal demineralization.

Carboxylic acids can cause chelation attacks. In citric acid ($C_6H_8O_7$), whose structure is reported in **Figure 1.9**, found in fruits and soft drinks, the COOH group is dissociated, forming H^+ for H_3O^+ and allowing a COO^- anion to cause calcium chelation [71]. Two anions may form a complex of soluble chelates with three calcium ions, depending on the strength of dissolution of the anion compared to the calcium bound in HA and forms a chelate at a pH of 3.8 to 4 (the pH of fruit and fruit drinks) [72]. Chelate can be transported from the enamel surface because it is soluble, leading to a net loss of minerals to the teeth.

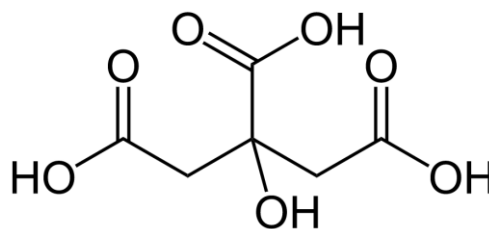


Figure 1.9: Citric acid structure [151]

Citric acid can damage teeth, as it can eliminate phosphate and calcium from HA [73]. Carbonic acid behaves like citric acid, but it has a lower dissolution constant ($\text{pK}_a(\text{H}_2\text{CO}_3) = 3.6$, $\text{pK}_a(\text{C}_6\text{H}_8\text{O}_7) = 6.4$) and it can dissociate to form both bicarbonate anions HCO_3^- and orthocarbonic acid $\text{C}(\text{OH})_4$, increasing the acid attack probability on teeth [65, 74].

The equilibrium constant for acid dissociation (K_a) and its logarithmic value (pK_a) represent the ratio of ionized to-nonionized acid groups in aqueous solution [75].

Phosphoric acid (H_3PO_4), found in soft drinks, does not contain a carboxylic group, but it does attack teeth through direct path and chelation [74, 76]. Two hydrogens dissociate from phosphoric acid, enabling the formation of two hydronium ions for the direct attack of the acid [35, 73]. The other phosphate ion (PO_4^{3-}) can chelate with calcium cations at ratio of 2:3, producing soluble calcium phosphate, and hydrogen phosphate (HPO_4^{2-}) chelates with calcium cations in a 1:1 ratio. Both routes contribute to demineralization with acidic and fizzy beverages and occur at low pH [68, 76].

1.3.2 Chemical erosion mechanisms

HA dissolution in enamel at lower pH is faster and more severe than at higher pH, indeed at low pH, HA surface is destabilized by chelation, causing weak phosphate coordination bonds [48]. Tooth erosion is due not only to pH [77].

Another parameter is the molar acid concentration present in drinks, measured with the titratable acidity (the amount of alkali necessary to titrate the subject to its natural value) [79].

While pH measures only the dissociated ions in a solution, which can form acids or alkalis, titratable acidity gives a more general overview of a solution's potential acidity because it even measures the bound compounds [48, 77].

An increase in titratable acidity is related to an increase in enamel loss in model studies and to the undissociated acid concentration [80]. The undissociated acid concentration is a measure of the inactive acidity of a solution: this describes solute that does not contribute to the pH of a solution [78]. These uncharged molecules permit a localized increase in hydrogen ions (once diffused into the HA), which favours enamel dissolution at the mineralization front. Hydrogen ions react with water to form hydronium ions that are supplied to the enamel [72].

The equilibrium constant for acid dissociation (K_a) and its logarithmic value (pK_a) indicate the ratio of ionized to-nonionized acid groups in aqueous solution and pK_a values change due to structural changes, environment, and solvent, but they are not connected to the severity of an acid [75]. The pK_a value indicates how an acid affects HA in the teeth. A carboxylic acid with a low pK_a value in water may produce many chelating ions, whereas a higher pK_a value is connected to a direct attack of hydrogen ions [48].

The temperature influences the dissolution kinetics, in fact the ambient temperature in the mouth is higher than the room temperature, and therefore the kinetic rate of reaction rises [45].

1.3.3 Modifying factors

Demineralization and the subsequent erosion are dynamic processes dependent on many modifying variables.

Dietary acid consumed through food or drink and microbial attack from bacteria present in the mouth are the main causes of an acid attack [47].

These modifying factors are split into two main groups, extrinsic and intrinsic, which can be altered by the modifying factors [4].

Extrinsic factors include eating habits and medication, while intrinsic ones are primarily diseases that may be treated with medications, like gastroesophageal reflux, indeed endogenous acids have a pH of 1.2, lower than the critical pH for fluorapatite (FAP) and HA dissolution [43, 81], and they lead to demineralization. Modifying factors can be changes in the biochemical characteristics of an intrinsic or extrinsic factor, behavioural factors (regular toothbrushing, types of drinks consumed, method to consume them, and frequency of drinking) or socioeconomic factors [72].

Weak demineralised areas are targets for dental cavities [66] and bacteria can easily colonize these areas, penetrating dentine and forming their own acids [82].

Glucose, sucrose, and fructose create an acidic environment that causes demineralization and carious lesions [81].

There are many theories about the kinds of oral bacteria acquisition. At birth, the oral cavity is sterile, but bacteria are transmitted through food/milk/water, from oral mucosa shedding surface during eruption of primary dentition or from parents.

The “ecological hypothesis” is the most accepted theory about the role of bacteria in acid production and caries formation: non-mutans bacteria are key players in dental plaque (a dynamic microbial ecosystem) for maintaining dynamic stability [72].

Initial studies reported the presence of acidogenic streptococci mutans in dental caries [83], and other studies proposed that also lactobacilli species cause dental caries due to the production of lactic acid following sugar fermentation [84, 85].

In vitro studies on bacterial species in caries lesions using PCR and specific DNA probes [86, 87] indicated that dental cavities contain several cariogenic bacterial species, like *Veillonella* or *Corynebacterium* [88].

The enamel is demineralized due to low pH [89, 90], microbes, saliva-buffering capacity, tooth characteristics, dietary habits, and host immune system [91].

The buffering capacity and the secretion rate of saliva influence pathogenesis of tooth erosion [92]. Saliva's composition influence demineralization, in fact the inorganic components of saliva (calcium and phosphorus) keep the mineral balance between the hydroxyapatite of enamel and saliva. If saliva cannot neutralize the acid metabolites of microbes, the dental plaque pH decreases, promoting enamel demineralization [93].

The dependence of these multifactorial and dynamic processes (demineralization, erosion and/or loss of tooth surface) on several modifying factors is shown in **Table 1.1**:

Table 1.1: Interaction of different factors in relation to tooth surface loss [4]

Biological	Chemical	Health and education	Behavioural
Saliva flow	pH type	Health status	Eating habits
Soft tissue anatomy	Acid type	Socioeconomic status	Drinking habits
Tooth anatomy	Chelation potential	Medication and drugs	Brushing frequency

1.4 Remineralization

Remineralization is a natural process of restoration of minerals as mineral ions to the hydroxyapatite structure for non-cavitated lesions. Through calcium and phosphate ions, a new surface is constructed on existing crystal leavings in subsurface lesions, forming acid-resistant remineralized crystals, that are less soluble than the original mineral [22].

Remineralizing agents, which can inhibit and remineralize enamel, are compounds used to increase mineral saturation (fluorides, casein phosphopeptide–amorphous calcium phosphate (CPP-ACP), bioactive glass, tricalcium phosphate (TCP), nano HAP particles, and beta tricalcium phosphate (TCP)), biofilm modifiers like arginine, triclosan, xylitol, and probiotics, and herbal compounds [22].

Preventive systems for tooth demineralization are fluoride therapy, saliva, probiotic bacteria and diet control. Dental composites containing different forms of calcium phosphates (CaPs), nanotechnology in preventive dentistry and biomimetic remineralization are also used to treat the demineralized tooth or incipient caries [94].

The most common remineralizing agent is fluoride, which stops enamel dissolution, caused by an acid attack to the enamel, and leads to an increase of pH and to new and larger fluoride crystals containing fluorhydroxyapatite form [95].

Fluoride affects enamel in many ways [95]. At first, the fluorapatite crystals resistance to acid attack is higher than the one of hydroxyapatite crystals, and it inhibits demineralization. The second mechanism is related to the acceleration of formation of new fluorapatite crystals due to the combining of calcium and phosphate ions, that interfere with the synthesis of phosphoenol pyruvate.

The calcium in HA is displaced by fluorine, forming FAP, which is less soluble than either hydroxyapatite or calcium-deficient HA and increases the enamel resistance to dissolution during the acid attack. Their structures are reported in **Figure 1.10**.

FAP forms a solid-state solution with the phosphate-rich HA, with a hydroxide being displaced [42]. Methods for fluoride delivery are toothpastes, varnishes, mouth rinses, gels and solutions [96].

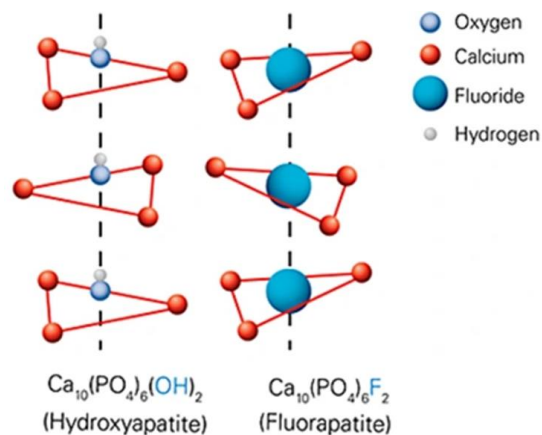


Figure 1.10: Formula of hydroxyapatite and fluorapatite [152]

There are two main advantages of FAP over HA:

1. Fluoride acts as a catalyst, helping for the enamel remineralization with phosphate ions dissolved in saliva [97].
2. The weakness in HA to lactic acid is eliminated due to the displacement of hydroxide with fluoride, consequently FAP $[\text{Ca}_{10}(\text{PO}_4)_6\text{F}_2]$ is not dissolved by this in the mouth [66].

For the formation of FAP, for every two fluoride ions, ten calcium ions and six phosphate ions are required, in fact the presence of inadequate calcium and phosphate can limit the remineralization process. Casein phosphopeptide-ACP (CPP-ACP) prevents the precipitation of calcium phosphate and demineralization and enhancing remineralization [98].

Saliva is an important biological factor due to its buffering capacity, cleansing, antibacterial action, and secretion rate [92, 99].

It is also a source for calcium and phosphate, used to inhibit tooth demineralization during periods of low pH maintaining supersaturation, and to promote remineralization in cases of neutral pH. In addition, it is a constant source of fluoride on the surface of the tooth, used to prevent tooth demineralization and to enhance remineralization [99].

Bacterial therapy implies the use of probiotic (“for life”) bacteria, which are “live microorganisms which, when administered in adequate amounts, confer a health benefit on the host” (definition by the World Health Organization, WHO) [100]. Probiotics used for oral health benefits are *Lactobacillus* (*reuteri* [101], *rhamnosus* [102], *salvarius* [103]) and *Bifidobacterium* (part of normal oral flora) [104].

Other preventive systems for tooth demineralization are the electrically assisted enhanced remineralization, that is a new technology developed by Reminova Ltd [105], dental composites with remineralizing action, which are resin-based composites used as dental filling materials for more than 50 years [106], composites containing ACP, composites containing HA, composites containing TTCPs, composites containing mono-, di-, and tricalcium phosphates [4].

1.5 Caries detection methods

Tooth decay is a dynamic disease process of progressive demineralization of the inorganic portion of the tooth and of disintegration of the organic component. The detection of early lesions should be the main goal because, prior to clinical expression, early lesions undergo several cycles of demineralization and remineralization.

Diagnostic methods that were commonly used earlier were based on visual examination using mouth mirrors, probes, and conventional radiography. Many studies demonstrate that the probe is not efficient for caries detection and disrupts remineralization [107] and sharp tooth explorers damage weakened enamel [108, 109]. Non-cavitated caries are difficult to detect because they are not visible to the unaided eye.

To identify the presence of dental caries many measurement criteria have been developed and one of the most widely recognized is the International Caries Detection and Assessment System (ICDAS). This is a standardized visual detection procedure with a clinical scoring system used to reduce the operator-dependent variability, for the identification and evaluation of caries activity, in dental education, clinical practice, research, and epidemiology [11]. In clinical practice, additional diagnostic methods are necessary to evaluate lesions invisible to visual examination, in particular on the areas of the proximal teeth [110].

Conventional tools are qualitative in nature, therefore they have mediocre validity with low sensitivity and moderate specificity, while advanced diagnostic methods, used to detect lesions at an earlier stage, are quantitative in nature and more reliable than the conventional methods [111].

New diagnostic methods typically exhibit high sensitivity and a good reproducibility, but a low specificity [112], therefore the favourite choice is the visual examination, as it is reliable, simple, and accurate [113, 114].

Usually, visual examination is combined with bitewing radiography (BWR) [115], a method to register tooth decay extensions in dental pulp [116].

Bitewing radiography provides an image of the crowns of the upper and lower teeth line up on a single film. The name is due to the fact that the film is placed into the patient's mouth using a cardboard film holding device, that is bitten down upon as the camera that, pressed against the cheek, takes the picture. This tab contains x-ray film in the centre which allows for a clear internal examination of the teeth without the gums and jawbone obscuring the image.

The choice to use many X-ray-free diagnostic methods, as Laser Fluorescence measurement (LF), Near-Infrared Light Transillumination (NILT), and Electrochemical Impedance Spectroscopy (EIS), is caused by the need to reduce the health risk from exposure to ionizing radiation [113, 117, 118, 119].

The NILT method is an imaging technique based on the light transmission through the tooth and it is used for monitoring enamel caries using various wavelengths, but not to accurately determine the depth of the lesion in the dentin [120]. The NILT method produces an image that can be captured, saved, and stored in digital format through an experimental setup formed by a transillumination system with a near-infrared light source, an imaging camera (a charge-coupled device, CCD), and a computer-controlled scan software.

The light shines on a tooth and two phenomena can occur: absorption, where photons are lost to the material, and scattering, which is the predominant process both in enamel and dentine, where the direction of photons is changed without loss of energy.

Laser or light fluorescence methods are used to assess early enamel lesions in visually inaccessible areas, because there is a difference in fluorescence between demineralized and healthy enamel that changes the light characteristic [121].

Two of the most promising approaches are based on Impedance Spectroscopy (IS) and Electrical Conductance Measurements (ECM) [119].

The optimal caries detection method should be minimally invasive, reliable, accurate, easy to apply, able to identify caries adjacent to restorations, cost-effective and applicable to all types of dental surfaces [107].

There are other advanced methods for caries detection that are [122]:

- Digital radiographic methods are digital image enhancement, digital subtraction radiography and tuned-aperture computed tomography (TACT).
- Optical caries monitor, quantitative fibre-optic transillumination, Digital Image fibre-optic transillumination (DIFOTI) and Quantitative light/laser-induced fluorescence (QLF) are based on visible light.
- A laser light method is DIAGNOdent – Laser autofluorescence.
- Electrical conductance measurement and electrical impedance measurement are methods that use electrical current.
- Ultrasonic caries detector uses ultrasounds.

The first digital radiographic method create an image formed by a spatially distributed set of discrete sensors and pixels. It may be direct (the direct image receptor that collects X-ray directly, for example, RVG) and indirect (for example, video camera used to create digital images of a radiograph), but it is time-consuming.

Digital subtraction radiography (digital bitewing radiograph) detects demineralization emergence or progression, but with a difficult image registration.

Tuned-aperture computed tomography is a sensitive technique used to detect small primary and secondary carious lesions, constructing radiographic section through teeth [122].

In white spot carious lesion, scattering is stronger than in sound enamel surface. In the optical caries monitor, a fibre bundle is used to transport the light to the tip of handpiece; the tip is placed against the tooth surface and different fibres of the tip reflect light [123].

Digital imaging fibre-optic transillumination (DIFOTI) is based on the combination of FOTI with a digital CCD camera, minimizing FOTI deficiency. DIFOTI detects initial areas of demineralization, cracks, and tooth fractures, using safe white light, with only dental diagnostic imaging instrument approved by the Food and Drug Administration.

Quantitative light/laser-induced fluorescence method (QLF) uses fluorescence, which results from change in the characteristics of light caused by a change in wavelength of incident light rays following reflection from the surface of material. It detects progression or regression of white spots of smooth surface lesions [122].

DIAGNOdent is a variation of QLF, and it was introduced in 1998 to help diagnose occlusal cavities as a complement to visual and X-ray examination. It uses infrared laser fluorescence of 655 nm to detect occlusal caries with smooth surfaces [124], with high sensitivity and specificity, precision, and reliability.

This method is easy and quick to use, pain-free, non-invasive, safe and without radiation exposure but expensive.

DIAGNOdent technology compares the reflection wavelength against a well-known healthy baseline using a simple laser diode to uncover decay. At specific wavelength, healthy tooth structure exhibits little or no fluorescence, whereas carious tooth exhibits fluorescence proportionate to the degree of caries. Healthy tooth leads to a very low scale readings, while carious tooth results in elevated scale readings on the display [125].

The device features a fibre optic cable that transfers the light source to a handpiece that contains a fibre optic eye in the tip. The baseline reading is achieved by putting the diode to the healthy enamel tooth structure, and then it inspect all the surfaces of the teeth, reflecting fluorescent light with particular wavelength. The light is absorbed by the organic and inorganic components of the tooth which induce infrared fluorescence, that is collected at the top of handpiece and transmitted back to the DIAGNOdent unit. The light is measured by the receivers, converted into an acoustic signal, and assessed electronically to reveal values between 0 and 99 [126].

DIAGNOdent pen is a development of DIAGNOdent technology. DIAGNOdent pen 2190 is an appropriate tool for detecting smooth surface cracks and caries accurately [127]. It is cordless, simple, handy, precise but expensive [122].

Electrochemical machining (ECM) was first proposed in 1878 and it is based on the principle that a demineralized tooth surface is more conductive than healthy one because it has more pores filled with water or saliva. The electrical conductivity across the enamel is directly proportional to the importance of demineralization [128]. This technique has two methods of application: site specific and surface specific.

The measurement of electrical impedance is a measure of the degree to which an electrical circuit is expected to have resistance to electrical current when a voltage is applied across two electrodes. Caries tissue has a lower impedance than sound tooth [122].

Impedance spectroscopy is a non-invasive method used in many applications and scientific fields for electrical impedance measurements, like characterization of protective coatings and biomaterials [129, 130], including dental alloys [131], physiological molecules monitoring and drug delivery [132, 133] and preservation of cultural heritage [129].

In medical field, impedance spectroscopy techniques can represent a risk-free alternative to ionizing radiography for the detection of caries, thus suitable to children and pregnant women [122], and a low-cost instrumentation [133].

Tissue impedance changes because of the decay process, which results in mineral loss and increased porosity, and consequently in a higher liquid content than healthy tissue, containing different ions coming from the oral environment [134].

The first studies to investigate the feasibility of using impedance spectroscopy for cavity detection date back about twenty years [135].

Impedance measurements are employed to evaluate root canal length, to investigate microleakage between tooth and filling materials difficult to detect [136, 137], to investigate the effect of smear layer [138] and dentine conditioners [139, 140] and to characterize the enamel and dentin structures; in fact, due to dentinal tubules full of liquid, the conductivity of the dentine is significantly higher than the enamel.

CarieScan Pro™ (Orangedental, Biberach, Germany) is a popular device which uses alternating current impedance spectroscopy technique. This instrument is made of a wire bundle, which makes the measuring process not straight forward into the small area of the teeth. The device shows a low accuracy and its tip, made by a bundle of wires, and makes it difficult to perform repeated measurements in a small area [141, 142].

The use of ultrasound to detect early carious lesions on smooth surfaces has generated renewed interest over the past ten years. The ultrasound pulse-echo technique is used to evaluate demineralization of natural enamel, in fact the echo amplitude changes are correlated to the mineral content of the body of the lesion [143].

Current and future technologies focus on scattering reflection, absorption, and fluorescence (objective measurement of the properties of light waves) [143]. Newer technologies are [122]:

1. Multiphoton imaging [126].
2. Infrared fluorescence [126].
3. Infrared thermography [144].
4. Terahertz imaging [145].
5. Optical coherence tomography [146].
6. Polarized Raman spectroscopy [146].
7. Modulated (frequency-domain) infrared photothermal radiometry [147].

1.5.1 Electrochemical Impedance Spectroscopy (EIS)

Electrical impedance spectroscopy (EIS) is a sensitive, rapid, non-invasive and non-destructive method to measure the resistance to alternating current flow through a given material, which can be a conductive material but also an insulating one. It is commonly used for the characterization of electrical properties of solids or liquids in the bulk and in the interface [153]. Impedance measurement detects the higher liquid content in tooth, related to the increase of porosity due to the loss of mineral caused by the caries process.

Electrical impedance spectroscopy may be used to measure electrical resistance of biological tissues, like dental one [154-159], skin [160], blood cells [161], and bone [162].

If these materials are penetrated by an electrolyte, they will conduct, and conductive properties are highly affected by the microstructure. Changes in the microstructure, caused by variations in the chemical constituents, may be directly related to the properties contained in the impedance spectra. Changes in ultrastructure and chemical components can be measured by using SEM (Scanning Electron Microscopy), FESEM (Field Emission Scanning Electron Microscopy), EDX (Energy Dispersive X-ray Analysis), XRD (X-Ray Diffraction) and TMR (Total Mixed Rations), giving a complete overview of microstructural changes in dental tissue.

In clinical practice, visual inspection, the most common decay detection system, and bitewing radiography are used to identify early caries, but they are based on subjective assessment and can only detect a limited amount of cavities [163]. On the other hand, EIS method can detect the first signs of tooth decay with reliability and precision [164].

To date, EIS techniques have been used for assessing the smear layer [155, 156], and to study enamel or earlier caries [157, 158].

Dentinal demineralization can be characterized using EIS because dentine demineralizes more rapidly than enamel, so in many cases, severe demineralization exists even though there are relatively few signs on the surface of the tooth [165]. Dentine has a tubular structure, which is composed of intertubular (a fibrous network of collagen with mineral crystals, mainly composed of hydroxyapatite) and peritubular dentine (a more highly mineralized tissue without collagen fibrils) [166]. EIS can be used in situ to investigate changes in the chemical composition and dentine ultrastructure caused by demineralization under simulated carious conditions [167].

EIS measurements can be performed with direct current (DC) [168] and two electrodes [169], but also with a three-electrode configuration (the third electrode is the reference one, used to determine the potential of the working electrode precisely) [170].

When measurements are carried out at a fixed frequency, contributions from many different electrical processes may arise. If impedance measurements are carried out over an appropriate frequency range, it is possible to relate the results to the physical and chemical properties of any material [156].

1.5.2 Raman Spectroscopy

Alternatives to traditional diagnostic techniques are represented by vibrational spectroscopic techniques such as Raman and Fourier transform infrared (FTIR), that are complementary techniques [171].

Raman spectroscopy is a simple, non-invasive and non-destructive technique, it requires minimal or no sample preparation [172] and it gives reproducible results [171].

Recently, there has been a significant increase in the use of Raman spectroscopy for biomedical applications, such as dentistry [173-176].

This technique can be used to diagnose diseased tissue as external tumours and, with the introduction of specially designed miniature fibre optical probes, pathologies of the oral cavity, gastrointestinal tract, brain tissue, and ocular tissue [178-182]. Even hard tissue pathologies, as normal and diseased bones and tooth tissues, can be diagnosed [183].

A further application consists in calculating the degree of conversion of polymeric materials, as resins and cements used in restorative dentistry [184], based on the variation of the intensity of specific vibrational modes. In particular, the technique makes it possible to monitor the development of peaks related to double bonds C=C which are converted into single bonds C-C with the photopolymerization process [185].

Spectral analysis in Raman spectroscopy is performed in reflection mode and tissues may be probed in their original state without any sample preparation. Several changes have been made to Raman spectroscopy imaging to characterize an area of particular interest in the medical and dental fields, to determine the specific peaks in the spectrum, used to discriminate between diseased and normal tissues. The Raman spectrum of human teeth can reveal its chemical composition. Organically induced fluorescence spectra often dominate much weaker Raman signals, and, as a result, the Raman spectroscopic studies were restricted to enamel, which contains only a small percentage of organic matter [186].

The technique can be used to monitor the vibrational modes related to hydroxyapatite, $\text{Ca}_{10}(\text{PO}_4)_6(\text{OH})_2$, which is one of the main components of tooth enamel and whose demineralization is related to the decay process. Hydroxyapatite, the main component of enamel, is placed in the teeth as polyhedral prisms aligned and joined by an inter-plasmatic substance that is highly mineralized. Cariogenic bacteria act through acidification and subsequent destruction of this inter-plasmatic substance and attachment to dentin. When this compound is dissolved, it encounters the demineralisation of enamel, which can promote the phenomenon of cavities. Therefore, the monitoring of the signal linked to molecular vibrations by Raman spectroscopy makes it possible to study the demineralization of the dental surface.

In Raman spectra, a well-defined peak at 959 cm^{-1} vibration both at the external surface of the enamel and in sectioned enamel [187] is related to changes in PO_4^{3-} vibrations resulting from hydroxyapatite in mineralized dental tissues. Examination of the different intensities of PO_4^{3-} vibrations (1043 , 590 and 431 cm^{-1}) showed a constant change in the intensity of carious lesion spectra compared to healthy enamel, linked to changes in morphology and/or orientation of enamel crystals induced by demineralization.

Recent studies on Raman spectroscopy have shown promising results in the diagnosis of early tooth cavities [174, 172, 188, 189].

1.5.3 Scanning Electron Microscopy (SEM)

Scanning electron microscopy is a characterization technique that works through a high-energy electron beam that interacts with the specimen surface. Morphological changes in emergent decomposing lesions have been characterised by scanning electron microscopy.

This technique uses the electrons that are reflected or knocked off the near-surface region of a sample to create an image. The wavelength of electrons is much smaller than that of light, so the resolution of SEMs is superior to that of a light microscope.

In SEM, the electron beam, that is focused on the sample surface thanks to magnetic lenses, scans the sample in a raster pattern. Electrons are generated at the top of the column by the electron source, which is reported in **Figure 1.11**, and they are emitted when their thermal energy overcomes the work function of the source material. The entire electron column must be under vacuum. Then these electrons are accelerated and attracted by the positively charged anode [197].

Vacuum protects electron source from being contaminated and it allows to avoid electron scattering before reaching the sample.

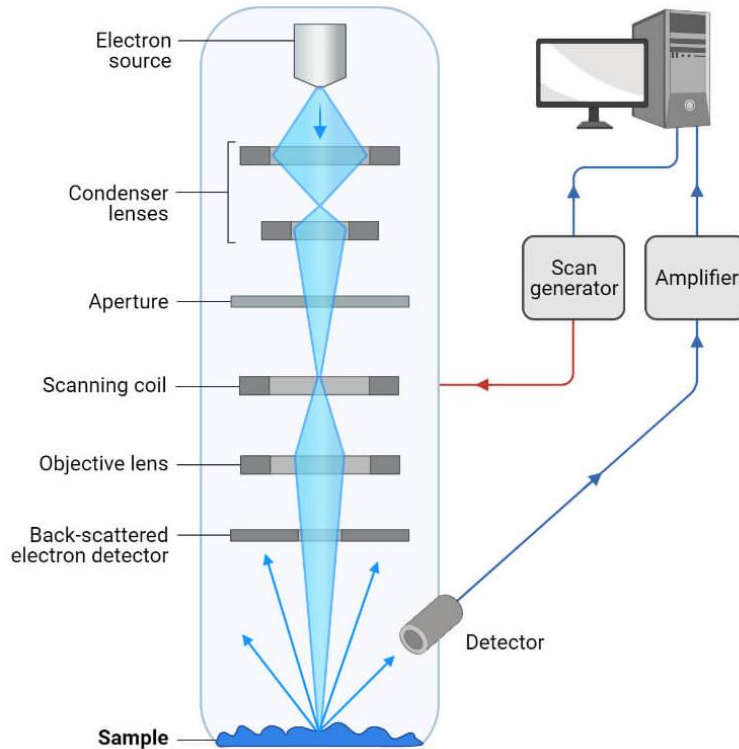


Figure 1.11: Basic components of a SEM [197]

In freshly extracted teeth with varying degrees of interproximal and fissure caries, the prism cores were preferentially demineralized. The demineralization starts at prism's neck, and it can involve the whole nucleus; prism sheaths show resistance to demineralisation [190].

After the removal of plaque, the white enamel patches on approximal surfaces following disclosed a honeycomb-like structure constructed of enamel prisms, whose cores have been preferentially dissolved [191].

In natural incipient carious lesions, carious enamel surfaces have small defects about the size of the "prism ends" and larger, more diffuse areas of apparent destruction [192].

Cariou lesions of the emerging natural enamel show areas of apparently intact enamel, focal holes, a prismatic pattern of destruction with an alveolar appearance, and an irregular type of destruction [193].

The remineralised surfaces have a more regular, smooth and uniform appearance than before and the crystals are more homogeneous, regular and larger than those of the unprocessed surfaces [194].

1.6 Aim of the work

The purpose of this thesis is to analyse the process of dental demineralization using electrochemical impedance spectroscopy measurements to assess the feasibility of using this technique for non-invasive caries diagnosis.

The analysis of the phenomenon of demineralization in the samples taken into consideration, a set of fifty healthy teeth, is aimed at identifying chemical and dielectric characteristics of teeth.

The samples were examined before being subjected to demineralisation, induced by a laboratory-prepared demineralizing solution, and after treatment, in order to differentiate them by electrochemical, morphological and chemical properties.

2. Materials Characterization and Methodologies

2.1 Human Teeth Samples Preparation

Healthy teeth (un-erupted human third molars and decayed canines) used for this survey were extracted from no more than one year, for periodontal reasons, by several patients after informed consent at the 'Department of Surgical Sciences-Dental School' of the University of Turin. The ethics committee of the University of Turin approved the study protocol DS 00071 2018.

For this study a set of fifty teeth was used. The root of the selected teeth is completely intact, and teeth have no dental fillings or sealants on their surface.

After the extraction, the teeth, examined and classified by an experienced dentist, were cleaned and soft tissues and bone fragments remaining on the surface were removed. To avoid dehydration, the extracted teeth have been stored in hermetically sealed test tubes (test tubes or vials) containing a 0.5% w/v solution of sodium hypochlorite (NaClO).

The first tests were performed on healthy teeth, which then were demineralized using a demineralizing solution.

The demineralising solution (1 L) was prepared using distilled water and had the following chemical composition [195]:

- distilled water,
- 0.05 mol/L of acetic acid (CH₃COOH),
- 1.28 mmol/L of calcium chloride (CaCl₂),
- 0.74 mmol/L of potassium dihydrogen phosphate (KH₂PO₄),
- sodium hydroxide (NaOH) or hydrochloric acid (HCl) to adjust pH.

The demineralising solution was prepared by taking 2.86 mL of acetic acid using a pipette and a piglet and transferring it into a beaker which contains 500 ml of distilled water. Then the beaker was placed on a magnetic stirrer and the solution was slowly shaken by inserting a magnetic hook. Through the appropriate trays, 0.1882 g of calcium chloride and 0.1007 g of potassium dihydrogen phosphate were weighted on an analytical balance. The salts are progressively added to the solution, which was shaken until dissolved.

At the end, the pH of the solution was measured, and, through a funnel, the solution was transferred to a 1000 mL flask, and it was made up to the mark with distilled water to one litre by buffering with sodium hydroxide or hydrochloric acid up to pH 5.

Primarily, healthy teeth were covered by an organic burnish to let only a small rectangular part of the surface in contact with the solution, as shown in **Figure 2.1**.



Figure 2.1: Tooth with an organic burnish

Teeth were then inserted into test tubes containing the demineralizing solution, which were placed in a climatic chamber at 38°C for 96 hours to induce demineralization.

2.2 Impedance Measurements and Data Acquisition

2.2.1 Main impedance concepts

Impedance Z is the sum of a real contribution, Z_{Re} , which is related to the ability of a circuit to withstand the flow of electric current, and an imaginary contribution, Z_{Im} , which is linked to the ability of a circuit to store electrical energy (formula 2.1).

$$Z = Z_{Re} + Z_{Im} \quad (2.1)$$

Impedance is measured through the application of an alternating potential $V(t)$, reported in formula 2.2, within an electrochemical cell and the measurement of the electric current that is generated within it $I(t)$, reported in formula 2.3 [205].

$$V(t) = V_0 \sin(\omega t) \quad (2.2)$$

$$I(t) = I_0 \sin(\omega t + \phi) \quad (2.3)$$

Where V_0 is the potential amplitude, I_0 is the current amplitude, $\omega = 2\pi f$ is the radial frequency (f is the frequency of the signal), and ϕ is the phase.

Therefore, the impedance is defined by formula 2.4 [205]:

$$Z^* = \frac{V(t)}{I(t)} \quad (2.4)$$

Using complex number theory, the impedance can be defined by formula 2.5, which can be used to obtain the formula for the phase (formula 2.6) [205]:

$$Z^* = Z_0(\cos\phi + i\sin\phi) = Z_{Re} + Z_{Im} \quad (2.5)$$

$$\phi = \arctan\left(\frac{Z_{Im}}{Z_{Re}}\right) \quad (2.6)$$

Impedance measurement data can be represented in two different ways [205]: the Bode diagram and the Nyquist diagram.

The Bode diagram, in which the X-axis is the logarithm of the frequency, and the Y-axis reports the logarithm of the impedance and the phase, is reported in **Figure 2.2**. Through this diagram it is possible to see more clearly what happens at high frequencies.

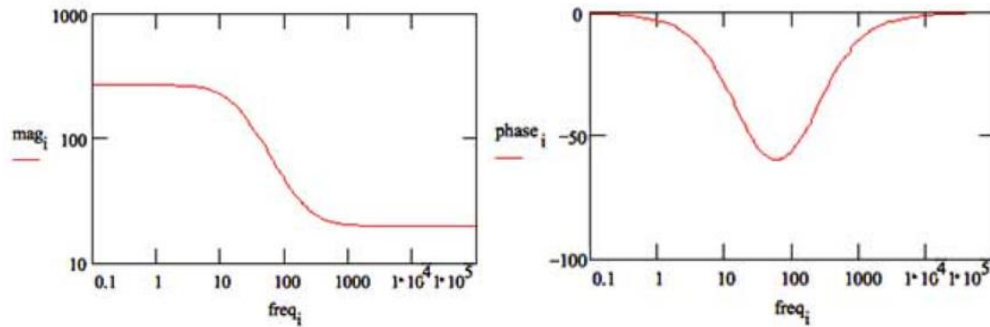


Figure 2.2: Bode Plot for 1 mm/year Corrosion Rate [206]

It is possible to model the electrochemical behaviour by using equivalent electrical circuits.

The Nyquist diagram, in which the X-axis is the real impedance Z_{Re} and the Y-axis is the opposite of the imaginary impedance $-Z_{Im}$, is reported in **Figure 2.3**. Through this diagram it is possible to compare the resistive contribution, given by the real part, with the capacitive one, given by the imaginary part.

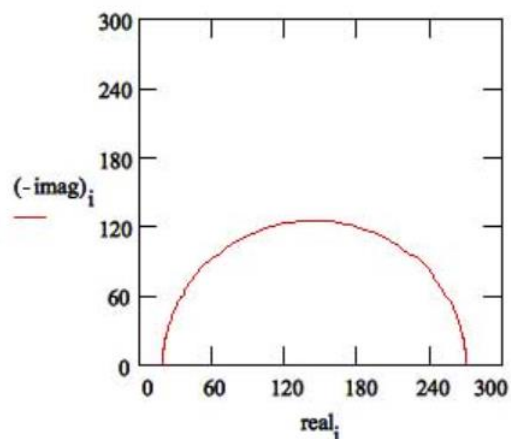


Figure 3.3: Nyquist Plot for 1 mm/year Corrosion Rate [206]

Moreover, information on conduction mechanisms and kinetics can also be obtained: a perfect half-semicircle represents a single charge transfer process, whereas two or more semicircles represent two or more transfer processes.

2.2.2 Impedance Measurements

The impedance measurements were carried out using an Ivium-n-Stat Potentiostat (Ivium Technologies BV, Netherlands), and the data were processed using the Iviumsoft software.

All measurements were carried out using a sample-holder, immediately after removing the samples from the hypochlorite solution, dried in air with tissue paper. The sample-holder is a designed 3D-printed PLA support, and it has been placed in the measuring cell to ensure proper measurement without damaging the tooth.

Approximately two-thirds to three-quarters of the tooth root were soaked in physiological saline solution. The 0.9% w/v sodium chloride (NaCl) solution offers good visibility of the sample while measuring and avoids drying of wet samples.

In **Figure 2.4** the experimental set-up is shown, composed by the measuring cell with a two-electrode configuration (platinum electrodes):

- the working electrode (WE) is a platinum wire in contact with the coronal access cavity, on the surface of the tooth,
- the counter electrode (CE or RE) is a Pt wire partially immersed in the physiological saline solution.

Both electrodes are connected to the computer controlled Potentiostat.

The experimental set-up is represented in **Figure 2.4**.

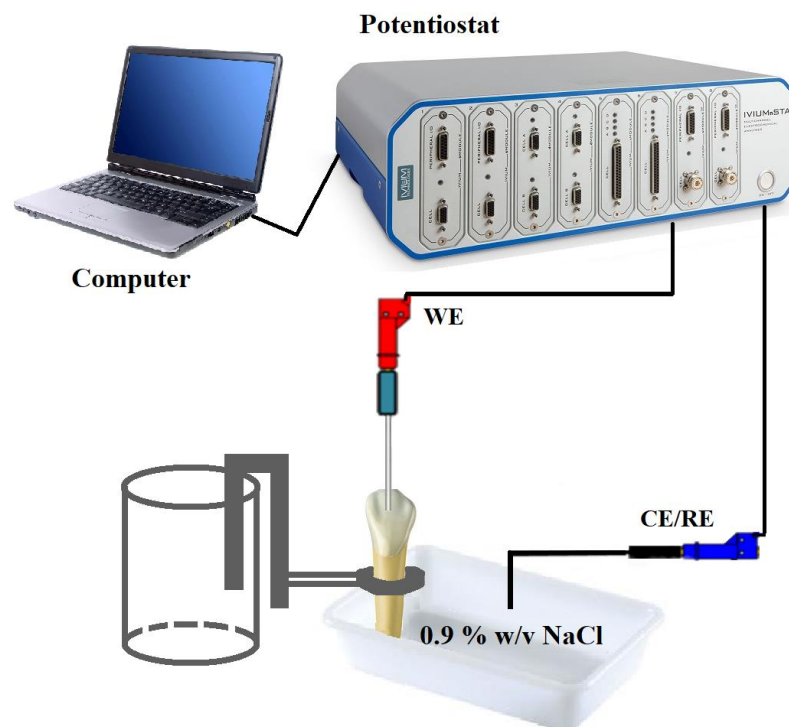


Figure 2.4: Experimental set-up for impedance measurements

After visual assessment of tooth surfaces, impedance measurements were carried out using a sinusoidal stimulus of 10 mV, in the frequency range from 10^{-1} Hz to 10^4 Hz, acquiring 5 points per frequency decade.

Numerous measurements have been made both on healthy and demineralized teeth. At different tooth surface investigation sites, successive measurements of impedance spectroscopy were performed, recording the values at each point.

A comparison is made for the frequency response of impedance magnitude and phase between healthy and decayed tooth.

2.3 Equivalent Electrical Circuit

2.3.1 Main aspects

Electrochemical Impedance Spectroscopy allows to distinguish the contribution of each individual element present in the sample through the modelling for equivalent electrical circuits: this is one of the reasons why it is preferred over other tests.

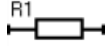
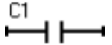
Within these circuits, the electrochemical phenomena are represented by passive electrical elements, such as resistors and capacitors.

It is important to select the most appropriate electrical circuit, in fact each electrical element has a chemical and physical meaning inside the system. On the other hand, it is preferable to choose a circuit as simple as possible [205]. The main electrical elements that can be found in a circuit are divided between ideals, such as resistor, capacitor, and inductor, and not ideals, such as the constant phase element (CPE) and the Warburg element [205].

In this thesis, the impedance measurements of the samples have been modelled using equivalent electrical circuits through the IviumSoft software.

Table 2.1 reports a list of the main equivalent elements with their symbol used in the IviumSoft software and the corresponding impedance expression.

Table 2.1: Principal equivalent elements present in equivalent circuits with IviumSoft symbols [206]

Equivalent element	Symbol	Impedance
Resistance R		R
Capacitance C		$1/j\omega C$
Inductance L		$j\omega L$
Warburg W		$1/[Y_0(j\omega)^{1/2}]$
CPE Q		$1/[Y_0(j\omega)^\alpha]$

where $j = \sqrt{-1}$, ω is the frequency, Y_0 is a constant independent of the frequency and α is the CPE power. The parameter $\alpha = 1$ represents an ideal capacitor, $\alpha = 0$ corresponds to a resistor, while there is an intermediate behaviour for other values.

An example of equivalent electrical circuit is the simplified Randles cell, which is one of the most common cell models and is reported in **Figure 2.5**. The Randles cell consists of a solution resistance R_{sol} in series with a double layer capacitor C_{dl} in parallel with a charge transfer resistance R_{ct} [205].

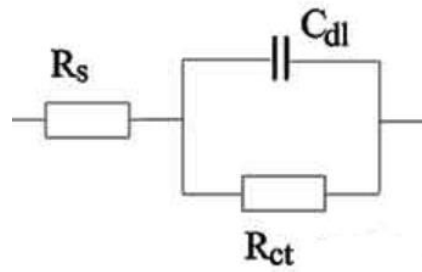


Figure 2.5: Simplified Randles cell schematic diagram [206]

2.3.2 Proposed Equivalent Electrical Circuit

For a more detailed analysis of the impedance measurement results, the spectra were modelled using a suitable equivalent electrical circuit. In **Figure 2.6** the proposed equivalent electrical circuit is reported, used to model the impedance spectra of healthy and decayed teeth.

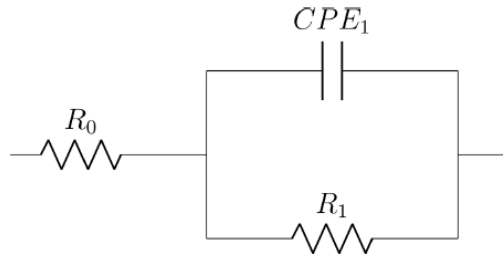


Figure 2.6: Equivalent electrical circuit

This equivalent circuit consists of a resistor R_0 connected to a constant phase element CPE_1 in parallel with a second resistor R_1 . R_0 is related to the interface resistance between the platinum wire and the tooth, CPE_1 represents the double layer capacitance modelled as a CPE, and R_1 is the charge transfer resistance. The parallel is related to the porous structure of the tooth due to the formation of caries and the electrical parameters associated with the structure of enamel and dentine [148, 149].

The first resistor R_0 is made up of two contributions: one related to solution resistance and another related to the interface resistance between the platinum wire and the tooth.

The measured impedance spectra were fitted using the IviumSoft software (release 4.982).

2.4 Scanning Electron Microscopy

The Scanning Electron Microscope (SEM) is a device capable of providing information on the topography and morphology of the surfaces of materials, with a magnification between 10x and 500kx. It allows to see the surface roughness, crystalline grains, porosities, and homogeneity of materials [207].

It has the same working principle as the optical microscope, but instead of working with visible light, it works through a beam of accelerated electrons. It analyses secondary electrons and retro-diffuse electrons from the sample surface, affected by the primary electron beam [208].

Inside the microscope, a monochromatic beam of electrons is produced by an electron cannon, accelerated towards the sample, where it interacts with the atoms on its surface, which produces secondary electrons and retro-diffused electrons, which are then collected by a detector. It is possible to reconstruct the morphology and topography of the surface by analysing secondary electrons, while information on the composition of the sample is obtained by analysing the retro-diffuse electrons [209].

The SEM measurements were carried out through a Phenom Desktop SEM instrument, shown in **Figure 2.7**.



Figure 2.7: Phenom Desktop SEM [196]

First, teeth were dried in air and then they were placed in the chamber, which is reported in **Figure 2.7**. The camera can capture images of the exposed surface of the tooth considered. The user can modify magnification value and can explore all surface in different positions.

SEM images are obtained using different magnification values, an accelerating voltage equal to 15 kV and a pressure equal to 60 Pa.

2.5 Raman Spectroscopy

Raman spectroscopy measurements were performed using a portable modular spectrometer produced by BWTEK, which is reported in **Figure 2.8**.

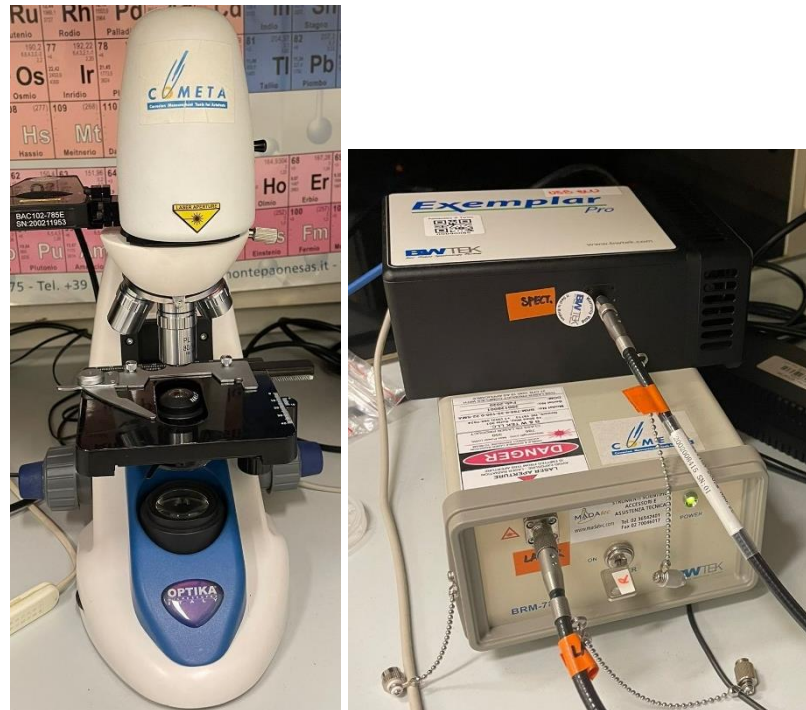


Figure 2.8: BWTEK portable modular spectrometer

The instrument is equipped with a monochrome laser (λ : 785 nm) and a BTC675N spectrometer (measuring range: 65 cm^{-1} to 3350 cm^{-1} , resolution equal to 6 cm^{-1}) coupled with a CCD sensor.

The analysis was carried out by connecting the instrument to a compact microscope (BAC151) that allows to observe the area of analysis and to focus the beam on the surface.

3. Results and discussion

3.1 Analysis of the demineralization process through SEM and Raman measurements

The demineralization process is initially analysed with two techniques in order to better understand the electrochemical impedance spectroscopy measurements: scanning electron microscopy and Raman spectroscopy.

A healthy tooth can be differentiated from a demineralized tooth through these analysis, which were carried out for many teeth of the set.

Figure 3.1 shows the surface of a healthy tooth: it looks smooth, without defects which can be correlated with demineralisation. Marks which can be observed are probably related to normal defects present in human teeth.

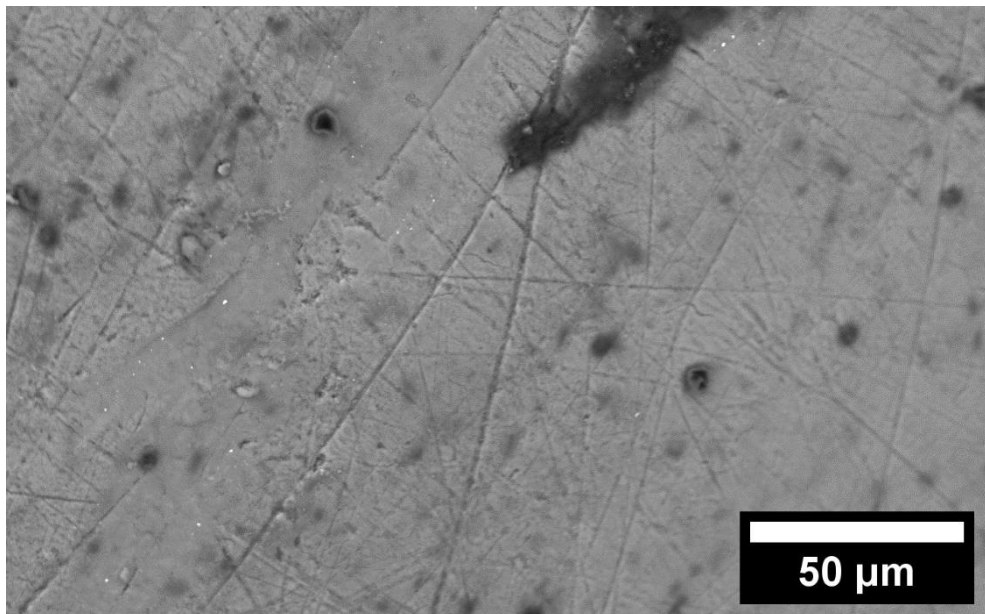


Figure 3.1: SEM image of a healthy tooth

Figure 3.2 displays the SEM image of the demineralized tooth obtained at the same magnification (2200 x).

In contrast to the results presented in **Figure 3.1**, the enamel surface contains the hexagonal structures denoted by the red rectangular. These structures represent prisms composed of hexagonal hydroxyapatite crystals [198].

These structures have a honeycomb appearance and it becomes visible only after the demineralization.

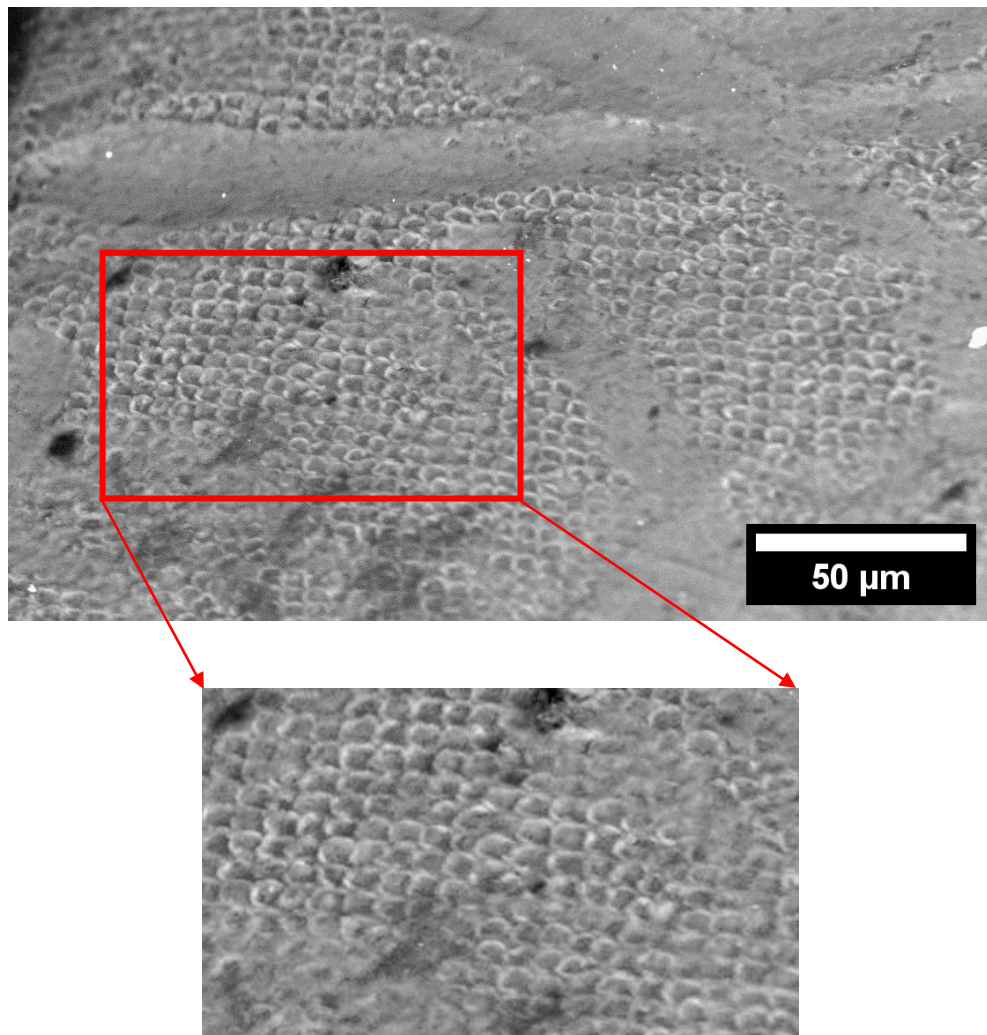


Figure 3.2: SEM image of a demineralized tooth

In some teeth, at low magnification, the enamel surfaces showed the presence of small depressions due to dissolution of the extremities of the prism, as shown in **Figure 3.3**. A few focal holes can be also seen, indicated by red rods [199].

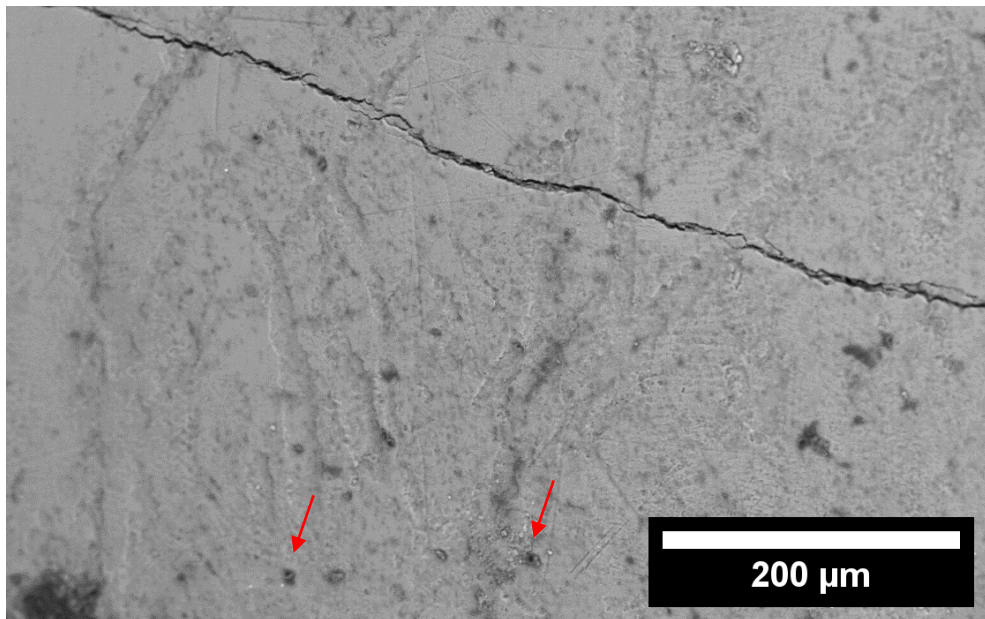


Figure 3.3: SEM image at lower magnification

At higher magnifications, the depressions appeared wedge-shaped (**Figure 3.4**) [199].

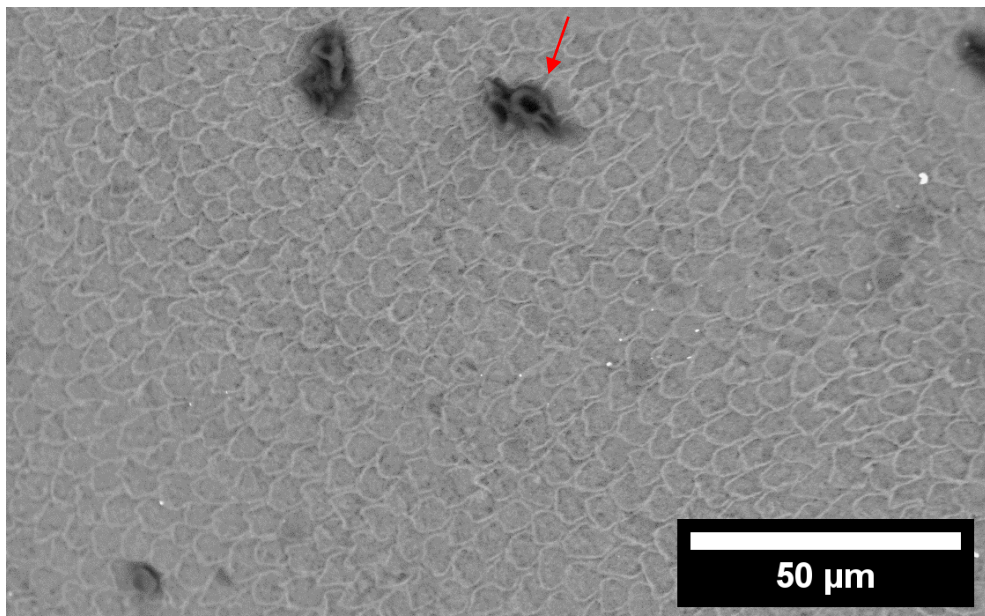


Figure 3.4: SEM image of a demineralized tooth

Figure 3.5 displays two spectra acquired on the surface of a healthy tooth and a demineralized one, in which it is possible to compare the change in intensity of the peak relative to hydroxyapatite. The acquired spectra allow to evaluate the degree of enamel demineralization by monitoring the variations of the peak at 960 cm^{-1} .

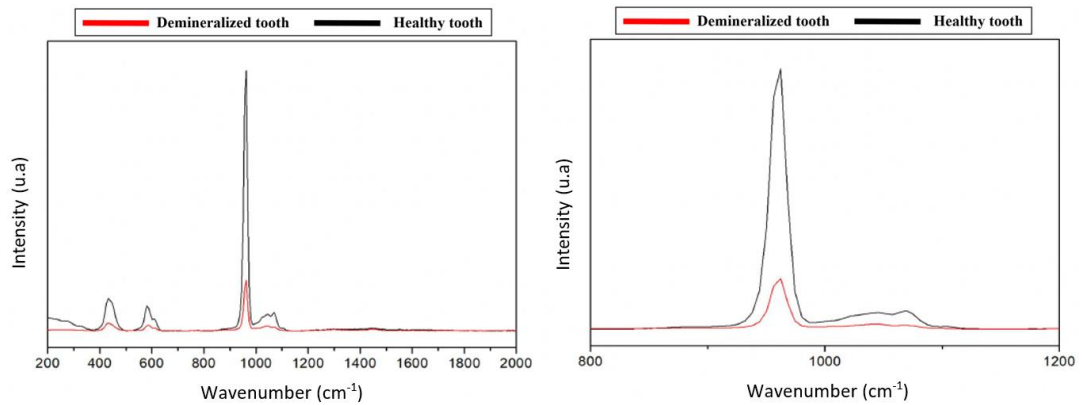


Figure 3.5: Raman spectra acquired on a healthy and demineralized tooth

In the left spectrum the peak is in the range $200\text{-}2000\text{ cm}^{-1}$, while in the right spectrum is shown an enlarged section, in the range $800\text{-}1200\text{ cm}^{-1}$.

The intensity of the peak, related to the vibration of group PO_4^{3-} in the hydroxyapatite, decreases with the increase of the degree of demineralization.

In the next sections, the chemical information derived from Raman spectroscopy will be coupled to the data from impedance spectroscopy measurements, to obtain a complete picture of the state of health of the tooth.

3.2 Experimental set-up

The experimental configuration used for impedance measurements is reported in **Figure 2.4**.

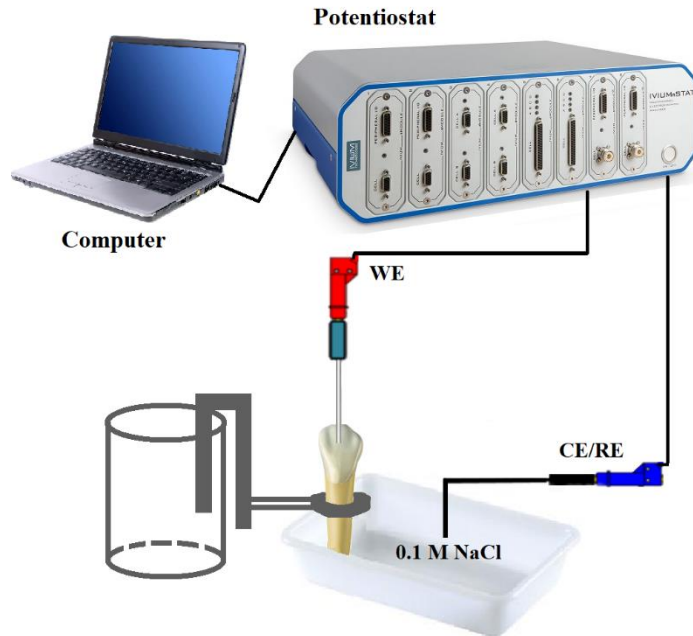


Figure 2.4: Experimental set-up for impedance measurements

The experimental set-up is composed by the sample, that is the tooth whose two-thirds to three-quarters are soaked in physiological saline solution, the Potentiostat and the computer.

The counter-electrode is partially immersed in saline solution, while the working-electrode is directly in contact with the teeth.

This system is simple and easy to apply to in-vivo applications because it involves two electrodes, one in contact with the tooth and the other on the oral cavity immersed in the saliva, so it does not lead to a tooth fracture.

In addition, this allows to use portable and low-cost instrumentation and it does not use X-rays, so it is suitable for young patients and pregnant women [122].

Furthermore, the impedance values are not normalized with respect to the sample area because it would be impossible to measure the surface area of teeth during in-vivo measurements.

3.3 Impedance measurements

Impedance spectroscopy coupled to Raman spectroscopy allows to correlate the current response to chemical information, to obtain a full overview of the dental condition.

The impedance spectroscopy measurements are used to distinguish healthy teeth from decayed ones. For this purpose, two sets of measurements were performed on fifty healthy teeth and on the same samples but after demineralization.

The objective is to demonstrate that, in the presence of a demineralized areas, a modification of the electrical characteristics of dental tissue occurs.

Figure 3.6 shows a Bode diagram representative of a healthy tooth (green lines) and a demineralized tooth (red lines).

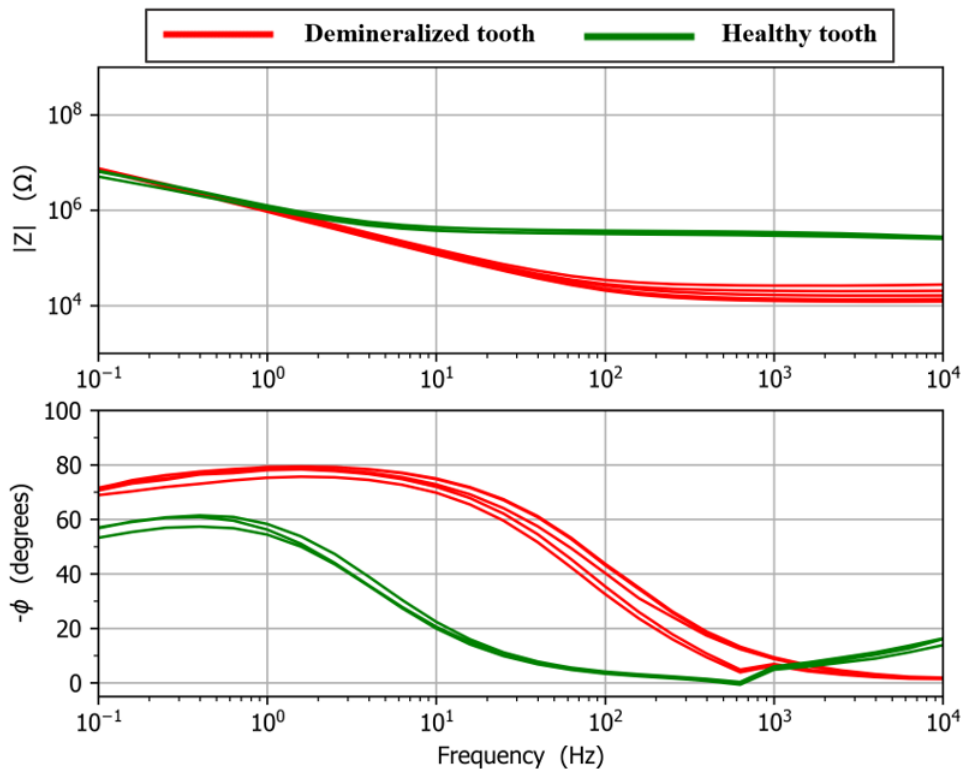


Figure 3.6: Impedance spectra of healthy (green lines) and demineralized (red lines) teeth as Bode diagram

These impedance spectra show as many lines as measurements made at different points on the surface, in fact green lines are multiple measurements collected on different points of the same healthy tooth and red lines are multiple measurements collected on different points of the same demineralized tooth.

All spectra for sound teeth show the same shape, which is a bit different from the spectra related to the demineralized teeth. These spectra show a resistive behaviour at high frequencies, related to the contact resistance platinum/tooth, which becomes capacitive-like at low frequencies, due to the double-layer capacitance.

In the case of healthy teeth (green lines) the resistive part of the graph is larger than that related to demineralized samples.

While the shape of the curves related to sound and demineralized samples is similar, it is possible to observe that the two kinds of samples have a different electrochemical behaviour. Indeed, in the case of the demineralized tooth, at high frequencies, the impedance module has lower values than the healthy tooth. In addition, in the case of the healthy tooth, the impedance phase remains at 0° for a higher frequency range and tends to close to -60° only below 1 Hz, while it reaches its maximum at about a value equal to -70° in the case of the demineralized tooth.

As previously written, these findings revealed a shift from resistive to capacitive behaviour that occurs at different frequencies if the measurement is performed on a healthy tooth or on a carious one, allowing to discriminate between healthy and carious teeth.

3.4 Equivalent electrical circuits

In order to further analyse the results of impedance measurements, the spectra were modelled using an appropriate equivalent electrical circuit, which represents a quantitative model describing the electrochemical system.

The proposed equivalent circuit, shown in **Figure 2.6**, consists of a resistor connected to a constant phase element (CPE) in parallel with a second resistor.

The first resistor, R_0 , represents the contact resistance between the platinum wire and the tooth, the constant phase element, CPE_1 , stands for the capacitance of double layer and the second resistor, R_1 , is the charge transfer resistance. The second part of the circuit (CPE_1 and R_1) represents the tooth/solution interface and is influenced by the outer portion of the tooth [200, 201].

In **Figure 2.6** is reported the proposed equivalent electrical circuit used to model the impedance spectra.

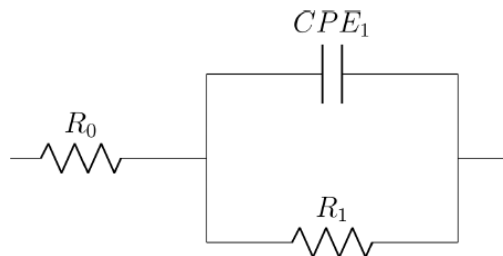


Figure 2.6: Equivalent electrical circuit

All spectra have a resistive behaviour at high frequencies and a capacitive-like behaviour at low frequencies. The resistive part is related to the interface of the tooth, while at lower frequencies the phase reaches -60° (healthy tooth) and -70° (demineralized tooth) because of the double layer capacitance formed at the interface between the probe and the tooth.

As already mentioned, the transition from resistive to capacitive behaviour takes place at different frequencies depending on whether the measurement is performed, on a healthy tooth or on a carious one.

Results from equivalent electrical circuit modelling are reported in **Table 3.1**, which shows measurements performed on a healthy tooth and on a decayed tooth. These data are referred to the sample whose impedance measurement is reported in **Figure 3.6**.

Table 3.1: Equivalent electrical circuit parameters computed for a healthy and a demineralized tooth (results coming from the spectra reported in Figure 3.6)

	R_0 (Ω)	R_1 (Ω)	Q_1 (s^N/Ω)	N_1
Healthy tooth	$3.17 \cdot 10^5$	$1.41 \cdot 10^7$	$2.46 \cdot 10^{-7}$	$8.22 \cdot 10^{-1}$
Decayed tooth	$2.64 \cdot 10^4$	$3.44 \cdot 10^7$	$1.83 \cdot 10^{-7}$	$8.80 \cdot 10^{-1}$

The parameter showing the larger changes between healthy and demineralized teeth is the value of R_0 , that is the contact resistance, obtained from the high frequency impedance value. This parameter has a lower value in correspondence of the demineralized area.

In addition, there are very limited variations in double-layer capacitance, Q_1 , which therefore does not seem to be affected by the presence of cavities in the tooth. There is a negligible increase in Q_1 in the demineralized tooth, but the order of magnitude has not changed.

These results are also supported from previous literature [1]. Actually, in a study related to the impedance characterisation of sound and carious teeth, it was found that some changes are also present in R_1 values, i.e. the charge transfer resistance, but they are subject to a significant estimation error. Actually, this error is present because the impedance spectra do not reach the resistive plateau at low frequency, so the parameter can not be correctly estimated by the software.

The impedance values are not normalized with respect to the sample area because all samples have different areas and shapes. It is important to consider that the variation of these parameters from tooth to tooth is related not only to the presence of demineralization, but also to the size of the samples.

These measured data are not normalized because, while it would be possible to measure the surface area of samples analysed during these in-vitro measurements, it would be impossible to apply this procedure in-vivo.

Equivalent electrical circuits, processed through the software IviumSoft, can model well these impedance measurements. This is demonstrated by the **Figure 3.7**, which reports the equivalent circuit fit for a sample pre demineralization.

Figure 3.7 shows a good fitting for impedance data of a healthy tooth, indeed some points at high frequencies are not considered to find the best fitting set of parameters of the circuit.

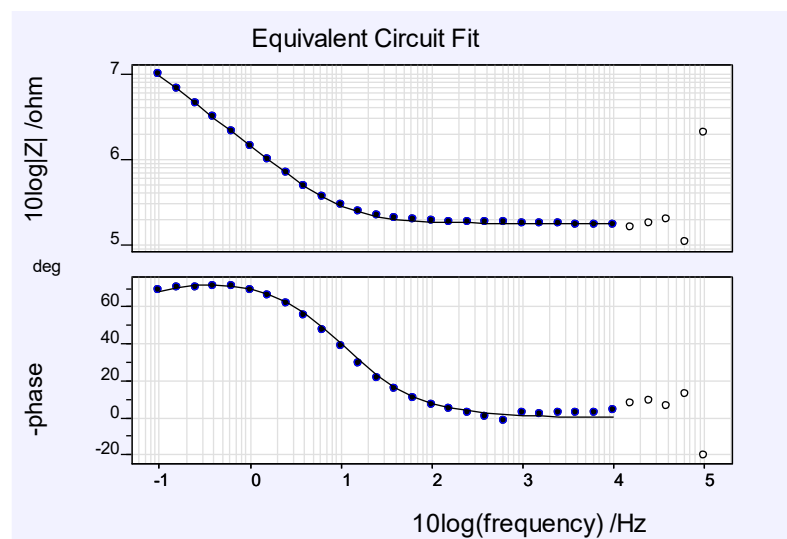


Figure 3.7: Bode diagrams of a healthy tooth modelled through IviumSoft software, blue dots are experimental data, while the continuous line represents the model

Figure 3.8 show the Nyquist diagram as the fitting for the same impedance data of the same healthy tooth. Also in this case, is shown a good fitting, but a difference between measured data and the model can be observed for the highest values of impedance.

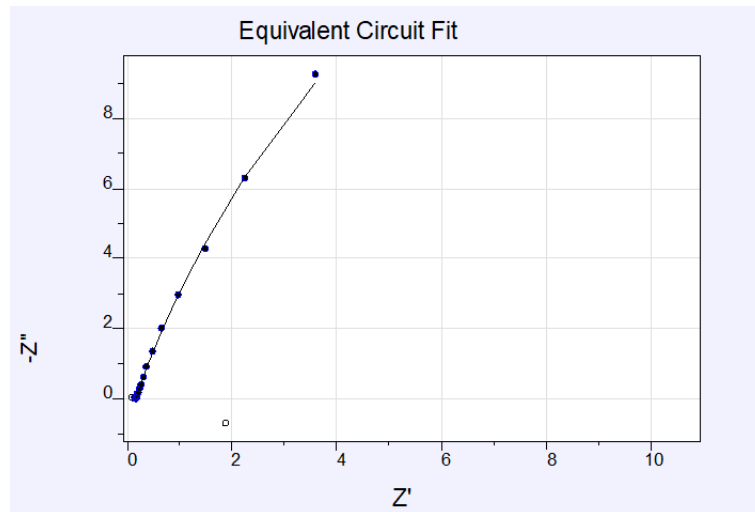


Figure 3.8: Nyquist diagram of a healthy tooth modelled through IviumSoft software, blue dots are experimental data, while the continuous line represents the model

The same behaviour is reported in **Figure 3.9** and **Figure 3.10**, which are related to the same tooth but after demineralization.

Even in this case a good fitting is shown both in Bode diagrams (**Figure 3.9**) and in Nyquist plot (**Figure 3.10**).

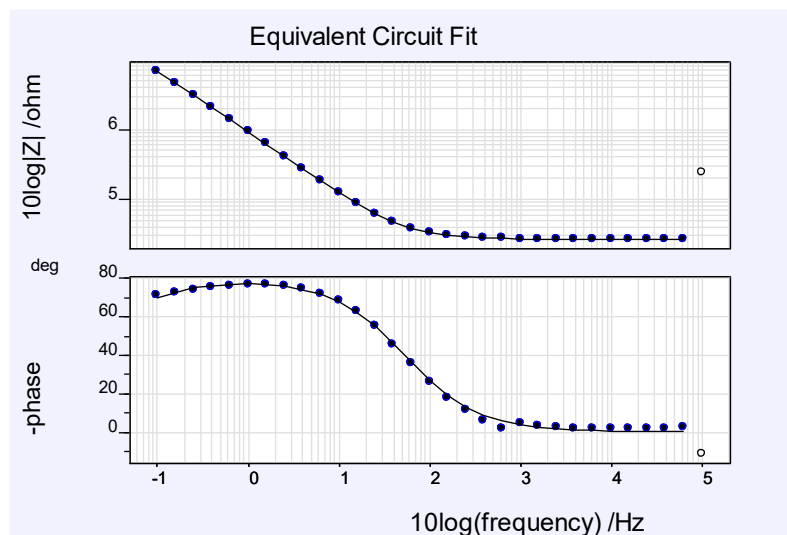


Figure 3.9: Bode diagrams of a demineralized tooth modelled through IviumSoft software, blue dots are experimental data, while the continuous line represents the model

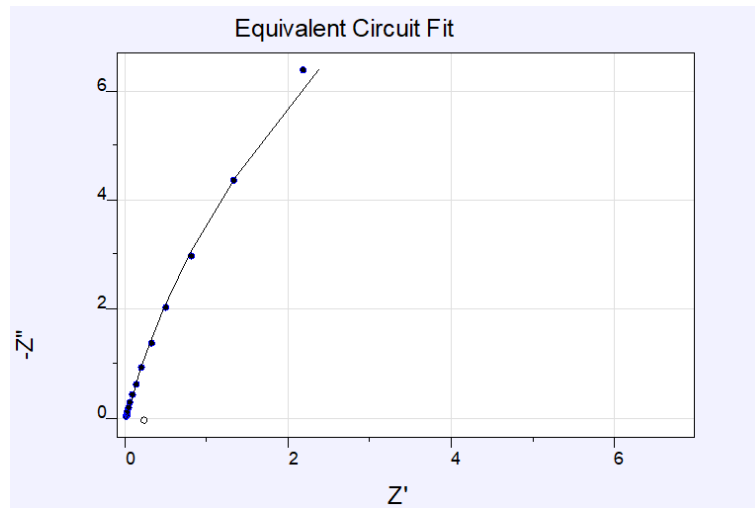


Figure 3.10: Nyquist diagram of a demineralized tooth modelled through IviumSoft software, blue dots are experimental data, while the continuous line represents the model

3.5 Variations in EEC Pre and Post Demineralization

Impedance measurements were performed for a set of fifty teeth, and an equivalent electrical circuit is developed for each measure.

Each measurement is characterized by percentage variations of electrical parameters, which are the contact resistance R_0 , the load transfer resistance, R_1 , and the double-layer capacitance, Q_1 .

In this chapter five representative samples are analysed and, for each of them, Bode diagrams are reported and percentage variation values of electrical circuits parameters pre and post demineralization are calculated.

Figure 3.11 reports a Bode diagram representative of the same tooth before demineralization (healthy) and after this treatment (demineralized).

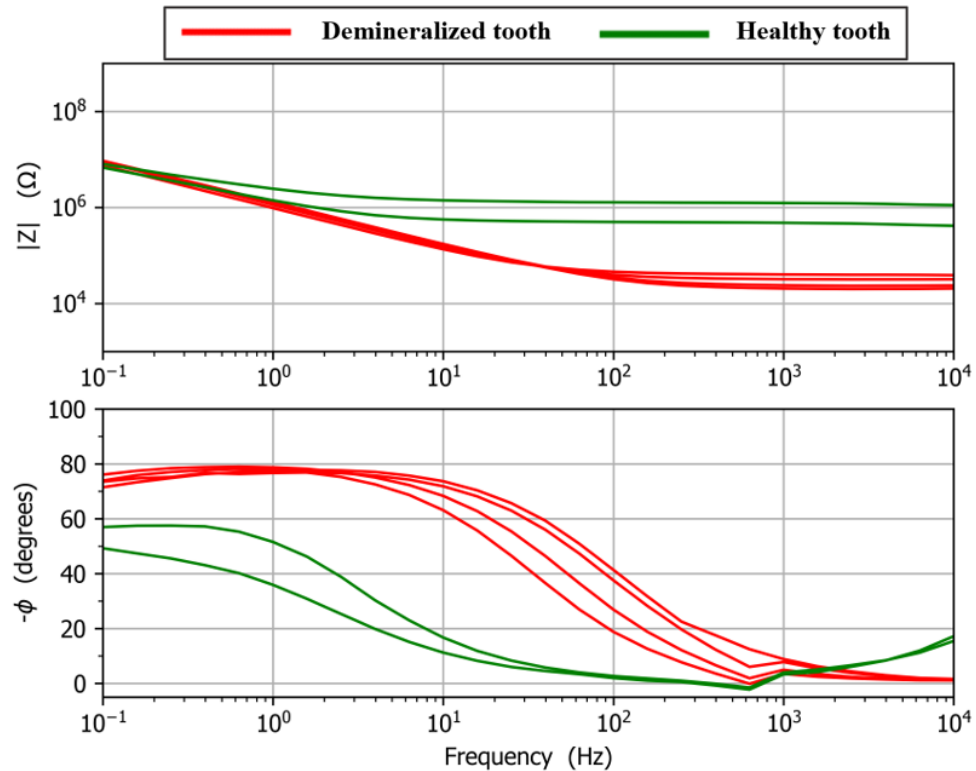


Figure 3.11: Impedance spectra of healthy (green lines) and demineralized (red lines) teeth as Bode diagram

Equivalent electrical circuit parameters referred to the sample whose impedance measurement is reported in **Figure 3.11** are reported in **Table 3.2**.

Table 3.2: Equivalent electrical circuit parameters computed for a healthy and a demineralized tooth (results coming from the spectra reported in Figure 3.11)

	R_0 (Ω)	R_1 (Ω)	Q_1 (s^N/Ω)	N_1
<i>Healthy tooth</i>	$4.48 \cdot 10^5$	$2.56 \cdot 10^7$	$1.96 \cdot 10^{-7}$	$8.11 \cdot 10^{-1}$
<i>Decayed tooth</i>	$3.90 \cdot 10^4$	$6.67 \cdot 10^7$	$2.02 \cdot 10^{-7}$	$8.95 \cdot 10^{-1}$

The most variable parameter is the contact resistance R_0 , that has a lower value in the case of the demineralized tooth. The double-layer capacitance, Q_1 , shows a very limited variation, a negligible increase for the decayed tooth with values in the same order of magnitude. On the other hand, R_1 values changes but they are subject to a significant estimation error (9.29% for healthy tooth and 29.91% for decayed tooth).

Percentage variations pre and post demineralization are reported in **Table 3.3**.

Table 3.3: Percentage changes relative to the equivalent electrical circuit parameters reported in Table 3.2

	R_0 (%)	R_1 (%)	Q_1 (%)
<i>Percentage change</i>	-91.29	160.55	3.06

In the formula used for these calculations:

$$\text{Percentage change} = \left(\frac{x_f - x_i}{x_i} \cdot 100 \right) \% \quad (3.1)$$

x_i is the initial value, relative to the healthy tooth, while x_f is the value of the parameters associated to the tooth after demineralization.

Figure 3.12 reports a Bode diagram representative of the same tooth before and after demineralization.

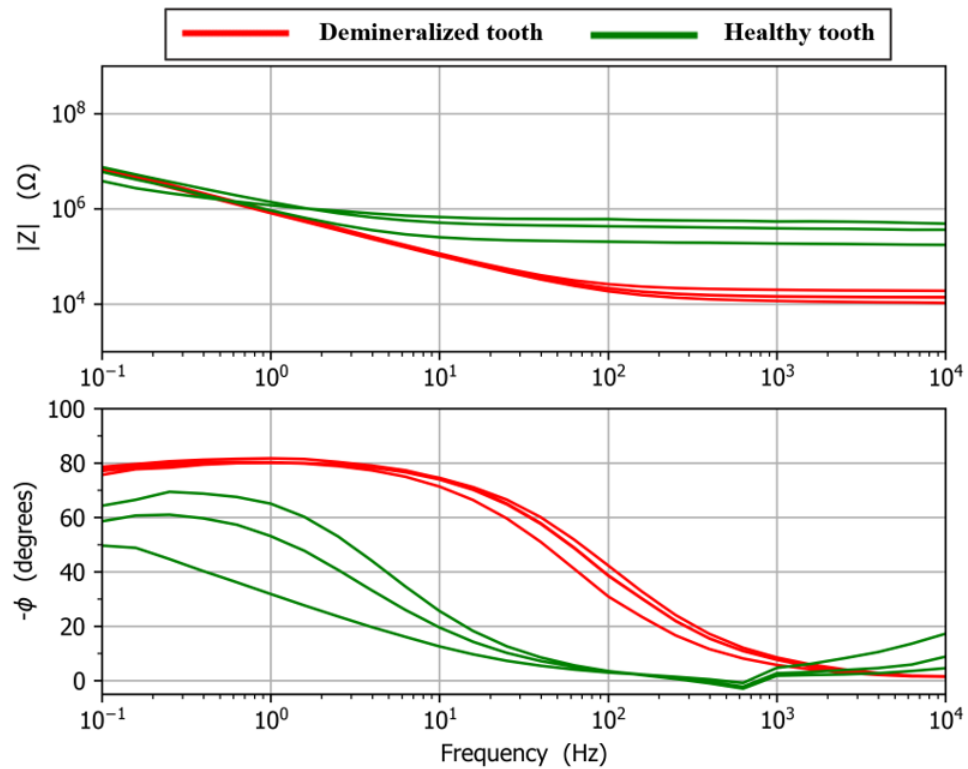


Figure 3.12: Impedance spectra of healthy (green lines) and demineralized (red lines) teeth as Bode diagram

Equivalent electrical circuit parameters referred to the sample whose impedance measurement is reported in **Figure 3.12** are reported in **Table 3.4**.

Table 3.4: Equivalent electrical circuit parameters computed for a healthy and a demineralized tooth (results coming from the spectra reported in Figure 3.12)

	R_0 (Ω)	R_1 (Ω)	Q_1 (s^N/Ω)	N_1
<i>Healthy tooth</i>	$4.04 \cdot 10^5$	$4.13 \cdot 10^7$	$1.94 \cdot 10^{-7}$	$7.93 \cdot 10^{-1}$
<i>Decayed tooth</i>	$1.06 \cdot 10^4$	$8.20 \cdot 10^7$	$2.39 \cdot 10^{-7}$	$8.98 \cdot 10^{-1}$

Even in this case, the most variable parameter is R_0 , Q_1 , shows a limited variation, and R_1 values are subject to a significant estimation error (29.99% for healthy tooth and 56.28% for decayed tooth). Percentual variations pre and post demineralization are reported in **Table 3.5**.

Table 3.5: Percentage changes relative to the equivalent electrical circuit parameters reported in Table 3.4

	R_0 (%)	R_1 (%)	Q_1 (%)
<i>Percentage change</i>	-97.38	98.54	23.19

Figure 3.13 reports a Bode diagram representative of the same tooth before and after demineralization.

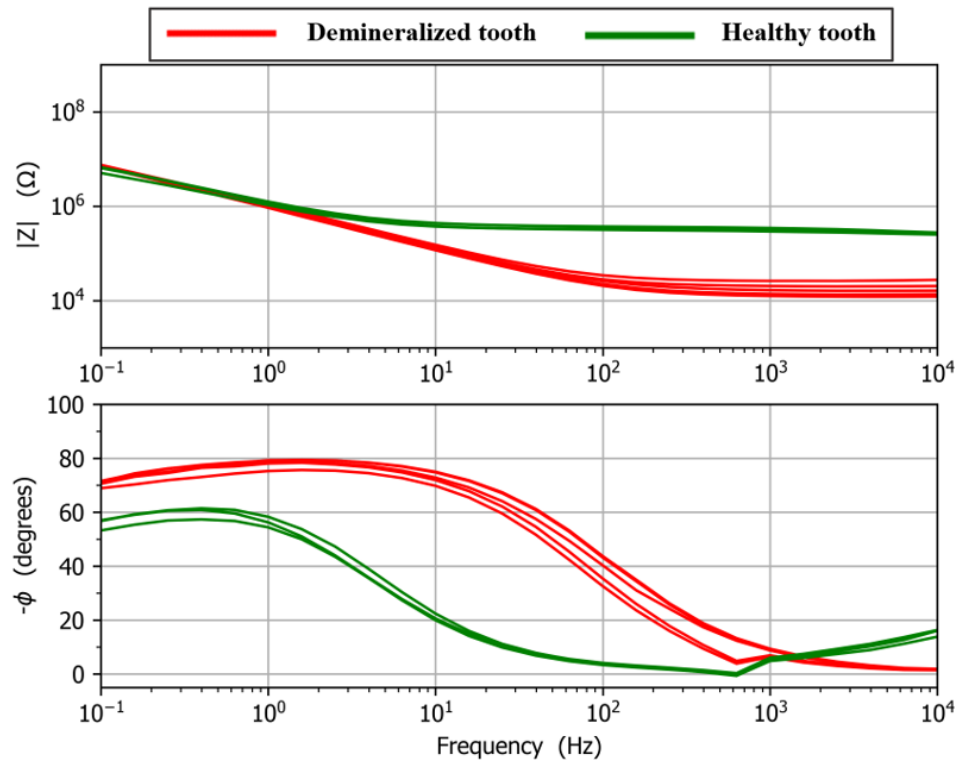


Figure 3.13: Impedance spectra of healthy (green lines) and demineralized (red lines) teeth as Bode diagram

Equivalent electrical circuit parameters referred to the sample whose impedance measurement is reported in **Figure 3.13** are reported in **Table 3.6**.

Table 3.6: Equivalent electrical circuit parameters computed for a healthy and a demineralized tooth (results coming from the spectra reported in Figure 3.13)

	R_0 (Ω)	R_1 (Ω)	Q_1 (s^N/Ω)	N_1
<i>Healthy tooth</i>	$3.17 \cdot 10^5$	$1.41 \cdot 10^7$	$2.46 \cdot 10^{-7}$	$8.22 \cdot 10^{-1}$
<i>Decayed tooth</i>	$2.64 \cdot 10^4$	$3.44 \cdot 10^7$	$1.83 \cdot 10^{-7}$	$8.80 \cdot 10^{-1}$

The same considerations as for the previous samples are valid. R_1 values have a significant estimating error equal to 6.90% for the healthy tooth and 15.09% for the demineralized one. Percentual variations pre and post demineralization are reported in **Table 3.7**.

Table 3.7: Percentage changes relative to the equivalent electrical circuit parameters reported in Table 3.6

	R_0 (%)	R_1 (%)	Q_1 (%)
<i>Percentage change</i>	-91.67	143.97	-25.61

Figure 3.14 reports a Bode diagram representative of the same tooth before and after demineralization.

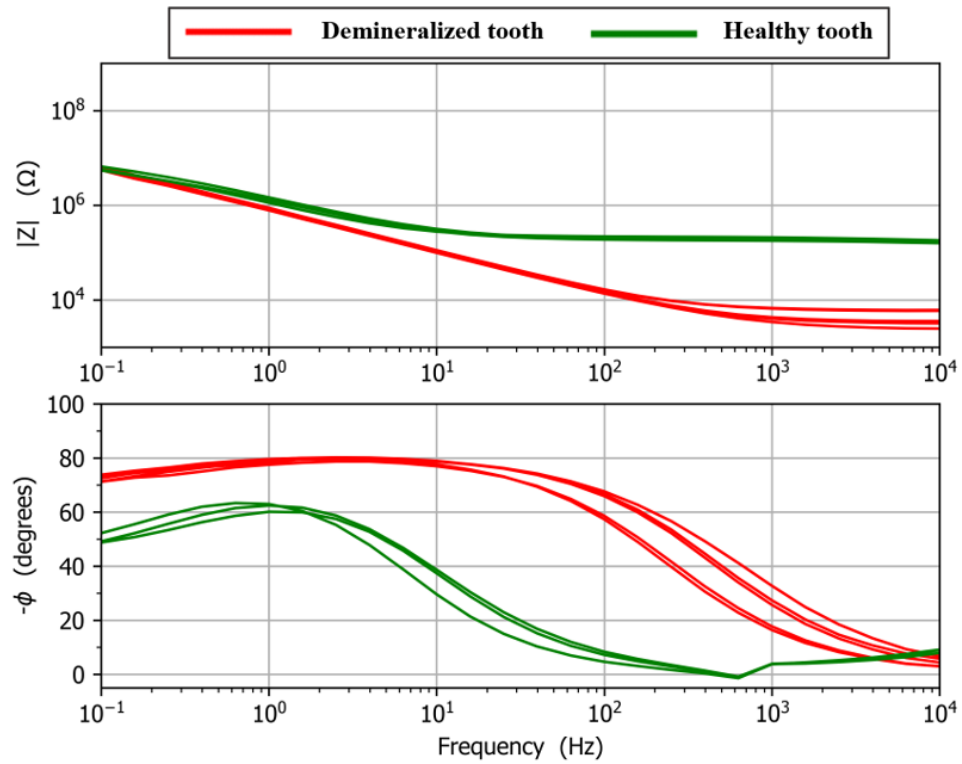


Figure 3.14: Impedance spectra of healthy (green lines) and decayed (red lines) teeth as Bode diagram

Equivalent electrical circuit parameters referred to the sample whose impedance measurement is reported in **Figure 3.14** are reported in **Table 3.8**.

Table 3.8: Equivalent electrical circuit parameters computed for a healthy and a demineralized tooth (results coming from the spectra reported in Figure 3.14)

	R_0 (Ω)	R_1 (Ω)	Q_1 (s^N/Ω)	N_1
Healthy tooth	$2.07 \cdot 10^5$	$1.30 \cdot 10^7$	$2.03 \cdot 10^{-7}$	$8.51 \cdot 10^{-1}$
Decayed tooth	$2.42 \cdot 10^3$	$4.80 \cdot 10^7$	$2.65 \cdot 10^{-7}$	$8.78 \cdot 10^{-1}$

The same considerations as for the previous samples are valid. R_1 values have a significant estimating error equal to 10.40% for the healthy tooth and 22.90% for the demineralized one. Percentual variations pre and post demineralization are reported in **Table 3.9**.

Table 3.9: Percentage changes relative to the equivalent electrical circuit parameters reported in Table 3.8

	R_0 (%)	R_1 (%)	Q_1 (%)
Percentage change	-98.83	269.23	30.54

Figure 3.15 reports a Bode diagram representative of the same tooth before and after demineralization.

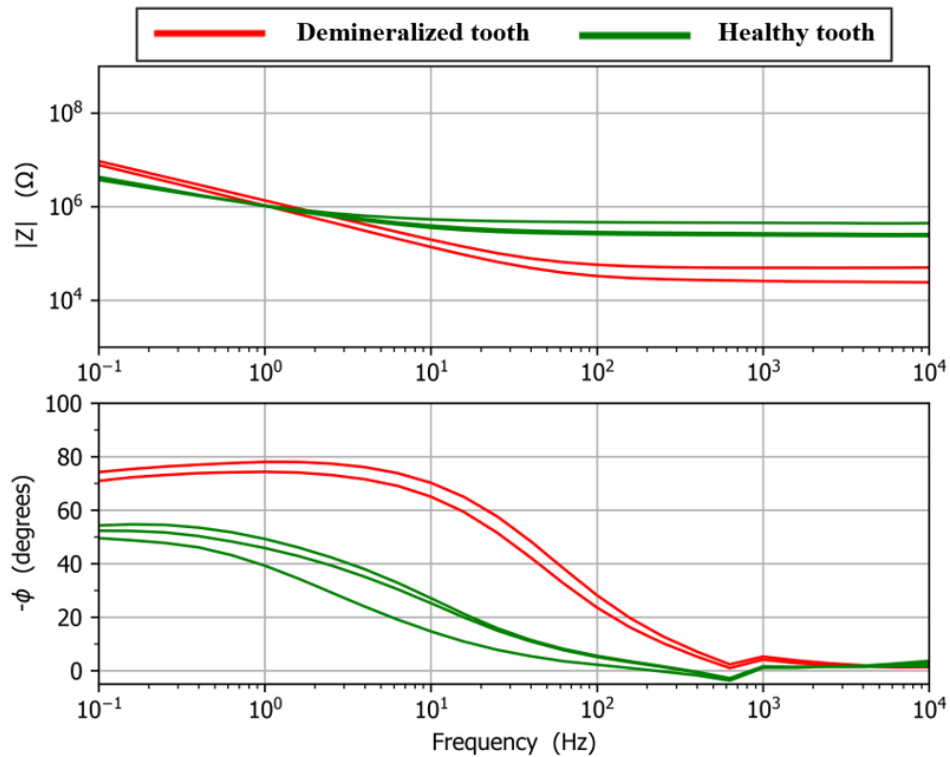


Figure 3.15: Impedance spectra of healthy (green lines) and demineralized (red lines) teeth as Bode diagram

Equivalent electrical circuit parameters referred to the sample whose impedance measurement is reported in **Figure 3.15** are reported in **Table 3.10**.

Table 3.10: Equivalent electrical circuit parameters computed for a healthy and a demineralized tooth (results coming from the spectra reported in Figure 3.15)

	R_0 (Ω)	R_1 (Ω)	Q_1 (s^N/Ω)	N_1
<i>Healthy tooth</i>	$2.70 \cdot 10^5$	$1.58 \cdot 10^7$	$3.04 \cdot 10^{-7}$	$7.01 \cdot 10^{-1}$
<i>Decayed tooth</i>	$4.86 \cdot 10^4$	$6.02 \cdot 10^7$	$1.52 \cdot 10^{-7}$	$8.72 \cdot 10^{-1}$

The same considerations as for the previous samples are valid. R_1 values have a significant estimating error equal to 21.80% for the healthy tooth and 16.80% for the demineralized one. Percentual variations pre and post demineralization are reported in **Table 3.11**.

Table 3.11: Percentage changes relative to the equivalent electrical circuit parameters reported in Table 3.10

	R_0 (%)	R_1 (%)	Q_1 (%)
<i>Percentage change</i>	-82.00	281.01	-50.00

These measurements show that, for all teeth examined pre and post demineralization, each parameter has the same order of magnitude:

- R_0 is about $10^5 \Omega$ for healthy teeth and $10^4 \Omega$ for demineralized ones,
- R_1 is about $10^7 \Omega$ for all samples,
- Q_1 is about $10^{-7} s^N/\Omega$ for all teeth.

These orders of magnitude can be useful to design a measuring device, indeed these values can be used to size the electronic part.

3.6 Discrimination using the phase value

Despite Bode diagrams represent a good choice for differentiating between a sound tooth and a demineralized one, there is another way to evaluate the demineralization: the use of the phase.

As discussed previously (see Section 3.3) the trend of the impedance phase was different comparing healthy and demineralized teeth. Actually, this value remains close to 0° in a larger frequency range for healthy teeth.

Figure 3.16 reports the frequency value at which the phase reaches -45° for all samples. If the phase value equal to -45° is not reached during the measurement, the lowest analysed frequency is reported.

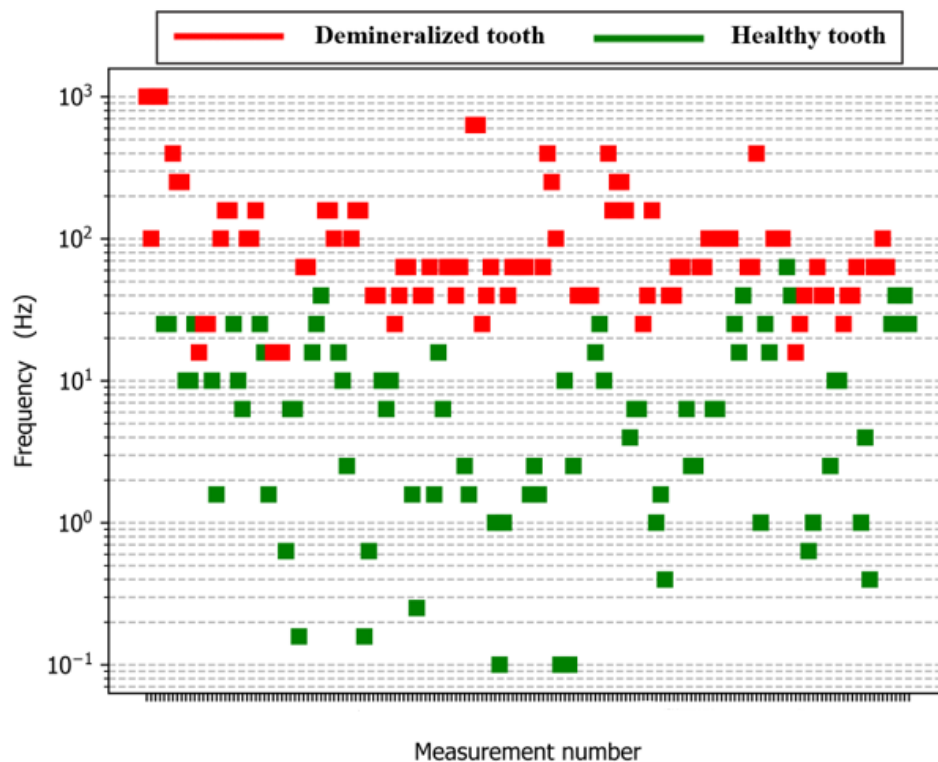


Figure 3.16: Frequency value at which the phase value of -45° is reached in each of the impedance measurements acquired on healthy teeth (green markers) and demineralized teeth (red markers) [1]

The red symbols at the top of the chart represent demineralized teeth, that reach the parameter at higher frequencies. On the other hand, green symbols in the lower part of the graph refer to sound teeth, indeed the phase value stays close to 0° for a larger frequency range.

In particular, it can be observed that the frequency at which the phase value is reached is higher than 10 Hz for teeth examined after demineralization, while it is lower than 10 Hz for healthy teeth.

The frequency at which the phase reaches a value equal to -45° is related to the different measured capacitance (equivalent electrical circuit modelling).

In conclusion, a significant difference between carious and non-carious teeth is related to the frequency at which the phase reaches -45° , so the phase value equal to -45° allows to discriminate samples in two different clusters.

This parameter is a threshold value to classify sound and carious teeth but, despite this, this method does not work with all measurements, indeed there are outliers.

3.7 Variability of measurements

Examined samples have different behaviour because they are human teeth, so they are different from each other. Some samples exhibit a strange behaviour, which can be caused by dental history, human or measurement errors, and surface defects.

There are some samples which show impedance spectra with an opposite trend to the behaviour observed in most teeth. **Figure 3.17** shows this result.

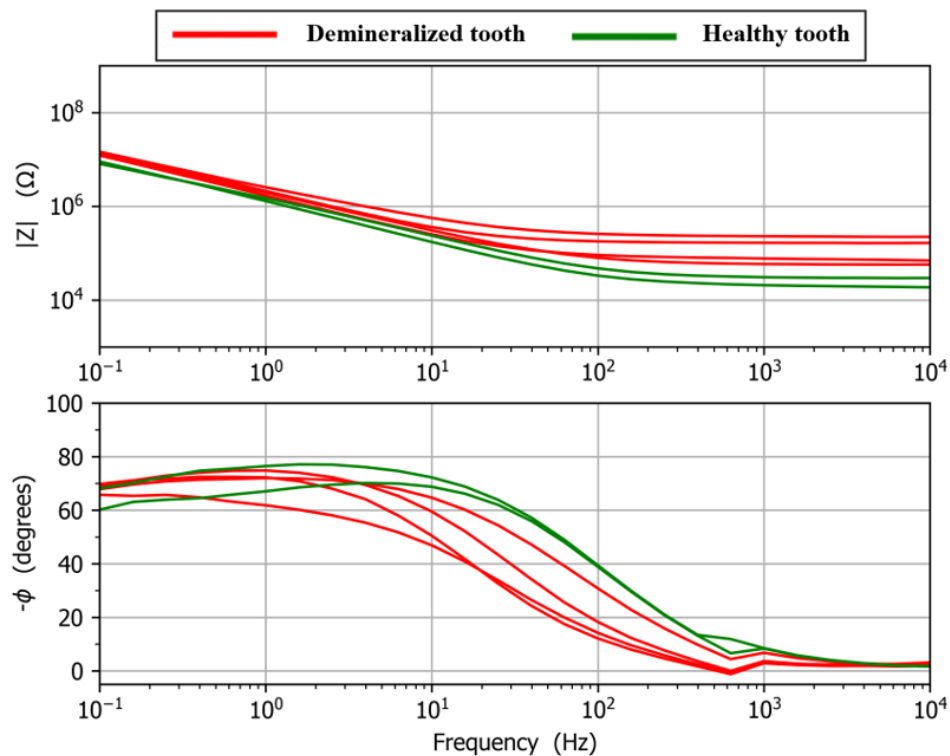


Figure 3.17: Impedance spectra, as Bode diagram, of the healthy (green lines) and demineralized (red lines) tooth which shows an opposite behaviour

This Bode diagram presents a different behaviour at high frequencies with respect to other results found previously, indeed impedance values at high frequencies are higher for the tooth after demineralization than for the same tooth but before the treatment. This result is opposed to the previous ones, so the data related to this sample can be seen as outliers.

In this case, the parameters of the equivalent electric circuits, one for each measurement, differs between each other. These variations can demonstrate that this sample does not have the behaviour shown by the most samples of the set.

This sample has been analysed by SEM in order to correlate these impedance results to the surface morphology of this tooth.

At low magnification (780 x), the SEM image, that is **Figure 3.18**, captured for that sample indicates demineralized areas (indicated by the red arrows) and smooth areas (indicated by the yellow arrow).

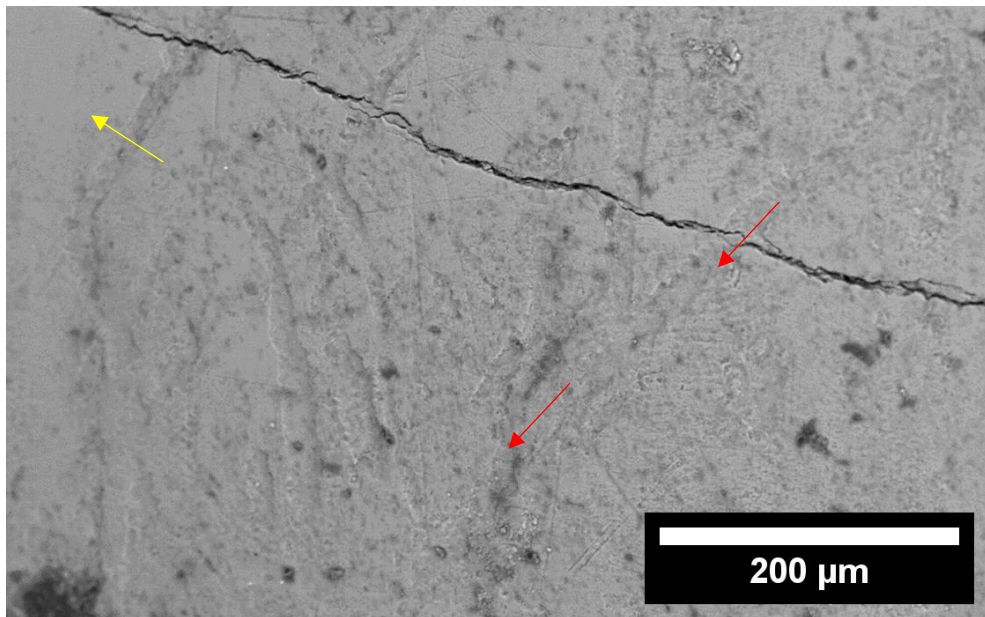


Figure 3.18: SEM image of a decayed tooth

This surface is characterized by both demineralized and intact areas, so the demineralization process did not affect the entire surface. This is correlated to the impedance measurements, which result different from each other and show an opposite trend for impedance values at high frequencies. At high magnification (2250 x), it is possible to see demineralized zones, as shown in **Figure 3.19**.

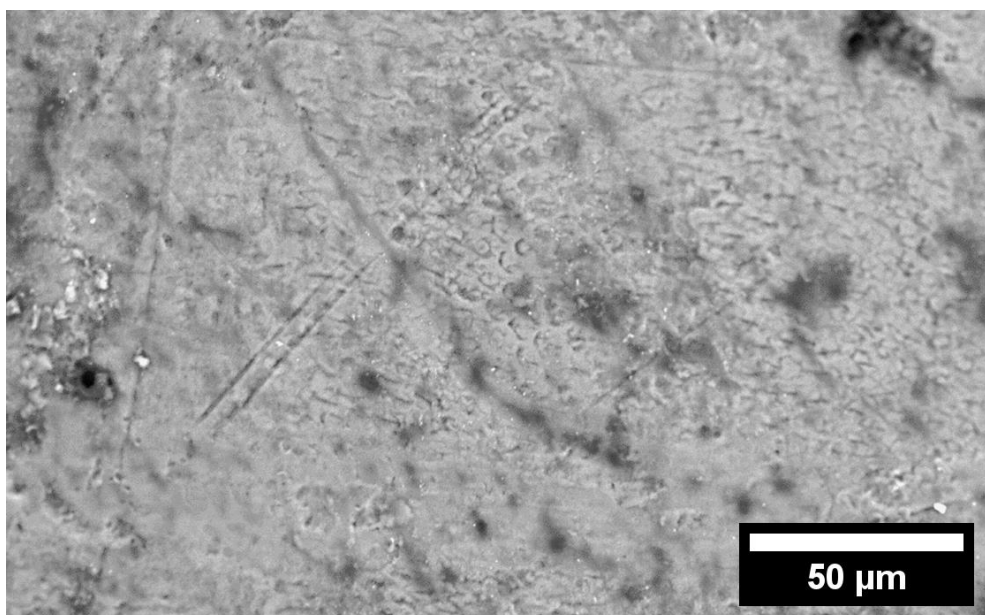


Figure 3.19: SEM image of a decayed tooth

There are other samples which show impedance spectra with different trends for each measurement done at different surface points.

In this case, some curves have a consistent trend in terms of what was discovered before, but others have an inverse trend.

Figure 3.20 represents impedance measurements:

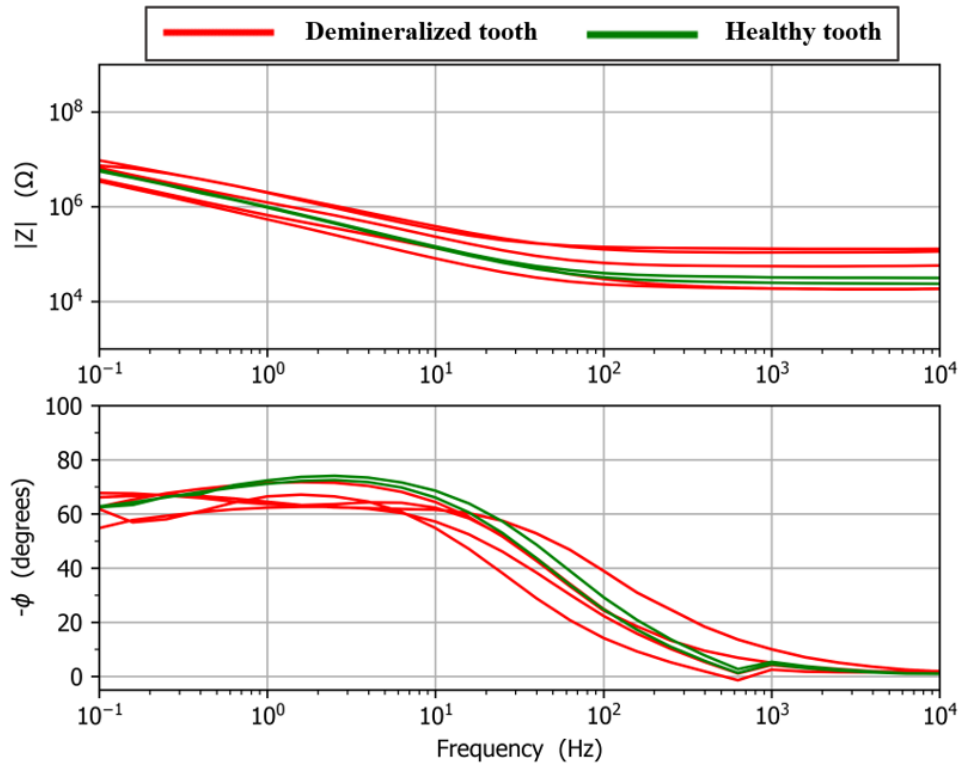


Figure 3.20: Impedance spectra, as Bode diagram, of the healthy (green lines) and demineralized (red lines) tooth which shows different trends

From these spectra a strange behaviour can be observed. At high frequencies, the impedance values related to the tooth after demineralization are not always lower than values of healthy tooth, as in the most cases. In fact, in this case only two sets of data show the “classical” behaviour at high frequencies (impedance values for demineralized teeth lower than the ones associated to healthy ones), while the other curves present a different trend at high frequencies.

This behaviour is examined through SEM analysis in order to understand how it can influence surface morphology.

At low magnification (760 x), the SEM image, captured for that sample and reported in **Figure 3.21**, show demineralized areas (red arrow) and smooth areas (yellow arrow). In that case, demineralised areas are hardly visible.

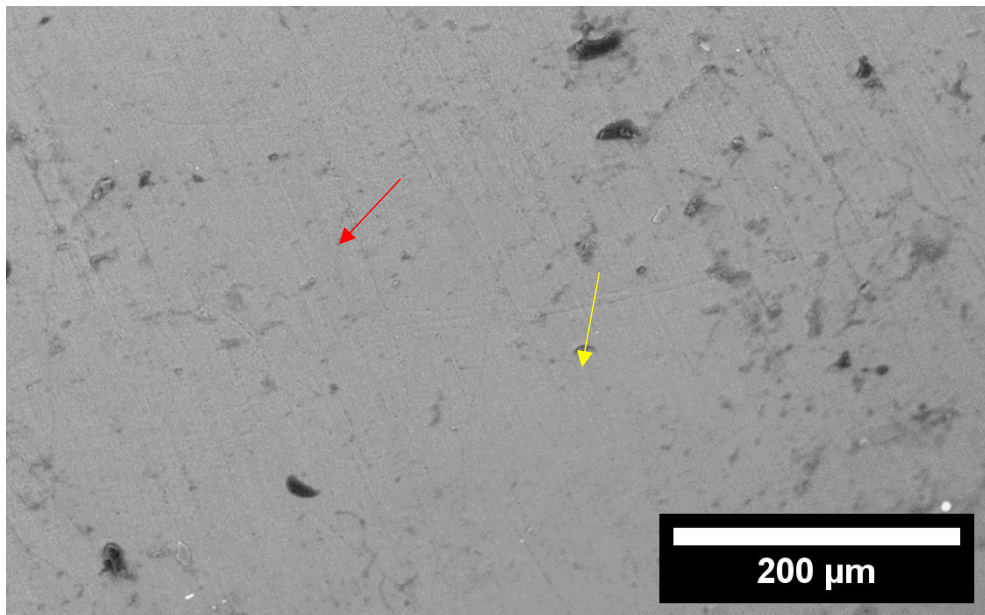


Figure 3.21: SEM image of a decayed tooth

Figure 3.22 shows demineralized zones, captured at high magnification (5500 x).

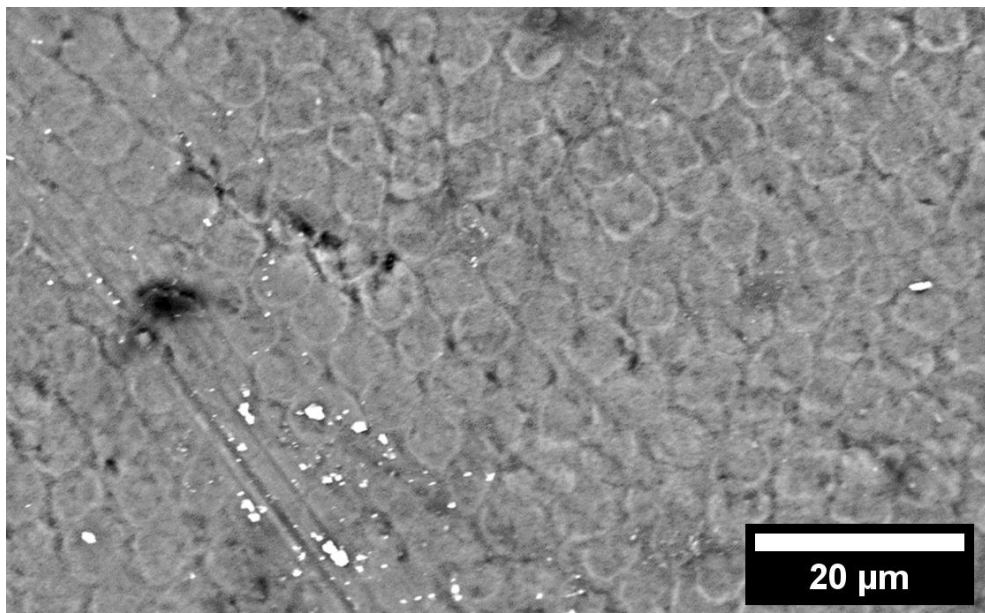


Figure 3.22: SEM image of a demineralized tooth

Even in this case the demineralization process did not affect the entire examined area, in fact the impedance spectra show an unexpected behaviour.

Figure 3.23 shows the impedance measurements represented by curves having a different tendency at each point where the measurement is made:

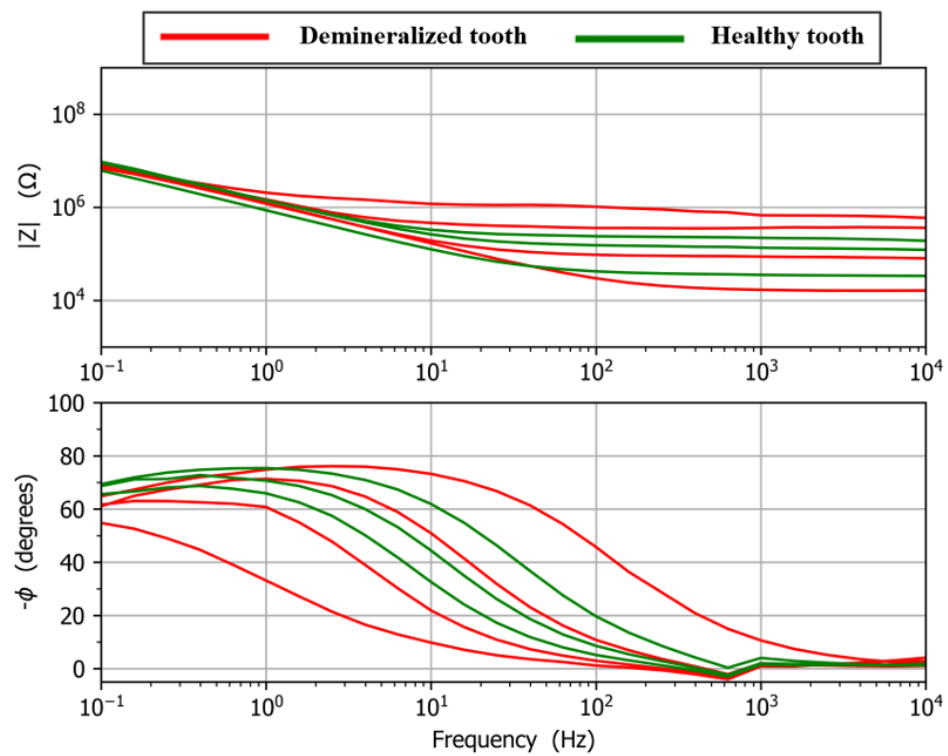


Figure 3.23: Impedance spectra, as Bode diagram, of the healthy (green lines) and decayed (red lines) tooth which shows different trends

At a magnification equal to 1950 x, the SEM image reported in **Figure 3.24** and **Figure 3.25**, show demineralized areas (red arrows) and smooth areas (yellow arrow). In this case, demineralized zones are hard to see.

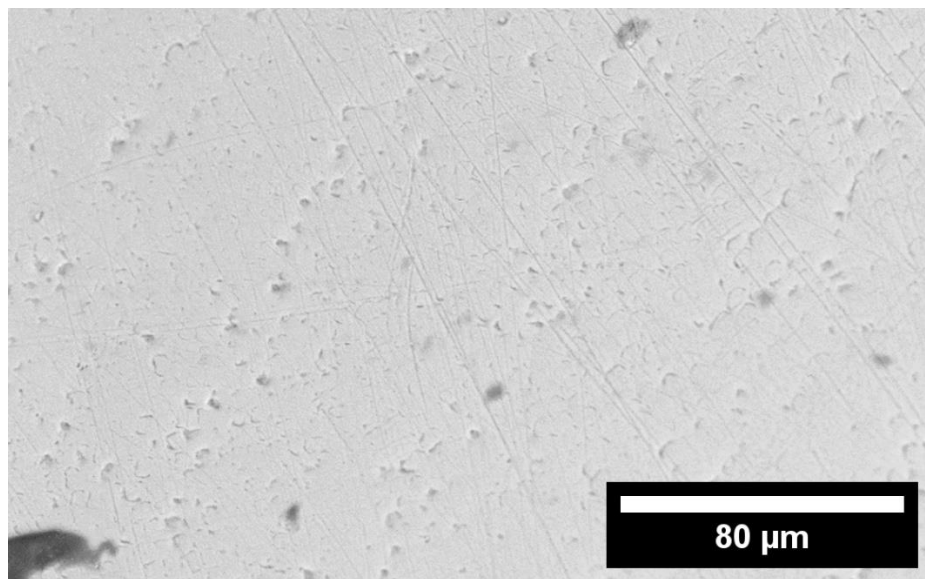


Figure 3.24: SEM image of a demineralized tooth

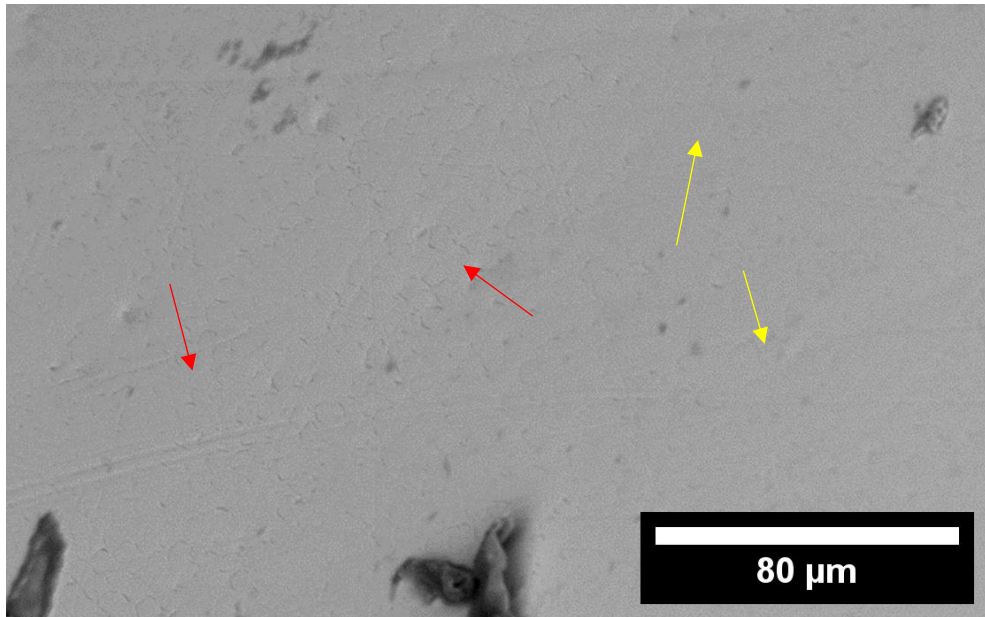


Figure 3.25: SEM image of a demineralized tooth

The same considerations reported for previous cases are valid.

The impedance measurements reported in **Figure 3.26** shows curves with different trends even if they represent measurements done on the same kind of tooth (healthy and demineralized):

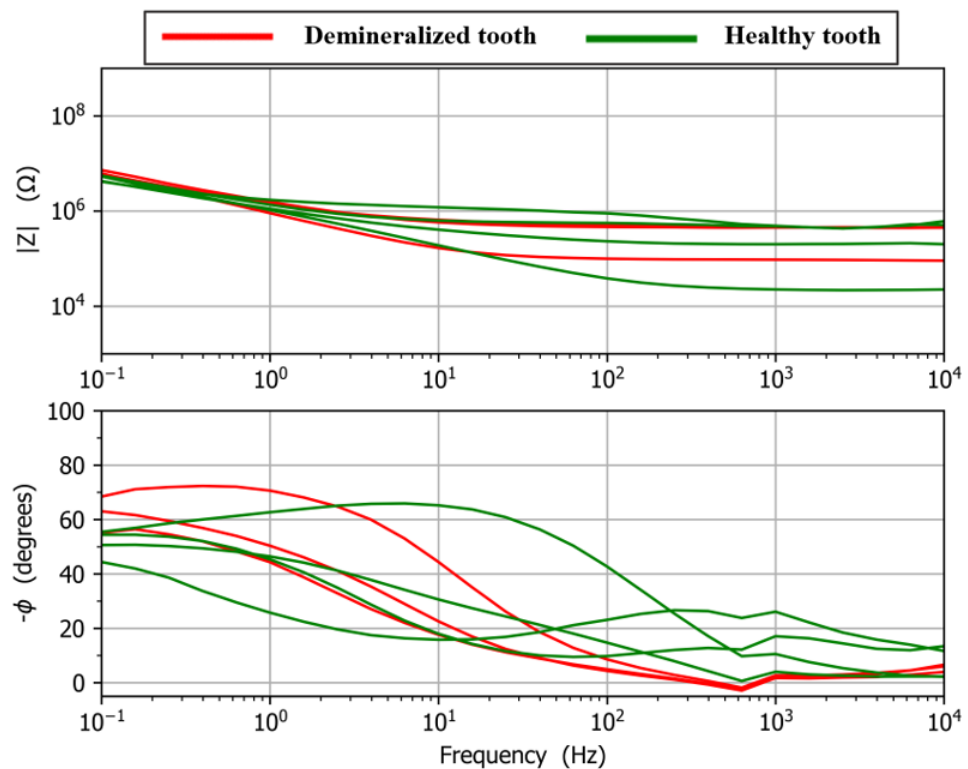


Figure 3.26: Impedance spectra, as Bode diagram, of the healthy (green lines) and decayed (red lines) tooth which shows different trends

In this case, demineralization is more visible, as shown in **Figure 3.27** (EIS image obtained with magnification equal to 2200 x):

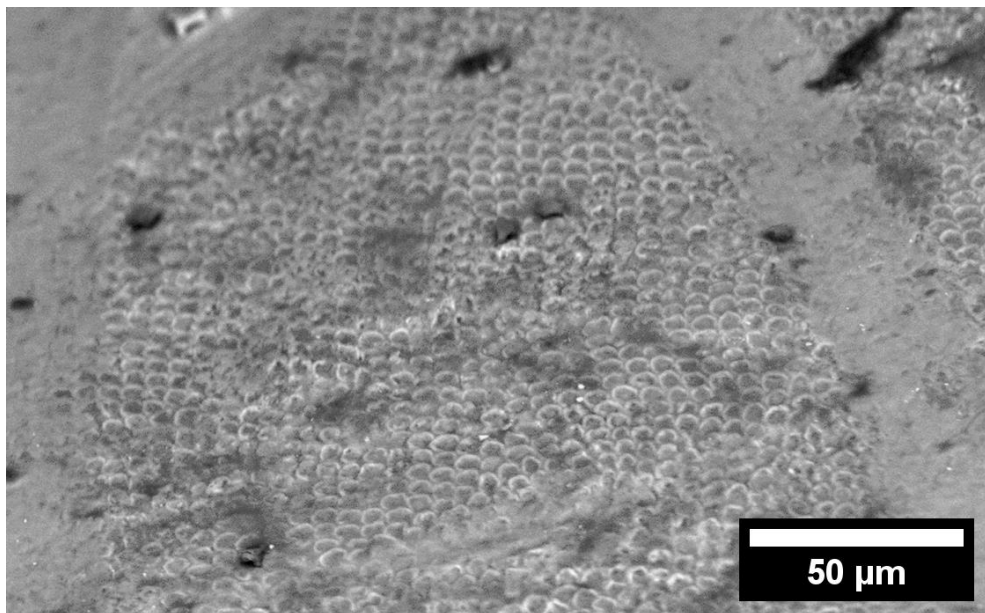


Figure 3.27: SEM image of a demineralized tooth

In this last case, despite impedance data show different trends, the demineralization process seems to be more important, in fact the honeycomb-like structure can be observed with a magnification equal to 2200 x.

3.8 Effect of outliers

In the previous chapter, the four examined teeth show an unexpected behaviour, in fact impedance measurements present trends which are not consistent with the trends shown by most of the samples.

These outliers can be examined by another point of view: the frequency at which the phase reaches a value equal to -45° .

This method can be used because, as already written, a significant difference between healthy and demineralized teeth is related to this parameter, so this phase value (-45°) allows to discriminate samples in two different clusters.

Figure 3.28 shows the frequency values at which the phase value equal to -45° is reached in each of the impedance measurements on the same tooth represented in **Figure 3.17** before and after the process of demineralization.

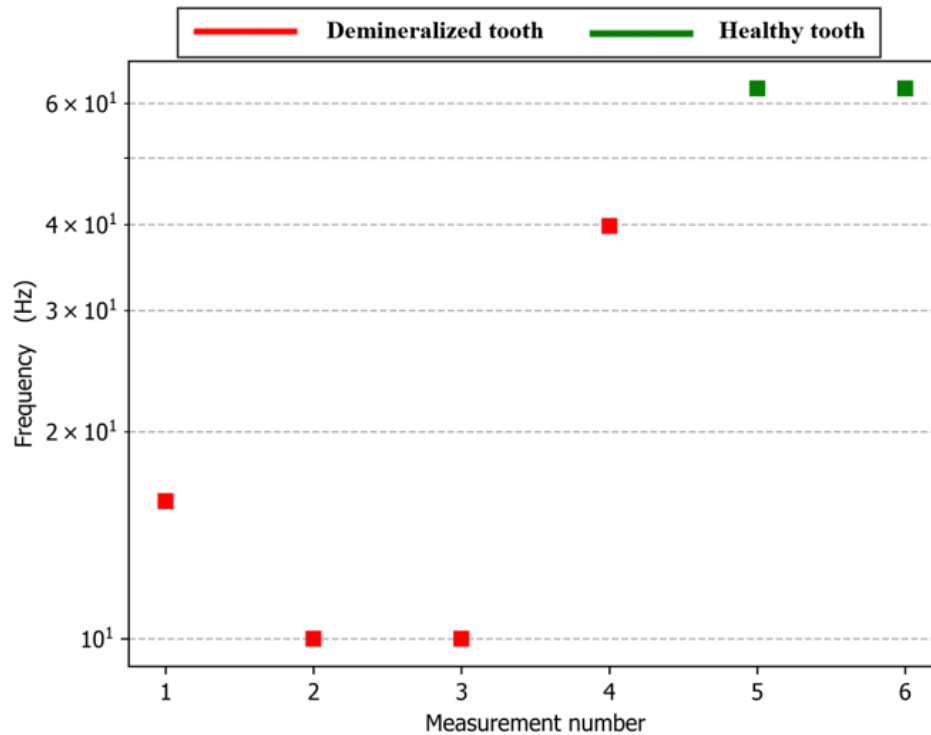


Figure 3.28: Frequency values at which the phase value of -45° is reached in each of the impedance measurements acquired on healthy tooth (green markers) and demineralized tooth (red markers) related to Figure 3.17

A strange behaviour can be observed also through this analysis; indeed, the threshold value is reached at higher frequency values in the healthy tooth than in the demineralised one. This result is not consistent with the results observed for most of the teeth.

Figure 3.29 shows the frequency values at which the phase value equal to -45° is reached in each of the impedance measurements on the same tooth represented in **Figure 3.20** before and after the process of demineralization.

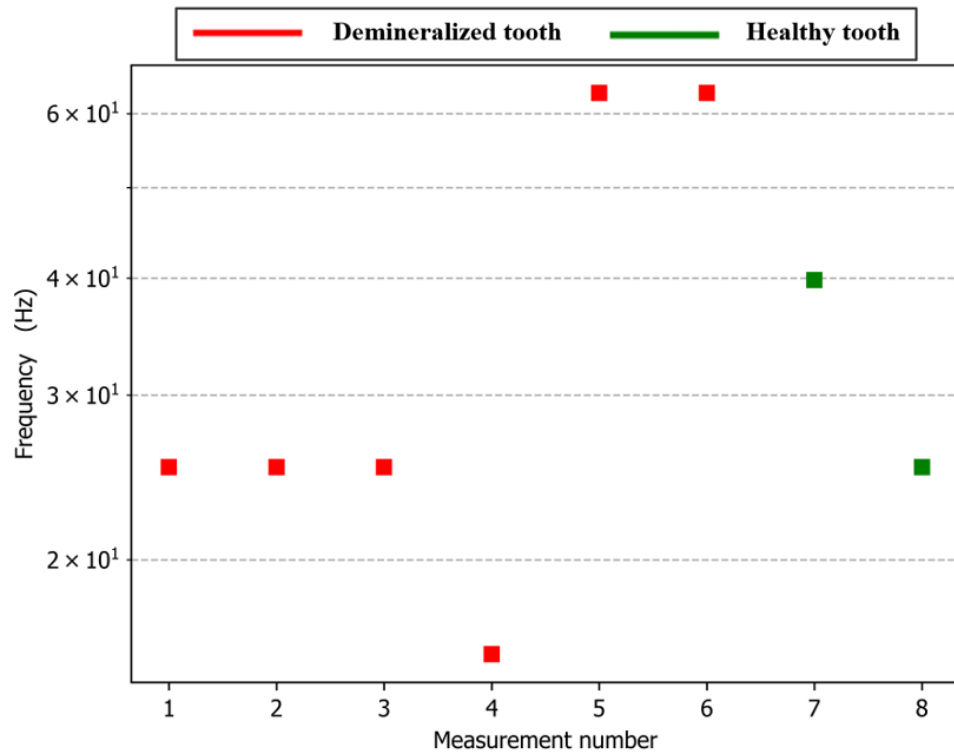


Figure 3.29: Frequency value at which the phase value of -45° is reached in each of the impedance measurements acquired on healthy tooth (green markers) and demineralized tooth (red markers) related to Figure 3.20

In this case, the phase value equal to -45° is reached at different frequency values between healthy and demineralized teeth: two impedance measurements on the demineralized tooth (green markers) reports a frequency value higher than that obtained for measurements on the healthy tooth, but most of measurements on the tooth after demineralization show a not consistent result.

Figure 3.30 shows the frequency values at which the phase value equal to -45° is reached in each of the impedance measurements on the same tooth represented in **Figure 3.23** before and after the process of demineralization.

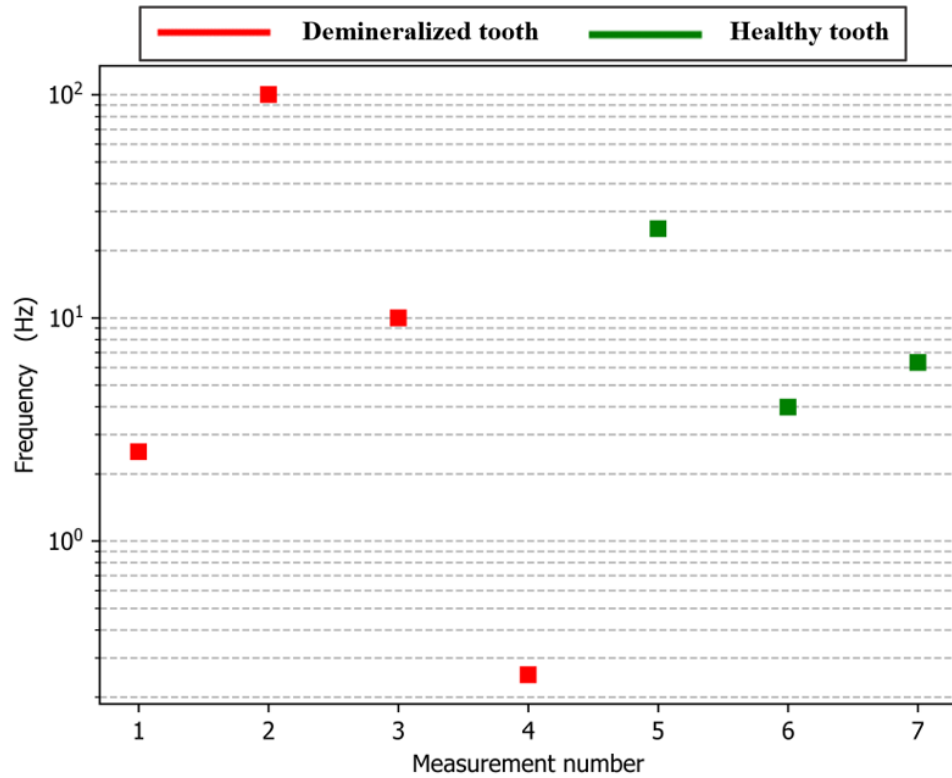
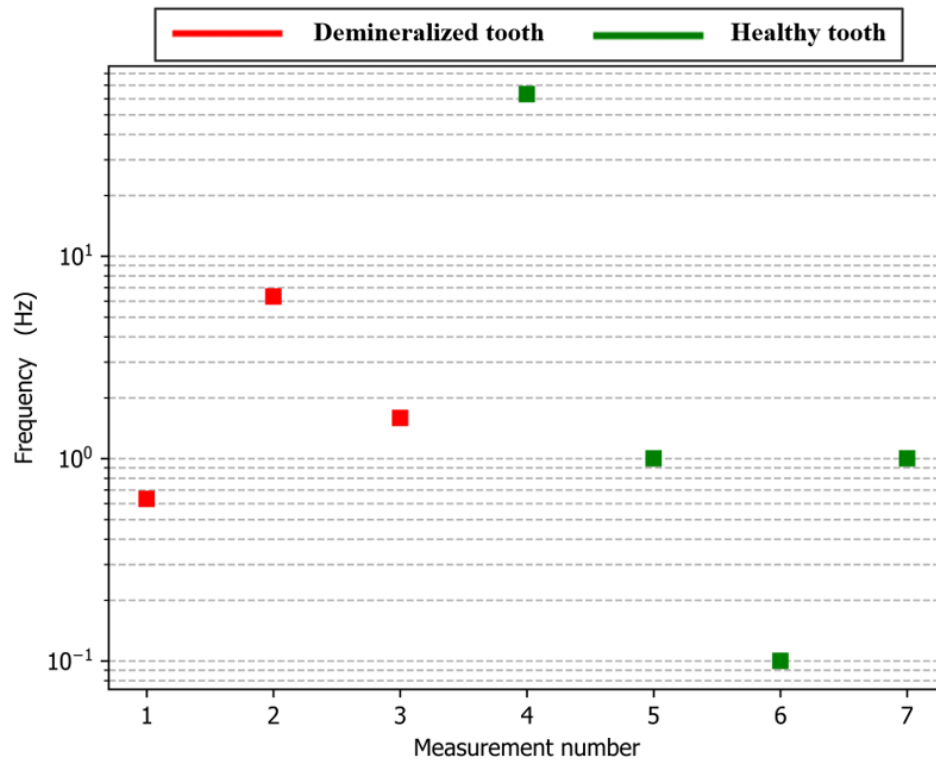


Figure 3.30: Frequency value at which the phase value of -45° is reached in each of the impedance measurements acquired on healthy tooth (green markers) and demineralized tooth (red markers) related to Figure 3.23

This case results similar with respect to the previous one, so it is impossible to discriminate between healthy and demineralised teeth.

Figure 3.31 shows the frequency values at which the phase value equal to -45° is reached in each of the impedance measurements on the same tooth represented in **Figure 3.25** before and after the process of demineralization.



***Figure 3.31:** Frequency value at which the phase value of -45° is reached in each of the impedance measurements acquired on healthy tooth (green markers) and demineralized tooth (red markers) related to Figure 3.25*

In this last case, related to **Figure 3.25**, impedance measurements, acquired on the same tooth pre and post demineralization, show higher frequency values at which the phase reaches -45° for the demineralized tooth than the healthy one for most of the measure, but in some points a different behaviour can be observed.

Figure 3.32 shows the frequency values at which the phase value equal to -45° is reached in each of the impedance measurements on some samples before and after the process of demineralization. In this graph not all measurements are reported, in fact measurements related to “problematic” teeth (outliers) are eliminated.

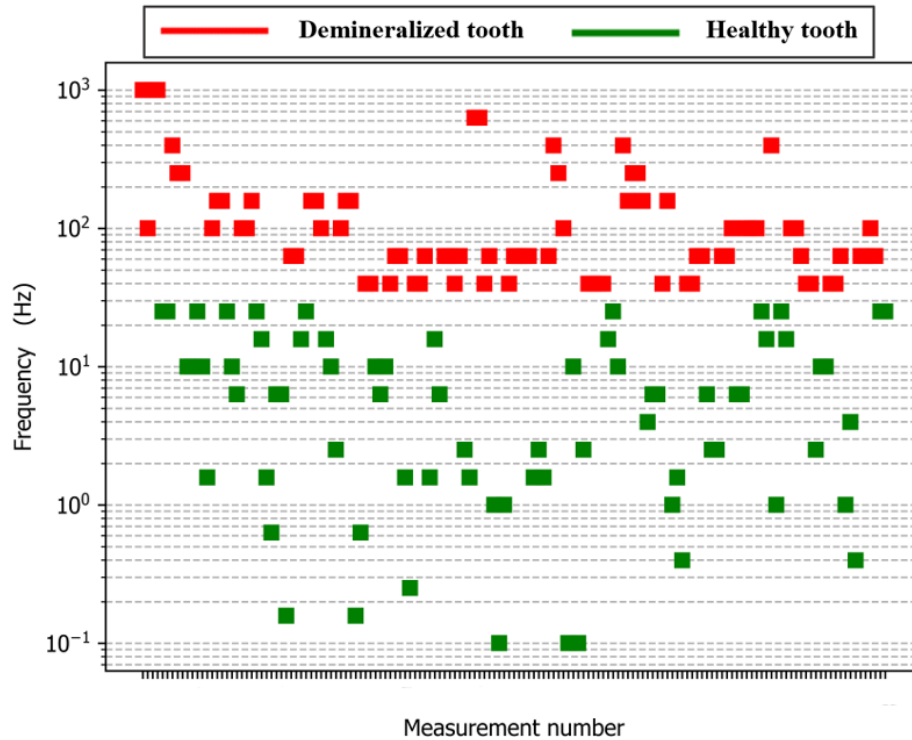


Figure 3.32: Frequency value at which the phase value of -45° is reached in each of the impedance measurements acquired on healthy teeth (green markers) and demineralized teeth (red markers)

In **Figure 3.32** a clear separation between samples pre and post demineralization can be seen. Consequently, it was decided to distinguish between healthy and decayed teeth by analysing the phase instead of the impedance module. In addition, the phase does not depend on the sample area, but only on its dielectric properties, so it can be a trustworthy parameter to differentiate teeth in the two clusters.

In conclusion, it has been decided to evaluate the frequency with which the phase reaches the -45° value to distinguish between samples before and after the treatment.

3.9 Demineralization process examined in different surface points

Impedance measurements are performed at five points per tooth because they provide a more detailed view of each sample.

Impedance spectra can display different curves, as well as overlapping curves. In fact, **Figure 3.33** shows curves with different trends for the sound tooth examined and overlapping curves for the demineralized tooth.

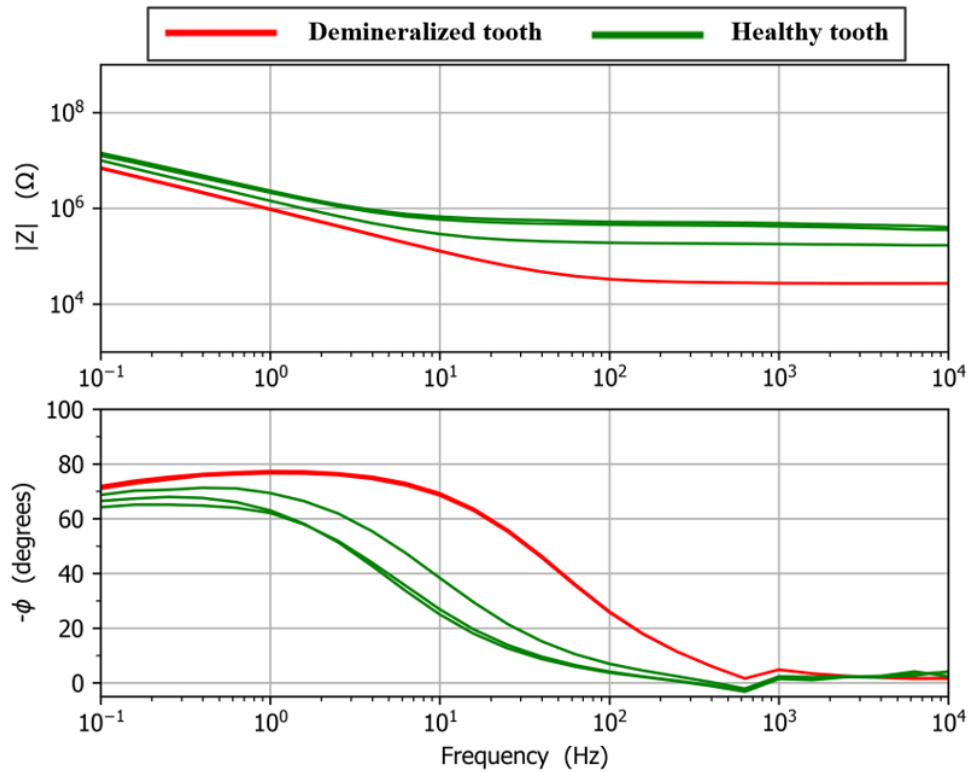


Figure 3.33: Impedance spectra, as Bode diagram, of the healthy (green lines) and demineralized (red lines) tooth

The shape is the same for all curves and some of them are very similar: this may be related to the fact that these impedance measurements are acquired in areas with similar properties. On the other hand, impedance measurements related to the demineralized tooth are represented by overlapping curves: this may be related to different measurements acquired in areas equally affected by demineralization.

At high magnification (4100 x), the SEM image, captured for this sample and reported in **Figure 3.34** demineralised areas are hardly visible.

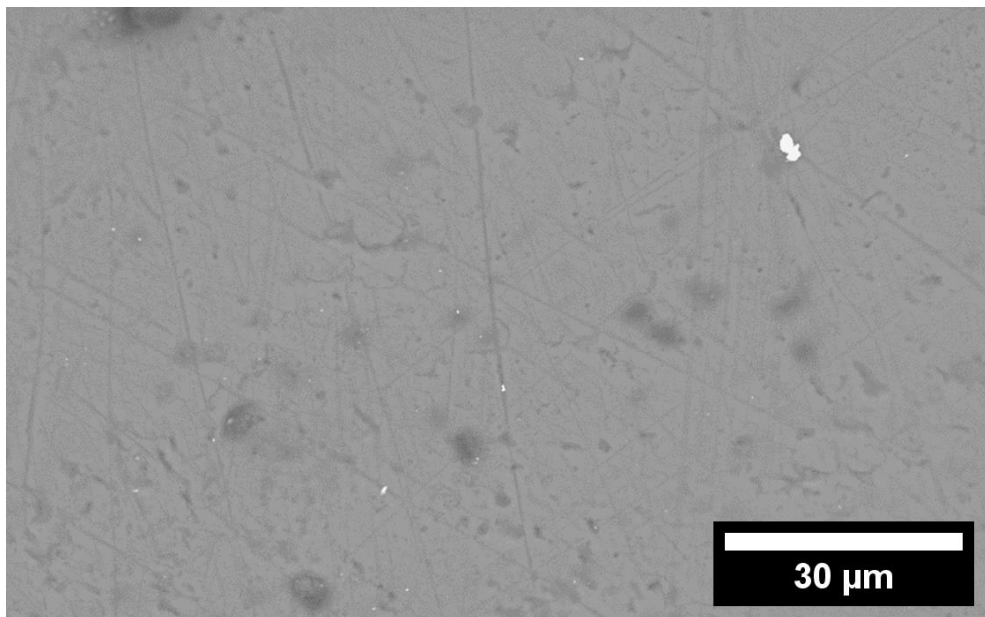


Figure 3.34: SEM image of a demineralized tooth

Figure 3.35 shows demineralized zones, captured at high magnification (5400 x).

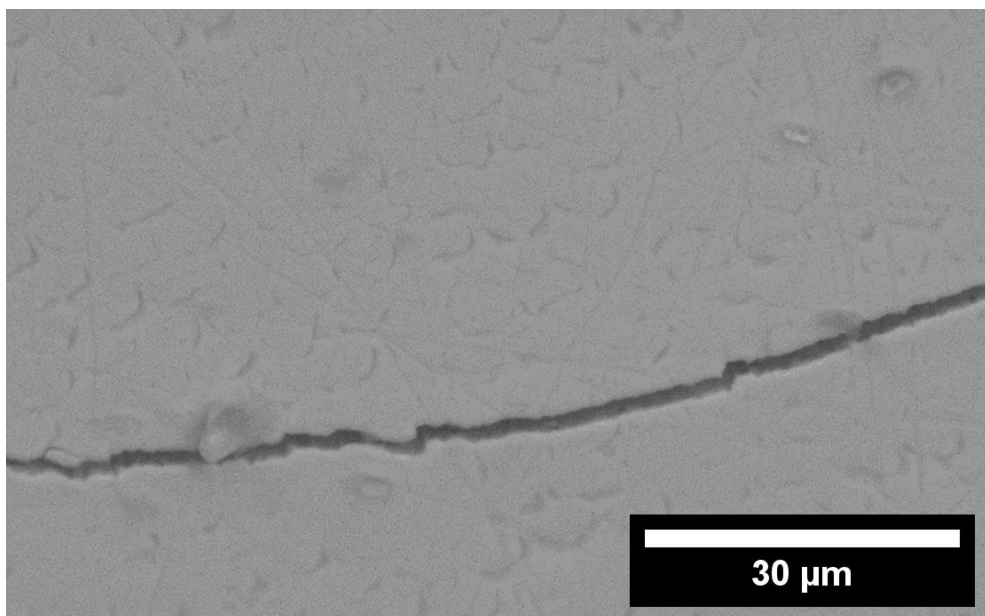


Figure 3.35: SEM image of a demineralized tooth

These SEM images show demineralized areas on the surface of the sample. Impedance measurements acquired on the healthy tooth are different than those acquired on the demineralized one due to the presence of these demineralized areas.

4. Conclusions and future developments

Dental disease management has been revolutionized by the scientific advances of the past century, but dental caries remains the most important chronic disease affecting people.

This experimental thesis proposes the use of impedance spectroscopy as additional diagnostic method in clinical practice to assess carious Raman spectroscopy and the use of the scanning electron microscope are used to verify the impedance findings.

The results obtained in this experimental thesis show the possibility of distinguishing healthy teeth from demineralized teeth through a variation in the electrical characteristics of the tooth.

In the case of demineralized teeth, the values of the impedance modulus at high frequencies are lower than that of healthy teeth, while the impedance phase maintains values close to 0° for a larger frequency range in the case of the healthy tooth and tends to values close to about -60° below 1 Hz. The phase reaches its maximum, below 1 Hz, at about a value equal to -70° in the case of the demineralized tooth.

Spectra modelled with an equivalent electrical circuit show capacitive behaviour, associated with double-layer capacitance, at low frequencies and resistive behaviour, associated with tooth interface, at high frequencies. The parameter with the highest variability between healthy and decayed teeth is the resistance R_0 , the double layer capacitance is not significantly affected by the carious process, while all parameters vary due to variability in the samples size.

The phase trend does not depend on the sample dimensions and the phase of 45° is reached at a frequency greater than 10 Hz for demineralized teeth and less than 10 Hz for healthy teeth. This parameter is a threshold to distinguish between healthy and demineralized teeth.

The SEM images of each sample acquired pre and post demineralization show a smooth and hard surface for healthy teeth and a surface characterized by hexagonal structures, with an alveolar appearance, for demineralized teeth. The intensity of the 960 cm^{-1} peak, monitored by Raman spectroscopy, decreases as the degree of demineralisation increases.

Significant variability in measurements between teeth belonging to the same group (pre-demineralization and post-demineralization) was observed due to morphological differences in the samples.

Future research will evaluate the proposed methodology in different solutions, like artificial saliva, or using different probes. Other studies will improve the statistics in order to validate this approach on a larger number of samples and with the purpose to assess its accuracy. In addition, once validated, the proposed method can also be used to evaluate the demineralisation state of human dentin and a new probe can be developed. In addition, impedance spectroscopy can also be proposed to study micro-leakages between dental and filler materials.

More complex processing algorithms will be studied, for example multidimensional analysis or machine learning tools [202-204].

List of Abbreviations

ICDAS	International Caries Detection and Assessment System
PDL	Periodontal ligament
HAP, HA	Hydroxyapatite ($\text{Ca}_{10}(\text{PO}_4)_6(\text{OH})_2$)
DEJ	Dentin-enamel-junction
OH	Hydroxyl
EDS	X-ray energy dispersive spectroscopy
ECM	Mineralized extracellular matrix
FAP	Fluorapatite
CPP-ACP	Casein phosphopeptide–amorphous calcium phosphate
TCP	Tricalcium phosphate
CaPs	Calcium phosphates
WHO	World Health Organization
BWR	Bitewing radiography
LF	Laser Fluorescence measurement
NILT	Near-Infrared Light Transillumination
EIS	Electrochemical Impedance Spectroscopy
IS	Impedance Spectroscopy
CCD	Charge-coupled device
ECM	Electrical Conductance Measurements
TACT	Tuned-aperture computed tomography
DIFOTI	Digital Image fibre-optic transillumination
QLF	Quantitative light/laser-induced fluorescence
ECM	Electrochemical machining
SEM	Scanning electron microscopy
FESEM	Field emission scanning electron microscopy
EDX	Energy Dispersive X-ray Analysis
XRD	X-Ray Diffraction
TMR	Total mixed rations
DC	Direct current
FTIR	Raman and Fourier transform infrared

List of Symbols

% w/v	Percent weight/volume
K_a	Equilibrium constant for acid dissociation or dissolution constant
pKa	Logarithmic value of K_a
Z	Impedance
Z	Impedance module
Z_{Re}	Real contribution of impedance
Z_{Im}	Imaginary contribution of impedance
V	Alternating potential
I	Electric current
V_0	Potential amplitude
I_0	Current amplitude
ω	Radial frequency
f	Frequency of the signal
ϕ	Phase
WE	Working electrode
CE	Counter electrode
R	Resistance
R_{sol}	Solution resistance
R_{ct}	Transfer resistance
C	Capacitance
C_{dl}	Double layer capacitor
L	Inductance
W	Warburg element
CPE	Constant phase element
Y_0	Constant independent of the frequency
α	CPE power
λ	Wavelength

References

- [1] Sannino I., Angelini E., Parvis M., Arpaia P., Grassini S., 2022, Impedance spectroscopy for monitoring sound teeth and carious lesions, *2022 IEEE International Instrumentation and Measurement Technology Conference (I2MTC)*, 1-5. [DOI: [10.1109/I2MTC48687.2022.9806564](https://doi.org/10.1109/I2MTC48687.2022.9806564)]
- [2] James S. L., Abate D., Abate K. H., Abay S. M., Abbafati C., Abbasi N., Abbastabar H., Abd-Allah F., Abdela J., Abdelalim A., et al., 2018, Global, regional, and national incidence, prevalence, and years lived with disability for 354 diseases and injuries for 195 countries and territories, 1990–2017: a systematic analysis for the global burden of disease study 2017, *The Lancet*, **392**(10159), 1789–1858.
- [3] Kassebaum N., Bernabe E., Dahiya M., Bhandari B., Murray C., Marcenes W., 2015, Global burden of untreated caries: a systematic review and metaregression, *Journal of dental research*, **94**(5), 650–658.
- [4] Abou Neel E.A., Aljabo A., Strange A., Ibrahim S., Coathup M., Young A.M., et al., 2016, Demineralization-remineralization dynamics in teeth and bone, *International Journal of Nanomedicine*, **11**, 4743-4763. [DOI: [10.2147/IJN.S107624](https://doi.org/10.2147/IJN.S107624)]
- [5] Selwitz R. H., Ismail A. I., Pitts N. B., 2007, Dental caries, *The Lancet*, **369**(9555), 51–59.
- [6] www.healthdirect.gov.au.
- [7] Thomson W., 2004, Dental caries experience in older people over time: what can the large cohort studies tell us?, *British dental journal*, **196**(2), 89–92.
- [8] Attivissimo F., Di Nisio A., Lucia Lanzolla A., Ragolia M., 2021, Analysis of position estimation techniques in a surgical em tracking system, *IEEE Sensors Journal*, **21**(13), 13389–13396.
- [9] Merchan M. T., Ismail A. I., 2021, Measurement and distribution of dental caries, in *Burt and Eklund's Dentistry, Dental Practice, and the Community*, Elsevier, 154–170.
- [10] Sannino I., Lombardo L., Angelini E., Parvis M., Arpaia P., Grassini S., 2022, Preliminary impedance spectroscopy study for carious lesions detection, *2022 IEEE International Symposium on Medical Measurements and Applications (MeMeA)*, 1-6. [DOI: [10.1109/MeMeA54994.2022.9856542](https://doi.org/10.1109/MeMeA54994.2022.9856542)]
- [11] Ismail A. I., Sohn W., Tellez M., Amaya A., Sen A., Hasson H., Pitts N. B., 2007, The international caries detection and assessment system (icdas): an integrated system for measuring dental caries, *Community dentistry and oral epidemiology*, **35**(3), 170–178.
- [12] Wheeler P., Burkitt H., Daniels V., 1987, Functional Histology: A Text and Colour Atlas, *Churchill Livingstone*.
- [13] www.vcdental.com.au.
- [14] www.mouthpower.org.jpg.
- [15] www.mouthhealthy.org.
- [16] <https://freemile.com/en/anatomy-of-the-mouth/tooth-anatomy/>.

- [17] Papagerakis P., Mitsiadis, T., 2018, Development and Structure of Teeth and Periodontal Teeth. In *Primer on the Metabolic Bone Diseases and Disorders of Mineral Metabolism*. [DOI:10.1002/9781119266594.ch117]
- [18] Ten Cate A.R., 1994, Oral Histology: Development, Structure, and Function 4th edn., Mosby.
- [19] I.M. Low et al., 2008, Mapping the structure, composition and mechanical properties of human teeth, *Materials Science and Engineering C* 28, 243–247.
- [20] Teruel J.deD., Alcolea A., Hernández A., Ruiz A.J., 2015, Comparison of chemical composition of enamel and dentine in human, bovine, porcine and ovine teeth. *Archives of oral biology*, 60(5), 768–775. [DOI:10.1016/j.archoralbio.2015.01.014]
- [21] Legeros R.Z., Legeros J.P., Phosphate minerals in human tissues. In: Nriagu JO, Moore P.B., Phosphate minerals, 1984, Springer; 351–85.
- [22] Anil A, I. Ibraheem W, A. Meshni A, et al., 2022, Demineralization and Remineralization Dynamics and Dental Caries., *Dentistry*. [DOI:10.5772/intechopen.105847]
- [23] Bigi A., Boanini E., 2017, Functionalized biomimetic calcium phosphates for bone tissue repair, *Journal of Applied Biomaterials and Functional Materials*, 15(4), e313-e325.
- [24] Lacruz R.S., Habelitz S., Wright J.T., Paine M.L., 2017, Dental enamel formation and implications for Oral health and disease, *Physiological Reviews*, 97(3), 939-993.
- [25] Reyes-Gasga J., Alcantara-Rodriguez C.M., Gonzalez-Trejo A.M., Madrigal-Colin A., 1997, *Acta Microscopica*, 6, 24-38.
- [26] Gutiérrez-Salazar M. del P., Reyes-Gasga J., 2003, Microhardness and chemical composition of human tooth, *Materials Research*, 6(3), 367–373. [DOI:10.1590/S1516-14392003000300011]
- [27] Teruel Jde D., Alcolea A., Hernández A., Ruiz A.J., 2015, Comparison of chemical composition of enamel and dentine in human, bovine, porcine and ovine teeth, *Arch Oral Biol*, 60(5), 768-775. [DOI:10.1016/j.archoralbio.2015.01.014]
- [28] Xu H.H., Smith D.T., Jahanmir S., Romberg E., Kelly J.R., Thompson V.P, Rekow E.D., 1998, Indentation damage and mechanical properties of human enamel and dentin, *J Dent Res*, 77(3), 472-80. [DOI: 10.1177/00220345980770030601]
- [29] Hart S., Hart T., 2007, Disorders of human dentin, *Cells Tissues Organs*, 186(1), 70–77.
- [30] Eastoe J., 1979, Enamel protein chemistry – past present and future, *J Dent Res*, 58(Spec Issue B), 753–764.
- [31] Weidmann S., Eyre D., 1967, Amino acid composition of enamel protein in the fully developed human tooth, *Caries Res*, 1(4), 349–355.
- [32] Felszeghy S., Holló K., Módis L., Lammi M., 2000, Type X collagen in human enamel development: a possible role in mineralization, *Acta Odontol Scand*, 58(4), 171–176.
- [33] Robinson C., Connell S., Kirkham J., Brookes S., Shore R., Smith M., 2004, The effect of fluoride on the developing tooth, *Caries Res*, 38(3), 268–276.
- [34] Barron M., McDonnell S., Mackie I., Dixon M., 2008, Hereditary dentine disorders: dentinogenesis imperfecta and dentine dysplasia, *Orphanet J Rare Dis*, 3, 31.

- [35] : Zheng X., Hu J., Chen Y., Zhu Y., Chen H., 2012, AFM study of the effects of collagenase and its inhibitors on dentine collagen fibrils, *J Dent*, **40**(2), 163–171.
- [36] Landis W.J., Song M.J., Leith A., McEwen L., McEwen B.F., 1993, Mineral and organic matrix interaction in normally calcifying tendon visualized in 3 dimensions by high-voltage electron-microscopic tomography and graphic image-reconstruction, *J Struct Biol*, **110**(1), 39–54.
- [37] Abou Neel E.A., Bozec L., Knowles J.C., et al., 2013, Collagen – emerging collagen based therapies hit the patient, *Adv Drug Deliv Rev*, **65**(4), 429–456.
- [38] Birk D., Silver F., 1984, Collagen fibrillogenesis in vitro: comparison of type I, II and II, *Arch Biochem Biophys*, **235**(1), 178–185.
- [39] Martinez E., da Silva L., Furuse C., de Araújo N., de Araújo V., 2009, Dentine matrix protein 1 (DMP1) expression in developing human teeth, *Braz Dent J*, **20**(5), 365–369.
- [40] Goldberg M., Kulkarni A.B., Young M., Boskey A., 2011, Dentin: structure, composition and mineralization: the role of dentin ECM in dentin formation and mineralization, *Front Biosci (Elite Ed)*, **3**, 711–735.
- [41] Depalle B., McGilvery C.M., Nobakhti S., Aldegaitner N., Shefelbine S.J., Porter A.E., 2021, Osteopontin regulates type I collagen fibril formation in bone tissue, *Acta Biomaterialia*, **120**, 194-202.
- [42] Almeida e Silva Júnior S., et al., 2011, Dental erosion: understanding this pervasive condition, *Journal of esthetic and restorative dentistry*, **23**(4), 205-16. [DOI:10.1111/j.1708-8240.2011.00451]
- [43] Shepherd T.J., Dirks W., Manmee C., et al., 2012, Reconstructing the life-time lead exposure in children using dentine in deciduous teeth, *Sci Total Environ*, **425**, 214–222.
- [44] Vanderby R., Provenzano P.P., 2003, Collagen in connective tissue: from tendon to bone; *J Biomech*, **36**(10), 1523–1527.
- [45] Burr D.B., 2004, Anatomy and physiology of the mineralized tissues: role in the pathogenesis of osteoarthritis, *Osteoarthr Cartil*, **12**(A), 20–30.
- [46] Ren Y.F., 2011, Dental erosion: etiology, diagnosis and prevention, *Dental Hygienist*, 75–84.
- [47] Scaramucci T., Carvalho J.C., Hara A.T., Zero D.T., 2015, Causes of Dental Erosion: Extrinsic Factors, *Dental Erosion and Its Clinical Management*, Springer International, 69–96.
- [48] Featherstone J.D., Lussi A., 2006, Understanding the chemistry of dental erosion, *Monogr Oral Sci*, **20**, 66–76.
- [49] <https://www.dentalcare.com/en-us/ce-courses/ce372>.
- [50] Machiulskiene V., Campus G., Carvalho J.C., Dige I., Ekstrand K.R., Jablonski-Momeni A., et al., 2020, Terminology of dental caries and dental caries management: Consensus report of a workshop organized by ORCA and cariology research group of IADR, *Caries Research*, **54**(1), 7-14.
- [51] Robinson C., Shore R.C., Brookes S.J., Strafford S., Wood S.R., Kirkham J., 2000, The chemistry of enamel caries, *Critical Reviews in Oral Biology and Medicine*, **11**(4), 481-495.

- [52] Silverstone L.M., 1973, Structure of carious enamel, including the early lesion, *Oral Sciences Reviews*, **3**, 100-160.
- [53] Palamara J., Phakey P.P., Rachinger W.A., Orams H.J., 1986, Ultrastructure of the intact surface zone of white spot and brown spot carious lesions in human enamel, *Journal of Oral Pathology*, **15**(1), 28-35.
- [54] Darling A.I., Mortimer K.V., Poole D.F., Ollis W.D., 1961, Molecular sieve behaviour of normal and carious human dental enamel, *Archives of Oral Biology*, **5**(3-4), 251-273.
- [55] Paris S., Schwendicke F., Keltsch J., Dorfer C., Meyer-Lueckel H., 2013, Masking of white spot lesions by resin infiltration in vitro, *Journal of Dentistry*, **41**(Suppl 5), e28-e34.
- [56] Marsh P.D., 1994, Microbial ecology of dental plaque and its significance in health and disease, *Advances in Dental Research*, **8**(2), 263-271.
- [57] Holly F.J., Gray J.A., 1968, Mechanism for incipient carious lesion growth utilizing a physical model based on diffusion concepts, *Archives of Oral Biology*, **13**(3), 319-334.
- [58] Moreno E.C., Zahradnik R.T., 1974, Chemistry of enamel subsurface demineralization in vitro, *Journal of Dental Research*, **53**(2), 226-235.
- [59] Mutahar M., Carpenter G., Bartlett D. *et al.*, 2017, The presence of acquired enamel pellicle changes acid-induced erosion from dissolution to a softening process, *Scientific Reports*, **7**(10920). [DOI:10.1038/s41598-017-11498-1]
- [60] Brown W.E., 1974, Physicochemical mechanisms of dental caries, *Journal of Dental Research*, **53**(2), 204-216.
- [61] Olek A., Klimek L., Bołtacz-Rzepkowska E., 2020, Comparative scanning electron microscope analysis of the enamel of permanent human, bovine and porcine teeth, *Journal of Veterinary Science*, **21**(6), e83.
- [62] De Medeiros R.C., Soares J.D., De Sousa F.B., 2012, Natural enamel caries in polarized light microscopy: Differences in histopathological features derived from a qualitative versus a quantitative approach to interpret enamel birefringence, *Journal of Microscopy*, **246**(2), 177-189.
- [63] Barbosa de Sousa F., Dias Soares J., Sampaio Vianna S., 2013, Natural enamel caries: A comparative histological study on biochemical volumes, *Caries Research*, **47**(3), 183-192.
- [64] Silverstone L.M., 1968, The surface zone in caries and in caries-like lesions produced in vitro, *British Dental Journal*, **125**(4), 145-157.
- [65] Wiegand A., Attin T., 2007, Occupational dental erosion from exposure to acids – a review, *Occup Med (Lond)*, **57**(3), 169–176.
- [66] Lussi A., Jaeggi T., 2008, Erosion – diagnosis and risk factors, *Clin Oral Investig*, **12**(S1), 5–13.
- [67] Zhang J., Du Y., Wei Z., Tai B., Jiang H., Du M., 2015, The prevalence and risk indicators of tooth wear in 12- and 15-year-old adolescents in Central China, *BMC Oral Health*, **15**(1), 120.
- [68] Lussi A., Von Salis-Marincek M., Ganss C., Hellwig E., Cheaib Z., Jaeggi T., 2012, Clinical study monitoring the pH on tooth surfaces in patients with and without erosion, *Caries Res*; **46**(6), 507–512.

- [69] Barbour M.E., Finke M., Parker D.M., Hughes J.A., Allen G.C., Addy M., 2006, The relationship between enamel softening and erosion caused by soft drinks at a range of temperatures, *J Dent*, **34**(3), 207–213.
- [70] Zheng J., Huang H., Shi M.Y., Zheng L., Qian L.M., Zhou Z.R., 2011, In vitro study on the wear behaviour of human tooth enamel in citric acid solution, *Wear*, **271**(9–10), 2313–2321.
- [71] Taji S., Seow W.K., 2010, A literature review of dental erosion in children, *Aust Dent J*, **55**(4), 358–367.
- [72] Shellis R.P., Finke M., Eisenburger M., Parker D.M., Addy M., 2005, Relationship between enamel erosion and liquid flow rate, *Eur J Oral Sci*, **113**(3), 232–238.
- [73] Tahmassebi J.F., Duggal M.S., Malik-Kotru G., Curzon M.E.J., 2006, Soft drinks and dental health: a review of the current literature, *J Dent*, **34**(1), 2–11.
- [74] Lussi A., Megert B., Peter Shellis R., Wang X., 2012, Analysis of the erosive effect of different dietary substances and medications, *Br J Nutr*, **107**(02), 252–262.
- [75] Perrin D.D., 1963, Buffers of low ionic strength for spectrophotometric pK determinations, *Aust J Chem*, **16**(4), 572–578.
- [76] Torres-Gallegos I., Zavala-Alonso V., Patiño-Marín N., Martínez-Castañón G.A., Anusavice K., Loyola-Rodríguez J.P., 2012, Enamel roughness and depth profile after phosphoric acid etching of healthy and fluorotic enamel, *Aust Dent J*, **57**(2), 151–156.
- [77] Cairns M., Watson M., Creanor S.L., Foye R.H., 2002, The pH and titratable acidity of a range of diluting drinks and their potential effect on dental erosion, *J Dent*, **30**(7–8), 313–317.
- [78] Sadler G.D., Murphy P.A., 2010, pH and Titratable Acidity, *Nielsen, S.S., Ed., Food Analysis, Springer, Boston, MA*, 219-238.
- [79] Singh S., Jindal R., 2010, Evaluating the buffering capacity of various soft drinks, fruit juices and tea, *J Conserv Dent*, **13**(3), 129–131.
- [80] Johansson K., Sorvari R., Birkhed D., Meurman J.H., 2001, Dental erosion in deciduous teeth – an in vivo and in vitro study, *J Dent*, **29**(5), 333–340.
- [81] Caufield P.W., Griffen A.L., 2004, Dental caries. An infectious and transmissible disease, *Pediatr Clin North Am*, **47**(5), 1001–1019.
- [82] Low I.M., Alhuthali A., 2008, In-situ monitoring of dental erosion in tooth enamel when exposed to soft drinks, *Mater Sci Eng C*, **28**(8), 1322–1325.
- [83] Loesche W.J., 1992, The specific plaque hypothesis and the antimicrobial treatment of periodontal disease, *Dental Update*, **19**, 70.
- [84] Becker M.R., Paster B.J., Leys E.J., Moeschberger M.L., Kenyon S.G., Galvin J.L., et al., 2002, Molecular analysis of bacterial species associated with childhood caries, *Journal of Clinical Microbiology*, **40**(3), 1001-1009.
- [85] Munson M.A., Banerjee A., Watson T.F., Wade W.G., 2004, Molecular analysis of the microflora associated with dental caries, *Journal of Clinical Microbiology*, **42**(7), 3023-3029.
- [86] Corby P.M., Lyons-Weiler J., Bretz W.A., Hart T.C., Aas J.A., Boumenna T., et al., 2005, Microbial risk indicators of early childhood caries, *Journal of Clinical Microbiology*, **43**(11), 5753-5759.

- [87] Aas J.A., Griffen A.L., Dardis S.R., Lee A.M., Olsen I., Dewhirst F.E., et al., 2008, Bacteria of dental caries in primary and permanent teeth in children and young adults, *Journal of Clinical Microbiology*, **46**(4), 1407-1417.
- [88] Belda-Ferre P., Alcaraz L.D., Cabrera-Rubio R., Romero H., Simon-Soro A., Pignatelli M., et al., 2012, The oral metagenome in health and disease, *The ISME Journal*, **6**(1), 46-56.
- [89] Kim M.J., Lee M.J., Kim K.M., Yang S.Y., Seo J.Y., Choi S.H., et al., 2021, Enamel demineralization resistance and remineralization by various fluoridereleasing dental restorative materials. *Materials (Basel)*, **14**(16), 223-230.
- [90] Lussi A., Schlueter N., Rakhmatullina E., Ganss C., 2011, Dental erosion—An overview with emphasis on chemical and histopathological aspects, *Caries Research*, **45**(Suppl 1), 2-12.
- [91] Ten Cate J.M., 2009, The need for antibacterial approaches to improve caries control, *Advances in Dental Research*, **21**(1), 8-12.
- [92] Meurman J.H., ten Cate J., 1996, Pathogenesis and modifying factors of dental erosion, *Eur J Oral Sci*, **104**(Pt 2), 199–206.
- [93] Bowden G.H.W., 2009, The microbial ecology of dental caries, *Microbial Ecology in Health and Disease*, **12**(3), 138-148.
- [94] Abou Neel E.A., Bozec L., Perez R.A., Kim H.-W., Knowles J.C., 2015, Nanotechnology in dentistry: prevention, diagnosis, and therapy, *Intell Surf.*, **10**, 6371–6394.
- [95] Ten Cate J.M., Buzalaf M.A.R., 2019, Fluoride mode of action: Once there was an observant dentist, *Journal of Dental Research*, **98**(7), 725-730.
- [96] Marinho V.C., Higgins J.P., Logan S, Sheiham A., 2003, Topical fluoride (toothpastes, mouthrinses, gels or varnishes) for preventing dental caries in children and adolescents, *Cochrane Database of Systematic Reviews*, **4**, 1-157.
- [97] Rios D., Honório H.M., Francisconi L.F., Magalhães A.C., de Andrade Moreira Machado M.A., Buzalaf M.A.R., 2008, In situ effect of an erosive challenge on different restorative materials and on enamel adjacent to these materials, *J Dent.*, **36**(2), 152–157.
- [98] Reynolds E., Cai F., Cochrane N., et al., 2008, Fluoride and casein phosphopeptide–amorphous calcium phosphate, *J Dent Res*, **87**(4), 344–348.
- [99] Dowd F., 1999, Saliva and dental caries, *Dent Clin North Am*, **43**(4), 579–597.
- [100] Twetman S., 2012, Are we ready for caries prevention through bacteriotherapy?, *Braz Oral Res*, **26**(Suppl 1), 64–70.
- [101] Keller M., Nøhr L., Karlsson I., Twetman S., 2014, Effect of tablets containing probiotic bacteria (*Lactobacillus reuteri*) on early caries lesions in adolescents: a pilot study, *Benef Microbes*, **5**(4), 403–407.
- [102] Lee S., Kim Y., 2014, A comparative study of the effect of probiotics on cariogenic biofilm model for preventing dental caries, *Arch Microbiol*, **196**(8), 601–609.
- [103] Wu C.C., Lin C.T., Wu C.Y., Peng W.S., Lee M.J., YC T., 2015, Inhibitory effect of *Lactobacillus salivarius* on *Streptococcus mutans* biofilm formation, *Mol Oral Microbiol*, **30**(1), 16–26.
- [104] Haukioja A., 2010, Probiotics and oral health, *Eur J Dent*, **4**(3), 348–355.

- [105] Stock M., 2015, Dental Device Promises Pain-Free Tooth Repair, <https://www.reuters.com/article/us-dental-device-idUSKCN0QU21C20150825>
- [106] Ferracane J.L., 2011, Resin composite – state of the art, *Dent Mater*, **27**(1), 29–38.
- [107] Zandoná A.F., Zero D.T., 2006, Diagnostic tools for early caries detection, *J Am Dent Assoc*, **137**, 1675-84.
- [108] Yassin O.M., 1995, In vitro studies of the effect of a dental explorer on the formation of an artificial carious lesion., *ASDC journal of dentistry for children*, **62**(2), 111–117.
- [109] Beltrami E., da Costa Silveira L., Perretto R., 1990, The effect of the exploratory probe on demineralized enamel, *Dens*, **6**(1-2), 1–4.
- [110] Ismail A., 2004, Visual and visuo-tactile detection of dental caries, *Journal of dental research*, vol. **83**(1 suppl), 56–66.
- [111] Traanaeus S., Shi X.Q., Lindgren L.E., Trollås K., Angmar-Mansson B., 2002, *In vivo* repeatability and reproducibility of the quantitative light-induced fluorescence method, *Caries Res*, **36**, 3-9.
- [112] Foros P., Oikonomou E., Koletsi D., Rahiotis C., 2021, Detection methods for early caries diagnosis: A systematic review and meta-analysis, *Caries Research*, **55**(4), 247–259.
- [113] Litzenburger F., Schäfer G., Hickel R., Kühnisch J., Heck K., 2021, Comparison of novel and established caries diagnostic methods: a clinical study on occlusal surfaces, *BMC Oral Health*, **21**(1), 1–10.
- [114] Topping G., Pitts N., 2009, Clinical visual caries detection, *Detection, assessment, diagnosis and monitoring of caries*, **21**, 15–41.
- [115] Schwendicke F., Tzschope M., Paris S., 2015, Radiographic caries detection: a systematic review and meta-analysis, *Journal of dentistry*, **43**(8), 924–933.
- [116] Kidd E., Pitts N., 1990, A reappraisal of the value of the bitewing radiograph in the diagnosis of posterior approximal caries, *British dental journal*, **169**(7), 195–200.
- [117] Söchtig F., Hickel R., Kühnisch J., 2014, Caries detection and diagnostics with near-infrared light transillumination: clinical experiences., *Quintessence International*, **45**(6).
- [118] Schaefer G., Pitchika V., Litzenburger F., Hickel R., Kühnisch J., 2018, Evaluation of occlusal caries detection and assessment by visual inspection, digital bitewing radiography and near-infrared light transillumination, *Clinical oral investigations*, **22**(7), 2431–2438.
- [119] Jablonski-Momeni A., Heinzl-Gutenbrunner M., Haak R., Krause F., 2017, Use of ac impedance spectroscopy for monitoring sound teeth and incipient carious lesions, *Clinical oral investigations*, **21**(8), 2421–2427.
- [120] Abdelaziz M., Krejci I., Perneger T., Feilzer A., Vazquez L., 2018, Near infrared transillumination compared with radiography to detect and monitor proximal caries: A clinical retrospective study, *Journal of dentistry*, **70**, 40–45.
- [121] Adeyemi A. A., Jarad F. D., Komarov G. N., Pender N., Higham S. M., 2008, Assessing caries removal by undergraduate dental students using quantitative light-induced fluorescence, *Journal of Dental Education*, **72**(11), 1318–1323.
- [122] Mohanraj M., Prabhu V.R., Senthil R., 2016, Diagnostic methods for early detection of dental caries - A review, *Int J Pedod Rehabil*, **1**, 29-36.

- [123] Vaarkamp J., ten Bosch J.J., Verdonschot E.H., Bronkhorst E.M., 2000, The real performance of bitewing radiography and fiber-optic transillumination in approximal caries diagnosis, *J Dent Res*, **79**, 1747-51.
- [124] Shi X.Q., Welander U., Angmar-Mansson B., 2000, Occlusal caries detection with KaVo DIAGNOdent and radiography: An *in vitro* comparison, *Caries Res*, **34**, 151-8.
- [125] Aleksejuniene J., Tranaeus S., Skudutyte-Rysstad R., 2006, DIAGNOdent – an adjunctive diagnostic method for caries diagnosis in epidemiology, *Community Dent Health*, **23**, 217-21.
- [126] Pretty I. A., 2006, Caries detection and diagnosis: novel technologies, *Journal of dentistry*, **34**(10), 727-39. [DOI:10.1016/j.jdent.2006.06.001]
- [127] Kühnisch J., Bücher K., Hickel R., 2007, The intra/inter-examiner reproducibility of the new DIAGNOdent Pen on occlusal sites, *J Dent*, **35**, 509-12.
- [128] Angmar-Mansson B., ten Bosch J.J., 1993, Advances in methods for diagnosing coronal caries – a review, *Adv Dent Res*, **7**, 70-9.
- [129] Es Sebar L., Iannucci L., Gori C., Re A., Parvis M., Angelini E., and Grassini S., 2020, In-situ multi-analytical study of ongoing corrosion processes on bronze artworks exposed outdoors, *Acta IMEKO*, **10**(1), 241–249.
- [130] No`e C., Iannucci L., Malburet S., Graillot A., Sangermano M., Grassini S., 2021, New uv-curable anticorrosion coatings from vegetable oils, *Macromolecular Materials and Engineering*, **306**(6).
- [131] Sun D., Frankel G. S., Brantley W. A., Heshmati R. H., Johnston W. M., 2021, Electrochemical impedance spectroscopy study of corrosion characteristics of palladium–silver dental alloys, *Journal of Biomedical Materials Research Part B: Applied Biomaterials*, **109**(11), 1777–1786.
- [132] Moccaldi N., Sannino I., 2020, A customized bioimpedance meter for monitoring insulin bioavailability, *2020 IEEE International Instrumentation and Measurement Technology Conference (I2MTC)*, 1–5, IEEE.
- [133] Sebar L. E., Iannucci L., Angelini E., Grassini S., Parvis M., 2020, Electrochemical impedance spectroscopy system based on a teensy board, *IEEE Transactions on Instrumentation and Measurement*, **70**(1–9).
- [134] Longbottom C., Huysmans M.-C., 2004, Electrical measurements for use in caries clinical trials, *Journal of Dental Research*, **83**(1 suppl), 76–79.
- [135] Huysmans M.-C., Longbottom C., Pitts N., Los P., Bruce P., 1996, Impedance spectroscopy of teeth with and without approximal caries lesions-an *in vitro* study, *Journal of dental research*, **75**(11), 1871–1878.
- [136] Andrei M., Pirvu C., Demetrescu I., 2014, Electrochemical impedance spectroscopy in understanding the influence of ultrasonic dental scaling on the dental structure–dental filling interface, *European journal of oral sciences*, **122**(6), 411–416.
- [137] Scotti N., Comba A., Cadenaro M., Fontanive L., Breschi L., Monaco C., Scotti R., 2016, Effect of lithium disilicate veneers of different thickness on the degree of conversion and microhardness of a light-curing and a dual-curing cement., *The International journal of prosthodontics*, **29**(4), 384–388.

- [138] Carrigan P.J., Morse D.R., Furst M. L., Sinai I.H., 1984, A scanning electron microscopic evaluation of human dentinal tubules according to age and location, *Journal of endodontics*, **10**(8), 359–363.
- [139] Ashley P., Blinkhorn A., Davies R., 1998, Occlusal caries diagnosis: an in vitro histological validation of the electronic caries monitor (ecm) and other methods, *Journal of dentistry*, **26**(2), 83–88.
- [140] Pradelle-Plasse N., Wenger F., Colon P., 2002, Effect of conditioners on dentin permeability using an impedance method, *Journal of dentistry*, **30**(5-6), 251–257.
- [141] Mortensen D., Hessing-Olsen I., Ekstrand K. R., Twetman S., 2018, In vivo performance of impedance spectroscopy, laser fluorescence, and bitewing radiographs for occlusal caries detection, *Quintessence Int*, **49**(4), 293–299.
- [142] Mortensen D., Dannemand K., Twetman S., Keller M. K., 2014, Detection of non-cavitated occlusal caries with impedance spectroscopy and laser fluorescence: an in vitro study, *The open dentistry journal*, **8**, 28.
- [143] Hall A., Girkin J.M., 2004, A review of potential new diagnostic modalities for carious lesions., *J Dent Res*, **83**, C89-94.
- [144] Kaneko K., Matsuyama K., Nakashima K., 1999, Quantification of early carious lesions by using an infrared camera in vitro, *Stookey GK, editor. Early Detection of Dental Caries II: Proceedings of the 4th Annual Indiana Conference*, 83-100.
- [145] Berry E., Fitzgerald A.J., Zinov'ev N.N., Walker G.C., Homer-Vanniasinkam S., Sudworth C.D., 2003, Optical Properties of Tissue Measured Using Terahertz Pulsed Imaging, *Proceedings of SPIE: Medical Imaging 2003: Physics of Medical Imaging*, 459-70.
- [146] Choo-Smith L.P., Dong C.C., Cleghorn B., Hewko M., 2008, Shedding new light on early caries detection., *J Can Dent Assoc*, **74**, 913-8.
- [147] Jeon R.J., Han C., Mandelis A., Sanchez V., Abrams S.H., 2004, Diagnosis of pit and fissure caries using frequency-domain infrared photothermal radiometry and modulated laser luminescence, *Caries Res*, **38**, 497-513.
- [148] www.chemtube3d.com.
- [149] encyclopedia.pub.
- [150] www.orthobullets.com.
- [151] it.wikipedia.org.
- [152] Qanbar A., Abdulla A.A.M., Abutayyem H., El Din Mohamed S.K., 2021, Comparative evaluation of the efficacy of silver diamine fluoride, sodium fluoride and GC tooth mousse plus and fluoride varnish as an antibacterial agent in childhood caries: As a literature review, *Dental Res Manag*, **5**, 1-7.
- [153] Bard A.J., Faulkner L.R., 1980, Electrochemical methods: fundamental and applications, *Wiley*.
- [154] Levinkind M., Vandernoot T.J., Elliott J.C., 1990, Electrochemical impedance characterization of human and bovine enamel, *Journal of Dental Research*, **69**, 1806–11.
- [155] Levinkind M., Vandernoot T.J., Elliott J.C., 1992, Evaluation of smear layers on serial sections of human dentin by means of electrochemical impedance measurements, *Journal of Dental Research*, **71**, 426–33.

- [156] Aziza H.E., Alec S.H., Girish M.K., 2004, In vitro analysis of smear layer on human dentine using ac-impedance spectroscopy, *Journal of Dentistry*, **32**, 547–54.
- [157] Huysmans M.C., Longbottom C., Pitts N.B., Los P., Bruce P.G., 1996, Impedance spectroscopy of teeth with and without approximal caries lesions-an in vitro study, *Journal of Dental Research*, **75**, 1871–8.
- [158] Longbottom C., Huysmans M.C., Pitts N.B., Los P., Bruce P.G., 1996, Detection of dental decay and its extent using a.c. impedance spectroscopy, *Nature Medicine*, **2**, 235–7.
- [159] Liao Y.M., Feng Z.D., Chen Z.L., 2007, In situ tracing the process of human enamel demineralization by electrochemical impedance spectroscopy (EIS), *Journal of Dentistry*, **35**, 425–30.
- [160] Ollmar S., Nyren M., Nicander I., Emtestam L., 1994, Electrical impedance compared with other non-invasive bioengineering techniques and visual scoring for detection of irritation in human skin, *British Journal of Dermatology*, **130**, 29–36.
- [161] Ackmann J.J., Seitz M.A., Dawson C.A., Hause L.L., 1996, Specific impedance of canine blood, *Annals of Biomedical Engineering*, **24**, 58–66.
- [162] Behari J., Singh S., 1998, Bioelectric characteristics of unstressed in vivo bone, *Medical and Biological Engineering and Computing*, **19**, 49–54.
- [163] Selwitz RH, Ismail AI, Pitts NB., 2007, Dental caries, *The Lancet*, **369**, 51–9.
- [164] Pretty I.A., 2006, Caries detection and diagnosis: novel technologies, *Journal of Dentistry*, **34**, 727–39.
- [165] Chan S.H., Su Y.C., 2008, A self-adaptive fluidic probe for electrical caries detection, *Biomedical Microdevices*, **10**, 447–57.
- [166] Gotliv B-A, Veis A., 2007, Peritubular dentin, a vertebrate apatitic mineralized tissue without collagen: role of a phospholipid– proteolipid complex, *Calcified Tissue International*, **81**, 191–205.
- [167] Zhang X., Koon G.N., Anil K., 2008, Monitoring acid demineralization of human dentine by electrochemical impedance spectroscopy (EIS), *Journal of Dentistry*, **36**, 1005–12.
- [168] Pincus P., 1951, A new method of examination of molar teeth grooves for the presence of dental caries (abstract), *Journal of Physiology*, **113**, 13–4.
- [169] Scholberg H.P., Borggreven J.M., Driessens F.C., 1982, Impedance of dental enamel membranes as a predictor for their permeability, *Medical & Biological Engineering & Computing*, **20**, 578–84.
- [170] Xu Zhang et al., 2008, Monitoring acid-demineralization of human dentine by electrochemical impedance spectroscopy (EIS), *Journal of dentistry*, **36**(12), 1005-12. [\[DOI:10.1016/j.jdent.2008.08.007\]](https://doi.org/10.1016/j.jdent.2008.08.007)
- [171] Movasaghi Z., Rehman S., and Rehman I.U., 2008, Fourier Transform Infrared (FTIR) spectroscopy of biological tissues, *Appl Spectrosc Rev.*, **43**, 134-179.
- [172] Krafft C., Sergo V., 2006, Biomedical applications of Raman and infrared spectroscopy to diagnose tissues, *Spectroscopy.*, **20**, 195-218.
- [173] Miyazaki M., Onose H., Moore B.K., 2002, Analysis of the dentin-resin interface by use of laser Raman spectroscopy, *Dent Mater.*, **18**, 576-580.

- [174] Ko A.C.T., Choo-Smith L.P., Hewko M., Sowa M.G., 2006, Detection of early dental caries using polarized Raman spectroscopy, *Opt Express.*, **14**(1), 203-215.
- [175] Venkatakrishna K., Kurien J., Pai M.K., Valiathan, M., Nagesh Kumar N., Murali Krishna C., Ullas G., Kartha, V.B., 2001, Optical pathology of oral tissue: A Raman spectroscopy diagnostic method, *Curr Sci.*, **80**(5), 665-669.
- [176] Kah J.C.Y, Kho K.W., Lee C.G.L, Richard C. J., Sheppard. Shen, Z.X. Soo, K.C. and Olivo M.C., 2007, Early diagnosis of oral cancer based on the surface plasmon resonance of gold nanoparticles, *Int J Nanomed.*, **2**(4), 785-798
- [177] Shim M.G., Wilson B.C., Marple E., Wach M., 1999, Study of fiber-optic probes for in vivo medical Raman spectroscopy, *Appl Spectrosc.*, **53**, 619-627.
- [178] Shim M.G., Wong Kee Song L.M., Marcon N.E., Wilson B.C., 2000, In vivo near-infrared Raman spectroscopy: demonstration of feasibility during clinical gastrointestinal endoscopy, *Photochem Photobiol.*, **72**, 146-150.
- [179] Schut T.C.B., Witjes M.J.H., Sterenborg H.J.C.M., Speelman O.C., Roodenburg J.L.N., Marple E.T., Bruining H.A., Puppels G.J., 2000, In vivo detection of dysplastic tissue by Raman spectroscopy, *Anal Chem.*, **72**, 6010-6018.
- [180] Buschmann H.P., Marple E.T., Wach M.L., Bennet B., Schut T.C.B., Bruining H.A., Brusckhe A.V., van der Laarse A., and Puppels G.J., 2000, In vivo determination of the molecular composition of artery wall by intravascular Raman spectroscopy, *Anal Chem*, **72**, 3771-3775.
- [181] Molckovsky A., Song L.M.W.K., Shim M.G., Marcon N.E., and Wilson B.C., 2003, Diagnostic potential of near infrared Raman spectroscopy in the colon: differentiating adenomatous from hyperplastic polyps, *Gastrointest Endosc.*, **57**, 396-402.
- [182] Crow P., Molckovsky A., Stone N., Uff J., Wilson B., Song L.M.W.K., 2005, Assessment of fiber-optic near infrared Raman spectroscopy for diagnosis of bladder and prostate cancer, *Urology.*, **65**, 1126-1130.
- [183] Boskey A.L., Mendelsohn R., 2005, Infrared spectroscopic characterization of mineralized tissues, *Vib Spectrosc.*, **38**, 107-114.
- [184] Es Sebar L. et al., 2022, Nanoindentation and Raman spectroscopy measurements on dual-cure luting cement for dental conservative restoration, *MeMeA Proceeding*.
- [185] Es Sebar L. et al., 2022, Measurements for restorative dentistry: shrinkage and conversion degree of bulk-fill composites, *MeMeA Proceeding*.
- [186] Ramakrishnaiah R., Ur Rehman G., Basavarajappa S., Al Khuraif A. A., Durgesh B. H., Khan A. S., Ur Rehman I., 2014, Applications of Raman Spectroscopy in Dentistry: Analysis of Tooth Structure, *Applied Spectroscopy Reviews*. [DOI: [10.1080/05704928.2014.986734](https://doi.org/10.1080/05704928.2014.986734)]
- [187] Ionita I., 2009, Diagnosis of tooth decay using polarized micro-Raman confocal spectroscopy, *Romanian Rep. Phys.*, **61**, 567-574.
- [188] Hill W., Petrou V., 2000, Caries detection by diode laser Raman spectroscopy, *Appl Spectrosc.*, **54**, 795-799.
- [189] Izawa T., Wakaki M., 2005, Lasers in dentistry XI: Application of laser Raman Spectroscopy to dental diagnosis, *Proceedings of SPIE*, **5687**, [DOI: [10.1117/12.590211](https://doi.org/10.1117/12.590211)]

- [190] Mortimer K.V., Tranter T.C., 1971, A scanning electron microscopic study of carious enamel, *Caries Res*, **5**, 240–63.
- [191] Lustman J., Sela M., Sela J., Ulmanky M., 1974, White enamel patches. A scanning electron microscope study of approximal surfaces following removal of plaque, *J Oral Pathol*, **3**, 123–6.
- [192] Wilson D.F., Shroff F.R., 1972, Scanning electron microscopy of carious enamel, *N Z Dent J*, **68**, 213–8.
- [193] Haikel Y., Frank R.M., Voegel J.C., 1983, Scanning electron microscopy of the human enamel surface layer of incipient carious lesions, *Caries Res*, **17**, 1–13.
- [194] Möller H., Schröder U., 1986, Early natural subsurface caries. A SEM study of the enamel surfaces before and after remineralization, *Caries Res*, **20**, 97–102.
- [195] Queiroz C.S., Hara A.T., Paes Leme A.F., Cury J.A., 2008, pH-cycling models to evaluate the effect of low fluoride dentifrice on enamel de- and remineralization, *Braz Dent J*, **19**(1), 21-7. [DOI: 10.1590/s0103-64402008000100004]
- [196] <https://www.thermofisher.com>.
- [197] <https://microbenotes.com/scanning-electron-microscope-sem/>.
- [198] Tsai M.T., Wang Y.L., Yeh T.W. et al., 2019, Early detection of enamel demineralization by optical coherence tomography, *Sci Rep*, **9**(17154). [DOI: 10.1038/s41598-019-53567-7]
- [199] Worawongvasu R., 2015, A Scanning Electron Microscopic Study of Enamel Surfaces of Incipient Caries, *Ultrastruct Pathol*, **39**(6), 408-12. [DOI: 10.3109/01913123.2015.1060284]
- [200] Morais A. P., Pino A. V., Souza M. N., 2014, Assessment of tooth structure using an alternative electrical bioimpedance spectroscopy method, *Brazilian dental journal*, **25**, 146-152.
- [201] Herencsar N., Freeborn T. J., Kartci A., Cicekoglu O., 2020, A comparative study of two fractional-order equivalent electrical circuits for modeling the electrical impedance of dental tissues, *Entropy*, **22**(10), 1117.
- [202] Iannucci L., 2021, Chemometrics for data interpretation: Application of principal components analysis (pca) to multivariate spectroscopic measurements, *IEEE Instrumentation and Measurement Magazine*, **24**(4), 42–48.
- [203] Giaquinto N., Scarpetta M., Spadavecchia M., Andria G., 2021, Deep learning-based computer vision for real-time intravenous drip infusion monitoring, *IEEE Sensors Journal*, **21**(13), 14148–14154.
- [204] Lindholm-Sethson B., Nyström J., Malmsten M., Ringstad L., Nelson A., Geladi P., 2010, Electrochemical impedance spectroscopy in label-free biosensor applications: multivariate data analysis for an objective interpretation, *Analytical and bioanalytical chemistry*, **398**(6), 2341–2349.
- [205] Lvovich V. F., 2012, Impedance spectroscopy: applications to electrochemical and dielectric phenomena, *Wiley*, 353.
- [206] <https://www.gamry.com/application-notes/EIS/basics-of-electrochemical-impedance-spectroscopy/>.
- [207] <https://photometrics.net/scanning-electron-microscopy-sem/>.

- [208] Mayeen A., Shaji L. K., Nair A. K., Kalarikkal N., 2018, Morphological characterization of nanomaterials, *Elsevier*, 335-364.
- [209] Akhtar K., Khan S. A., Khan S. B., Asiri A. M., 2018, Scanning electron microscopy: Principle and applications in nanomaterials characterization, *Springer International Publishing*, 113-145.

Acknowledgments

First, I would like to thank my supervisors, Sabrina Grassini and Leonardo Iannucci, for the opportunity they have given me and for the assistance and helpful advice in the development of this thesis. I also thank the PhD student Isabella for helping me during the realization of this work.

I want to thank my friends, in Turin and not, for all the support.

To my family and Bachisio, thank you for always being there.